

**The Effect of Input from the Cerebellar
Nuclei on Activity in
Thalamocortical Networks**

Julia Goncharenko

Submitted to the University of Hertfordshire in partial
fulfilment of the requirements of the degree of
Doctor of Philosophy

October 2021

UH Biocomputation Group
Centre for Computer Science and Informatics Research
University of Hertfordshire
Hatfield

Supervisors:

Dr Volker Steuber

Dr Reinoud Maex

Dr Christoph Metzner

Dr Neil Davey

Acknowledgments

I would like to thank Professor Volker Steuber for his support, patience and invaluable advice at every stage of my research.

I am very grateful to Dr Reinoud Maex for his insightful comments and suggestions which helped to accelerate the entire project towards the finish line.

I would like to express my sincere gratitude to Dr Arnd Roth and Professor Rod Adams for detailed feedback on my dissertation which enabled me to improve it greatly.

I would like to extend my thanks to Dr Neil Davey and Dr Maria Schilstra for supervising me during my first year of PhD studentship before their retirement. I will be always grateful for the hours of teaching at the beginning of my studentship to Dr Neil Davey and his guidance through my life in the UK to which I was totally novice.

I would like to thank our collaborator, Dr Freek Hoebeek for sharing with me the spike time recordings.

I am grateful to Dr Michael Scmuker for helping me with the *.pkl data format converting, to Sam Sutton of his friendly support and to Jean for agitating me to analyse my data in R.

I would like to thank Dr Ankur Sinha for helping me with the Linux Fedora system and guiding me through software installation at the early stages of my studentship.

I would like to express my gratitude to the Biocomputation research group for shaping my academic interest in computing.

I would like to thank all the people I shared the office with for making my student life brighter. In particular, Dr Deepak Panday and Dr Zaheed Mahmood and their families for their friendship and invaluable support.

At last but not least, I would like to mention how indebted I am to my family. I cannot be grateful enough to my husband Berdakh, who took care of the children and the household while I was doing my research. Thank you for believing in me, encouraging me at every step and for treating me with tenderness and respect. I am sincerely grateful to Leila and Tim, who bore my long erratic working hours and missed me while being close at reach. And of course, this PhD wouldn't happen without the huge contribution which my parents invested in me in terms of their time and education at all the stages of my growth and personal development, which shaped my personality to whom I am now.

Abstract

The cerebellum is a prominent brain structure that contains more than half of all neurons, in the brain, which are densely packed and make up 15% of the total brain mass (Andersen et al., 1992). It is well known for its contribution to the control of motor functions, but it also plays a pivotal role in non-motor behaviours. The cerebellum is also involved in numerous pathological conditions. This thesis contributes to the understanding of the pathophysiology of the cerebello-thalamo-cortical pathways. I concentrate on two cerebellar diseases, namely: absence epilepsy (Noebels, 2005) and downbeat nystagmus (DBN) (Strupp et al., 2007).

In this thesis the missing link in explaining the alleviating mechanism of a potassium channel blocker on downbeat nystagmus was found. A simulated single biologically detailed floccular target neuron (FTN) model was stimulated by input from cerebellar Purkinje cells (PCs). It was demonstrated that for both synchronised and unsynchronised input, irregular PC spike trains (which resembles the DBN condition) resulted in elevated FTN firing rates, in comparison with regular (4-AP treated) ones. This increase or decrease of the FTN firing rates during DBN, or after 4-AP treatment, respectively depended on short term depression (STD) at the PC - FTN synapses exclusively in the cases when the PC input was unsynchronised. In contrast, results of previous modelling studies (Glasauer et al, 2011; Glasauer and Rossert, 2008) were not in-line with the corresponding experimental findings (Alvina and Khodakhah, 2010) because they did not take into account the STD on the FTN-PC synapses.

It was also demonstrated here that the cerebellar output contributes to the control of absence epilepsy that originates in the thalamocortical network. Moreover, the cerebellar input was most effective when it arrived at the peak of the GSWD burst, with the least effective input arriving during the inter-ictal interval, showing clear phase-dependency. I have also shown that a three-fold increase in the inhibitory time constant, drives the asynchronous-irregular network into an ictal state. This increase reflects the GABA_A block. A change to GABA_B dominated inhibition results in GSWDs, in which the “wave” component is related to the slow GABA_B-mediated K⁺ currents (Destexhe, 1998).

Therefore, in this thesis two important contributions are made to the understanding of cerebellar pathological states: absence epilepsy and DBN, which might in turn be useful in the potential treatment of these conditions.

Contents

1. <u>Introduction</u>	1
1.1 Motivation	
1.2 Aims of the Thesis	
1.3 Contributions to knowledge	
1.4 Overview of the Thesis	
<hr/>	
2. <u>Background</u>	10
2.1 The cerebellum	
2.1.1 Introduction	
2.1.2 Structure of the cerebellum and its circuit	
2.1.2.1 Cerebellar cortex	
2.1.2.2 Cerebellar afferents and efferents	
2.1.2.3 Cerebellar nuclei neurons	
2.1.3 Cerebello-thalamo-cortical networks	
2.1.4 Functions of the cerebellum	
2.2 Cerebellar contribution to pathologies	
2.2.1 Tottering mice, an established model of absence epilepsy and nystagmus	
2.2.2 Nystagmus	
2.2.2.1 Aetiology	
2.2.2.2 4AP Ca ²⁺ channel blocker	
2.2.3 Absence epilepsy	
2.2.3.1 Aetiology	
2.2.3.2 Neuromodulation	
2.3 Chapter conclusions	
<hr/>	
3. <u>Methodology</u>	32
3.1 Downbeat nystagmus model (CN neuron model)	
3.1.1 Neuron model	
3.1.2 Synapse model	
3.1.3 Network model	
3.2 Absence epilepsy model	

3.2.1	Choosing a network model	
3.2.1.1	A single column thalamocortical network model	
3.1.1.2	McIntyre model	
3.1.1.3	Thalamocortical and thalamic reticular	
3.2.2	AdEx model: single neuron model	
3.2.3	Epilepsy model: synapse model	
3.2.4	Epilepsy model: network model	
3.3	Simulators	
3.3.1	Neuron	
3.3.1.1	P. Gleeson's implementation (the reason for a change from NEURON to Nest)	
3.3.2	PyNN	
3.3.2.1	NEO object model	
3.3.3	NEST	
3.4	Data analysis tools	
3.5	Chapter conclusions	

4. <u>Modelling downbeat nystagmus</u>	57
4.1 Experiment 1: Modelling downbeat nystagmus	
4.2 The robustness of the results	
4.3 The mechanism of the translation of input irregularity into the output firing rate	
4.4 Chapter conclusions	

5. <u>Replication of the thalamocortical models</u>	72
5.1 Experiment 2: Single neuron model replication	
5.2 Experiment 3: Replication of Destexhe 2009	
5.2.1 Replication of one-layer cortical model of 500 neurons	
5.2.2 Replication of two-layer cortical model of 2200 neurons	
5.2.3 Replication of thalamocortical model	
5.2.4 Clarifying adaptation units	
5.3 Experiment 4: Replication of Destexhe's paper with GSWDS	
5.4 Specific parameters to reduce model bistability	

5.5 Difference between ictal and asynchronous state

5.6 Chapter conclusions

6. Dynamics of the interictal asynchronous state87

6.1 Naud's single neuron model parameters

6.2 Synaptic model

6.3 Background input

6.4 Interictal state dynamics investigation

6.5 Modelling experimental response types

6.6 Chapter conclusions

7. The ictal state: generalised spike-and-wave discharges and their termination by optogenetic stimulation.....98

7.1 Generalised dpike-and-wave discharges (GSWDs) as indication of the ictal state

7.1.1 Outline of the main changes and parameters important for the ictal state

7.1.1.1 Alpha function

7.1.1.2 Inhibitory synaptic conductance

7.1.1.3 Model bistability and the adaptation time constant τ_w

7.1.1.4 A note on the role of adaptation parameter a in the ictal state

7.2 GSWDs

7.3 CN input to terminate seizures

7.4 Phase dependency of the CN input

7.5 Phase dependence of spontaneous GSWDs termination as a model of evoked one

7.6 Chapter conclusions

8. Validation of modelling results using experimental data.....118

8.1. Experiment 1: modified pre-recorded input to all TC neurons in ictal network

8.2 Experiment 2: varying the number of TC neurons receiving CN input

8.3 Experiment 3: could seizures be triggered with the CN input?

8.4 Chapter conclusions

9. Discussion.....126

10. Conclusions.....131

- 8.1 Summary of the results: findings and limitations
- 8.2 Open questions and future directions
- 8.3 List of publications

<u>Bibliography</u>	137
<u>Appendix</u>	152
i. Conference papers	
ii. Experimental data	

Introduction

Motivation

The nervous system is a complex structure which joins multiple interacting elements to perform various vital functions for the organism. To understand biological processes, to research how the normal neuronal activities are altered in different pathological states and how to alleviate these conditions, various scientific approaches are used. The methods that are utilised to study the nervous system include experimental, clinical, theoretical and simulation procedures. Each of these approaches has made a valuable contribution to the current neuroscience knowledge and understanding of brain functions, but also has its own downsides. For example, the results of experimental research are subjective to the limitations linked to the use of animal models, the complexity of experimental design and other factors, which makes the possibility to reproduce the results very low. To integrate the knowledge and to drive the conclusion from a number of research papers in order to answer the fundamental questions is a very complex task, because many research papers tackling the same problem use different preparations and experimental methods, which are not always plausible to compare.

The object of experimental studies could be either a cellular culture, the brain slice or the brain as a whole in the *in-vivo* approaches, which is a big difference by itself. With the introduction of optogenetics more than a decade ago, the identification of particular neural populations and their connections and interactions become a new reality.

In spite of the incredible similarity between humans and many other mammals, the results obtained from animal research cannot always be transferred to humans, and deviations may or may not be important. Also, ethical questions about animal use in research is still a contentious issue, which was the turning point personally to me while deciding to switch from experimental research to modelling. As for science in general, the best is the integrative approach, where the scientists from all the neuroscience areas are working in collaboration.

The imaging and electrophysiological measurement of neuronal electrical activity become the gold standard of the experimental approaches in neuroscience, allowing a huge variability in techniques used both extra- and intracellularly, especially now, when with the development of optogenetic techniques, the neuronal activity can be controlled noninvasively by light stimulation in a freely moving, awake animal. With the growth of electrophysiological data, the question of systematically processing and analysing these data gets more and more important. With this in mind, and to overcome ethical and experimental problems related to research on laboratory animals, computational methods are widely used. They can serve as explanatory or predictive tools. Depending on the problem, different modelling methods can be applied based on the level of detail. Also, computational methods become of significant help

with data that are difficult to obtain experimentally, such as studying the activity of many neurons simultaneously. That is also the reason why experimentalists and computational modellers usually work in collaborative groups, so that modellers can help with explaining connections, pathways and brain-behavior relationships.

By and large, computational models vary in the complexity, level of abstraction and computational power they require (Sterratt et al., 2011). To this purpose, models of different abstraction levels were created: single-neuron models which are detailed multicompartmental and biologically realistic, such as cerebellar nucleus (CN) neuron model (Steuber et al., 2011) or network models, where the single neuron properties are simplified in order to be able to observe neuronal ensembles behaviour in large networks. Neurons can still have their intrinsic properties according to their type, such as in the adaptive exponential integrate-and-fire (AdEx) model (Brette and Gerstner 2005).

In terms of the design of the experiments, the most productive outcomes might be collected when both experimental and computational researches are working in collaboration. Experimentalists usually define the general trend of research, and computational specialists seek for the mechanisms underlying these trends.

The cerebellum is a remarkable brain structure which contains more than half of all brain neurons, which are densely packed in around 15% of the total brain mass (Andersen et al., 1992), and four times more neurons than neocortex (Azevedo et al., 2009). The fact that the cerebellum increased its size in humans significantly faster as predicted by the change in neocortex size for the last million years (Clark et al, 2001) unequivocally shows how important this brain region is. The sole output of the cerebellar cortex is provided by the Purkinje cells (Thach, 1970). They are the main structural element of cerebellar cortex. They were named after Czech physiologist Johannes Purkinje in 1837. They are one of the largest neurons so that each Purkinje cell (PC) has around 200,000 inputs (Tyrrell and Willshaw 1992). The major part of PC synapses are formed with one of the smallest neurons – granule cells, whose axons grow upwards, thus forming parallel fibers. Apart from synapses with PCs they also synapse onto three other types of cerebellar neurons, which are stellate, basket and Golgi cells. Purkinje cell dendrites branch from one side of the soma in one plane, which is very unusual for neurons, which are normally grow without precise spatial orientation. They could form this special type of dendritic tree in order to increase the probability of the contact with parallel fibres while they grow, as parallel fibres are arranged in a transverse direction. Due to the strict spatial organisation of neurons in the Cerebellum, its morphology is very well studied. The first time the general principles of synaptic connections in the cerebellum were mentioned at the end of

XIX century in the studies of Spanish histologist Ramon Y Cajal. After that, there were many breakthroughs in cerebellar research.

Nonetheless, until recently the simplistic description of the cerebellum as purely motor structure was quite popular (Leiner et al., 1989). With the development of magnetic resonance imaging (MRI) research, it was shown that the cerebellum preserves high activity during actions not related to motor activity in humans (Leiner et al., 1993). It was also shown that the lesion of some cerebellar regions lead to disruption of motor-unrelated functions, such as quality of sensor perception (Bastian, 2011). Other studies have shown that the cerebellum is important for short-term memory (Silveri et al., 1998), attention (Courchesne et al., 1994) emotions, planning and even in the development of pathological states (Glickstein, 2007).

The research described in this project is focused on the contribution of the cerebellum to pathologies such as downbeat nystagmus and absence epilepsy. Experimental (Alvina and Khodakhah, 2010; Kros et al., 2015) and modelling studies (Glasauer and Rossert, 2008; Glasauer et al., 2011) attempted to research the nature of these channelopathies, but there is no clear agreement about the mechanisms that underlay these pathological conditions. Here an attempt is made to elucidate the mechanisms of these pathologies and possibly propose alleviating solutions.

Aims of the Thesis

The aim of the thesis is to research the contribution of the cerebellum to pathologies, in particular to downbeat nystagmus and absence epilepsy, and attempt to describe the mechanisms underlying them, in order to be able to propose possible treatment.

Downbeat nystagmus (DBN) is a common eye fixation disorder that is often caused by the pathological activity of neurons in the cerebellum (Hüfner et al., 2007). DBN is characterized by slow spontaneous upward eye drift and a compensatory fast phase directed downward. Patients suffering from DBN can be treated with 4-aminopyridine (4-AP), a non-selective potassium K⁺ channel blocker (Kalla et al., 2004).

The aim was to understand and propose the mechanism that underlies the therapeutic action of 4-AP in DBN based on the experimental data (Alvina and Khodakhah, 2010).

Absence seizures are the most common form of generalised epilepsy in children (Berg et al., 1999). It is a non-seizure type of epilepsy which is characterised by a temporal loss of consciousness which lasts up to ten seconds with sudden onset. The hallmark of the absence epilepsy is generalised spike-and-wave discharges (GSWDs) seen on electroencephalogram (EEG) (Crunelli, V. and Leresche, N., 2002). These GSWDs are based on neuronal oscillations in thalamocortical networks, which can be caused by excessive inhibition in the thalamus or excessive cortical activity (Kros et al., 2015). Absence seizures can be triggered by a switch from the normal asynchronous neuronal activity in thalamocortical networks to synchronised oscillations and terminated by the reverse process, switching from synchronised oscillations to asynchronous activity. Our collaborators have reported the potential therapeutic effect of cerebellar nuclei stimulation on absence epilepsy (Kros et al., 2015). They showed that input from the cerebellar nucleus neurons can disrupt oscillatory activity in thalamocortical networks. It was found that optogenetic activation of neurons in the cerebellar nuclei (CN) can stop epileptic absence seizures and reset the oscillatory activity, for example in a closed-loop system (Kros et al., 2015). Moreover, they showed a phase-dependency of the stimulation time with respect to the oscillation phase in thalamocortical networks. However, the underlying mechanism of the termination of absence seizures by CN stimulation is not yet clear.

The aim of the thesis was to reproduce these experimental results to be able to explain the potential mechanisms contributing to the absence seizure termination in response to the CN stimulation. To reach this aim there was a need to complete some intermediate tasks:

- Choose a suitable model with adequate abstraction level for the task
- Replicate / calibrate chosen model
- Change the model in order to produce generalised spike-and-wave discharges (GSWDs) (as the chosen model is designed to produce Up and Down states)
- Make a parameter search to find out which particular parameter is responsible for the oscillatory mode
- Simulate CN stimulation to thalamus to terminate GSWDs
- Propose a mechanism of GSWDs termination as a response to the CN stimulation.

Contribution to knowledge

As a result of the research documented in this thesis the cerebellar contribution to pathologies, in particular to downbeat nystagmus and absence epilepsy, were studied.

1. It was shown with single CN neuron modelling that for both synchronized and unsynchronized Purkinje cell input, irregular (which resembles the DBN condition) input trains resulted in higher floccular target neuron (FTN) spike rates than regular (4-AP treated) ones. In the presence of unsynchronized Purkinje cell input, the acceleration of the FTN spike output during simulated DBN and the corresponding deceleration during simulated 4-AP treatment depended on Short-Term Depression (STD) at the FTN - Purkinje cell synapses. STD at the PC-FTN neuron was the component which was not taken into account by the previous modelling studies (Glasauer et al, 2011; Glasauer and Rossert, 2008). Acceleration of the FTN firing rate leads to nystagmus and motor deficit, while 4-AP treatment restored regular PC firing and alleviated nystagmus, which is completely in-line with experimental findings.

2. It was shown that the network activity can exhibit oscillatory or asynchronous irregular (AI) dynamics, depending on the time constants of the inhibitory synaptic conductance. An increase in the inhibitory decay time constant reflects a change from GABA_A dominated inhibition to more GABA_B, which can result in GSWDs, given that the “wave” components of GSWDs are related to slow GABA_B-mediated K⁺ currents (Destexhe, 1998). The results described in this thesis confirm that input from the CN can control oscillatory activity in thalamocortical networks. Furthermore, I demonstrated that the effectiveness of this input exhibits phase-dependence. In the simulations, CN input terminates epileptic absence seizures most effectively when it arrives at the peak of GSWDs, while seizure termination is least efficient for input between the GSWD bursts. This finding is potentially relevant for therapeutic applications of CN stimulation to terminate seizures.

Overview of the Thesis

The thesis is organised as follows. In the **second chapter**, the background for the thesis is given. The elements that form the cerebellar circuit, such as cerebellar cortex, its afferents and efferents are described. The functions of the cerebellum are outlined, with its contributions to pathologies. The tottering mouse model is discussed as a commonly used model for DBN and absence epilepsy research. The two cerebellar pathologies, DBN and absence epilepsy described in terms of their aetiology and possible treatment solutions.

The **third chapter** describe the methodologies used in this thesis. These include the description of the CN neuron model used to research DBN and 4-AP as an alleviation option. The choice of the model of absence epilepsy was not straightforward, so the brief descriptions of possible models of choice are given, with the reasoning behind. The absence epilepsy was modelled with the AdEx model, which was adjusted to be able to replicate thalamocortical oscillations. Single neuron and network models are discussed. The modelling software such as NEURON and Nest, PyNN API for Python model and NEO object model are described, as well as the software that was used for the output processing. For this, the data analysis tools were used, such as Matlab and R programming language.

In **chapter four**, the background of the DBN research is given, which includes the two modelling paper outline: the system-level model (Glasauer and Rossert, 2008) and the integrate-and-fire (I&F) model of PCs. Their results are discussed and compared with the outcome of the experimental research (Alvina and Khodahah, 2010). The chapter include our findings of the crucial effect of the short term depression (STD) in the PC-FTN synapses together with regularity and synchrony.

The **fifth chapter** contains the description of the model of Up and Down and asynchronous irregular states by A.Destexhe (Destexhe, 2009). The issues were faced during the attempts to replicate different configurations of the model are mentioned here. Additionally, there is a detailed description of the thalamocortical model, which was obtained after the modification of the second layer of the two-layer cortical model. The single neuron model which was written to confirm the intrinsic properties of the cell types constitute the thalamocortical model is outlined here.

The **sixth chapter** contains the results of the absence epilepsy modelling. There is the reasoning behind the parameter choices and the specifications of the asynchronous interictal state.

In the **seventh chapter**, the transition from an asynchronous state to an oscillatory ictal state was made, so that generalised spike-and-wave discharges (GSWDs) are prominent. The

description of the ictal state is made, with parameter changes declared. The issues which arose are also described in this chapter, such as model bistability, and how they were handled. After the model was calibrated in order to produce GSWDs, the external excitatory input from CN neuron was modelled. This CN input was shown to be able to terminate absence seizures and drive the model back to the asynchronous interictal state. The effect of the CN input showed phase-dependency, which is also discussed in the chapter.

The **final conclusions chapter** provides a summary of the results and possible future work that can be conducted to continue with this research.

2

Background

2.1 The cerebellum

2.1.1 Introduction

From the top level hierarchy, the brain can be divided into the brainstem, cerebrum and cerebellum. The latter is situated behind the brain stem and beneath the posterior portions of the cerebral hemispheres (Figure 2.1), and its name is Latin for ‘little brain’. The cerebellum is a unique brain structure as it contains more than half of the brain’s neurons, taking only 10% of its volume (Kandel et al., 2000). This has incited the interest among various scientists to study the cerebellum. Its structure consists of repeating units with the same microcircuit, which contributed to the fact that it is probably the best understood part of the brain. Also, its contribution to pathologies is increasingly understood.

This chapter provides an overview of the physiology of the brain structures related to the thesis and to the models used. A brief description of the cerebellar structure and function will be given, with particular attention to the neurons of the Cerebellar Nuclei.

The basic cerebellar circuit will be described, together with its role in the cerebello-thalamo-cortical network. In the last part of the chapter the cerebellar contribution to pathologies will be outlined with particular focus on absence epilepsy and nystagmus, the two pathologies described in the thesis and to which mechanisms of alleviation are proposed.

2.1.2 Structure of the cerebellum and its circuit

The cerebellum is composed of the two hemispheres and centrally located vermis (“worm”) (Figure 2.1). The central branching framework inside the cerebellar hemispheres and the centre of the vermis is formed by white matter and is highlighted by the blue stain in Figure 2.2. The grey matter, which composes the cerebellar cortex, is shown in purple (hematoxylin) and red (eosin) on Figure 2.2. (Best and Taylor, 1965). This stained section makes it clear why the cerebellum is sometimes called the *Arbor Vitae*, a Latin phrase meaning “the tree of life”, and the separate subdivisions are called *folia* (from Latin for “leaf”) (Figure 2.2)

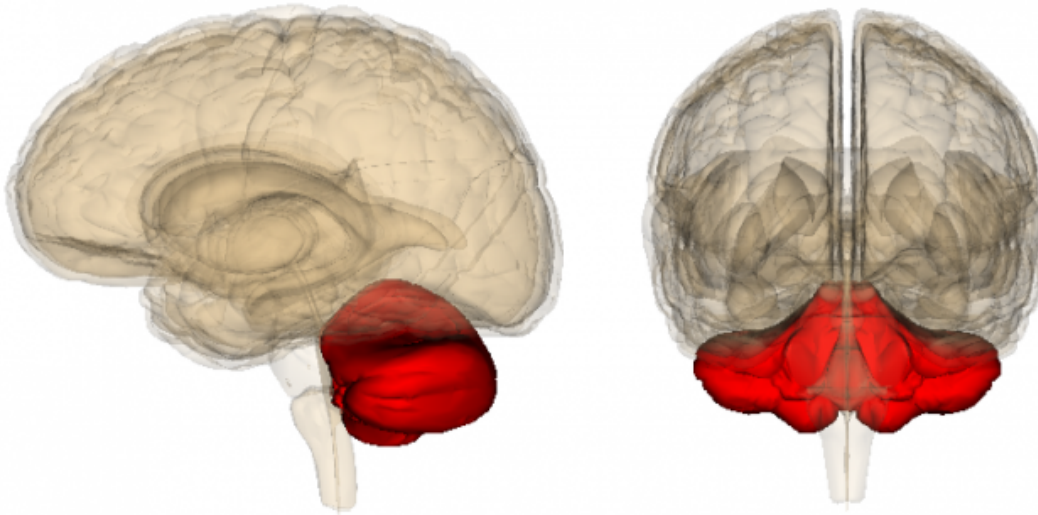


Figure 2.1 Picture of the human brain. Cerebellum marked in red. Source: Wikimedia Commons / Life Science Databases

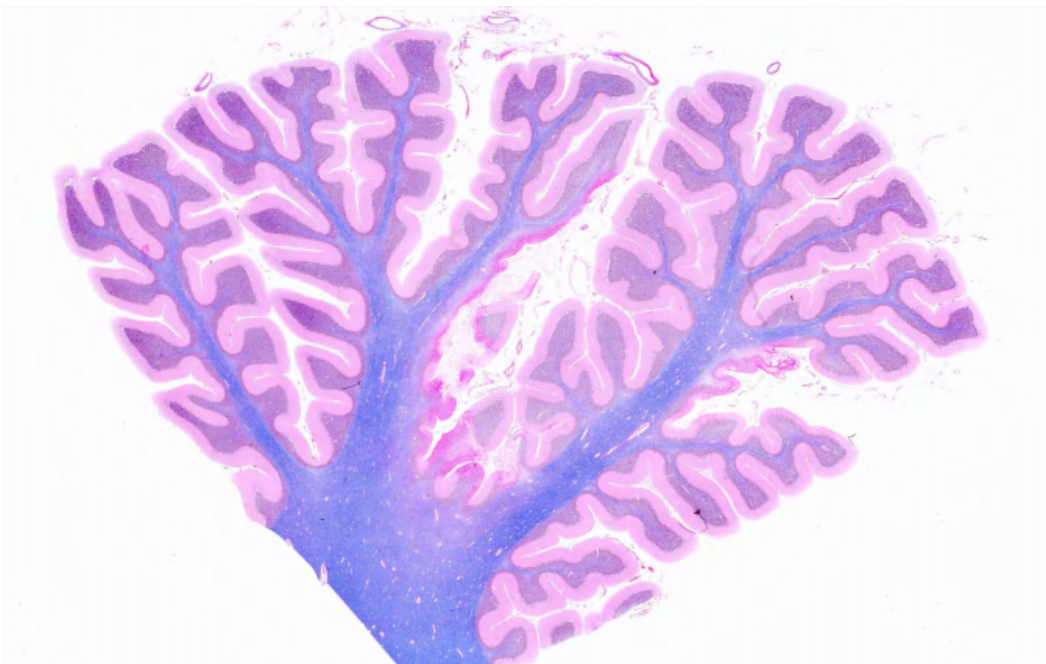


Figure 2.2 Picture of the central branching framework inside the cerebellar hemispheres with the white matter stained in blue and the grey matter in purple.

Source: Harvard Brain Tissue Resource Center, McLean Hospital, Belmont, MA. 1-800-BRAIN BANK

transmitted through the mossy fibers diverge to DCN and activate the granular layer (containing GrC and GoC). The ascending axon of the GrC bifurcates in the molecular layer (containing PC, SC, and BC) forms the parallel fibers (pf). The cerebellar circuitry is arranged as a feedforward excitatory circuit assisted by inhibitory loops: mfs excite GrCs, which activate other cortical elements. In the granular layer, inhibition is provided by GoC, in the molecular layer by SC and BC. After all, PC inhibit DCN. The IO, which is also activated by brain stem and spinal cord nuclei, controls PC activity through a single strong synapse. Thus, the whole system can be considered as a complex mechanism which controls the DCN output. Source: (D'Angelo and Casali 2012).

The deepest layer – **granular layer** – is mostly composed of small but most numerous densely-packed excitatory granule cells receive the input to the cerebellar cortex, and much fewer large inhibitory Golgi interneurons. Both of these cell types form synapses within complexes known as cerebellar glomeruli, where both neuron types receive mossy-fibre input and where Golgi axons inhibit granule cells. Each granule cell grows T-shaped axons to the molecular layer to form a parallel fibre. Mossy fibres, which are one of the two principal afferents to the cerebellum also terminate in this layer. Their terminals supply excitatory (AMPA, NMDA) synapses to granule cell dendrites. The mossy fibre – granule cell pathway is highly divergent, connecting 1 mossy fibre to around 500 granule cells, whereas only around 4 mossy fibres innervate each single granule cell.

The **Purkinje cell layer** is situated in the middle and composed of the Purkinje cell bodies. Their dendrites grow upwards to the molecular layer, where they receive inputs from climbing and parallel fibres, as well as from inhibitory interneurons. Purkinje cells are GABA-ergic neurons, thus they inhibit their efferent neurons in the deep cerebellar and vestibular nuclei. Their axons form the entire output of the cerebellar cortex.

The dendrites of the Purkinje cells occupy the entire molecular layer, which also contains inhibitory interneurons (stellate and basket cells). The molecular layer further contains the axons of the granule cells, which run parallel to the folia and perpendicular to the dendritic trees of the Purkinje cells, so that they are known as parallel fibres.

The **molecular layer** lies on the top of the Cerebellum. As stated above, it is formed out of the inhibitory interneurons – the stellate and basket cells, the Purkinje cells dendrites, as well as the granule cell axons - parallel fibres, which are oriented perpendicular to the dendrites on which they are prone to form synapses. The dotted appearance of the parallel fibres on a cross-section has given the name to this layer.

2.1.2.2 Cerebellar afferents and efferents

Afferent and efferent axons compose the white matter of the cerebellar cortex. The afferent fibres (mossy fibres and climbing fibres) form excitatory synapses with neurons in both the cerebellar cortex and the deep cerebellar nuclei.

The cerebellum is connected to the brain stem by three compact bundles of nerve fibres known as peduncles. The **middle peduncle** is purely afferent, no fibres leave the cerebellum via this peduncle. The middle peduncle is the largest of the three and transmits impulses from the pons to the cerebellum. Its axons terminate as mossy fibres carry sensory and motor information. Mossy fibres form excitatory synapses with the dendrites of granule cells which, on their turn, convergently connect to Purkinje cells. The middle peduncle also emits collaterals that terminate in the cerebellar nuclei (CN) (Voogd and Ruigrok, 2012).

The **inferior peduncle** contains the fibres arising in the vestibular nuclei of the medulla and fibres of the direct dorsal spinocerebellar tract to the cerebellum. It carries proprioceptive sensory input (posture and balance). According to one of the hypothesis, the movement “error signal” originates in the inferior olivary nucleus, which receives input from both periphery and cerebral cortex, and enters the cerebellum as climbing fibre via the inferior peduncle. Each climbing fibre connects to multiple Purkinje cells (1:10), forming multiple synapses with each. Like the mossy fibres, climbing fibres also project to the neurons in the deep cerebellar nuclei. The inferior peduncle also provides the output of the cerebellum to the vestibular nuclei.

The **superior peduncle** connects the cerebellum to the midbrain and transmits impulses to the red nucleus and thalamus, through which the impulses hit the motor area of the cerebral cortex. The superior peduncle also provides the input to the cerebellum from the ventral spinocerebellar tract. To summarise, most input to the cerebellum is coming through the middle and inferior peduncles, and most of the output from the cerebellum is coming through the superior peduncle.

To summarise, in the cerebellar cortex, all of the incoming information is collected by the Purkinje cells which project to the three pairs of deep nuclei. The deep nuclei in turn send projections to other parts of the brain. In addition to the inhibitory Purkinje cell input, neurons in the deep cerebellar nuclei also receive excitatory input from climbing and mossy fibre collaterals. Therefore the inhibitory output of the Purkinje cells modulates the excitatory signal from mossy fibres to deep cerebellar nuclei. This loop is sometimes referred to as a primary cerebellar circuit.

2.1.2.3 Cerebellar nuclei

The cerebellar nuclei are the main output of the cerebellum. As mentioned above, they also receive excitatory glutamatergic input from mossy and climbing fibre collaterals, which originate from spinal cord, vestibular nuclei, pontocerebellar nuclei etc. This excitatory input is modulated by inhibition from Purkinje cells via their recurrent collaterals.

In the depth of the cerebellum, they are organized as three discrete masses of grey matter, the largest of which is the **dentate** nucleus. It receives input from the lateral hemisphere and from cerebellar afferents that carry information from the cerebral cortex (via the pontine nuclei). It projects to the contralateral red nucleus and the ventrolateral (VL) thalamic nucleus.

There are two other cerebellar nuclei: the **interposed** and the fastigial. The latter is the most medial. Laterally to the fastigial nucleus, there lie two parts of the interposed nucleus, the **globose** and the **emboliform**. Their input is coming from the intermediate zone and from cerebellar afferents that convey spinal, proximal somatosensory, auditory, and visual information. They project to the contralateral red nucleus (the origin of the rubrospinal tract).

The most medially located **fastigial nucleus** receives input from the vermis and from cerebellar afferents that carry vestibular, proximal somatosensory, auditory, and visual information. Then these neurons run to the vestibular nuclei and the reticular formation.

A further group of nuclei – the **vestibular nuclei** – is located outside the cerebellum, in the medulla. In spite of that they do not strictly belong to the cerebellar nuclei, vestibular nuclei are considered to be functionally equivalent to cerebellar nuclei because their connectivity patterns are the same. The vestibular nuclei receive input from the flocculo-nodular lobe and the vestibular labyrinth. They project to various motor nuclei and give origin to the vestibulospinal tracts. (J.Knierim, Neuroscience Online).

2.1.3 Cerebello-thalamo-cortical networks

The cerebellum is recurrently connected to the cerebral cortex. The cerebral cortex projects to the cerebellum through relays in the pontine nuclei, whereas the cerebellum projects to neocortex through relays in the thalamus.

Thalamic nuclei are strategically situated between motor areas of cerebral cortex and cerebellum. There are three main elements in the thalamocortical circuitry, which include excitatory thalamocortical relay neurons (TC) that project to the cerebral cortex (thalamocortical fibres), inhibitory interneurons situated inside relay nuclei and GABA-ergic neurons of the thalamic reticular nucleus (RE) which project to the thalamus proper.

Thalamocortical and corticothalamic pathways run through the reticular nucleus, which modulates the excitability of thalamus by its afferent fibres. The thalamus and cerebral cortex are bidirectionally connected by axons. Collateral branches of thalamocortical and corticothalamic fibres form the principal excitatory pathway to the neurons of the RE nucleus (Grillner, 2010).

The density of corticothalamic terminals is very high and they form around 80 % of all synapses on TC neurons. The circuit includes three cortical populations (layer V and VI) of pyramidal cells (PY) and two order of thalamic nuclei. The first consists of the TC relay neurons with projections that allow the processing of peripheral sensory information and relay it to the cortex. The second is RE nucleus. PY axonal collaterals excite RE nucleus neurons, which provide a feed-forward inhibition to the TC neurons. Each TC neuron receives around 5000 synaptic inputs, which arrive from retina, cortex and brainstem, but here the focus will be only on the inputs coming from cortex and RE neurons (Sherman and Guillery, 2006). Cortical input to TC nucleus is glutamatergic.

Intranuclear collaterals of RE axons form inhibitory GABA-ergic connections with TC dendrites. Due to this disynaptic inhibition the hyperpolarization happens at disynaptic delay after excitation of RE neurons by collateral thalamocortical and corticothalamic inputs. Disynaptic inhibition is mainly mediated by GABA_A receptors. Chemical synapses between RE neurons with reduced GABA_A-mediated inhibition in thalamic neurons and cortical inhibition intact may synchronise RE activity (Destexhe, 1998) leading to the synchronised oscillations with TC relay neurons, displaying a prolonged bursting discharges shown at Figure 2.4 B (Scherman, 2011) and Figure 2.5 B (Destexhe, 1998).

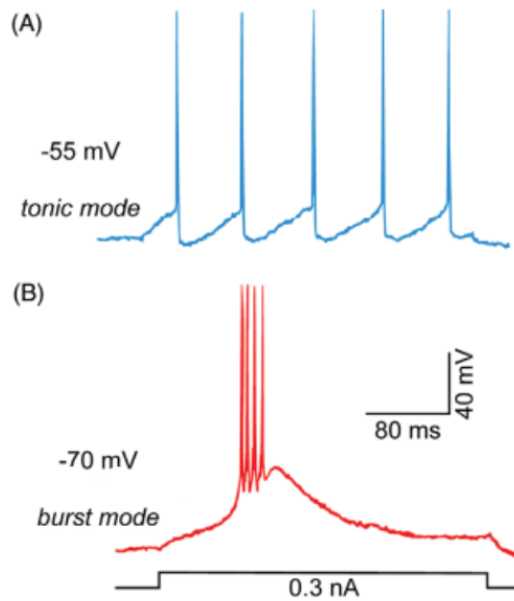


Figure 2.4 Example of tonic (A) and burst (B) firing. Source: (Sherman et al., 2011).

Bursting in TC neurons initiates excitatory postsynaptic potentials (EPSPs) and low-threshold Ca^{2+} spike-mediated bursts of action potentials (AP) in RE cells. The next burst in RE neurons leads to the large GABA_A receptor-mediated inhibitory postsynaptic potentials (IPSPs) in TC neurons. Some TC neurons in response to this activity generate rebound low-threshold Ca^{2+} spike-mediated bursts, which initiate the next oscillatory cycle. One such a cycle (RE – TC – RE) takes around 100 – 150 ms. Therefore, the network oscillates at 6 – 10 Hz (McCormick and Bal, 1997).

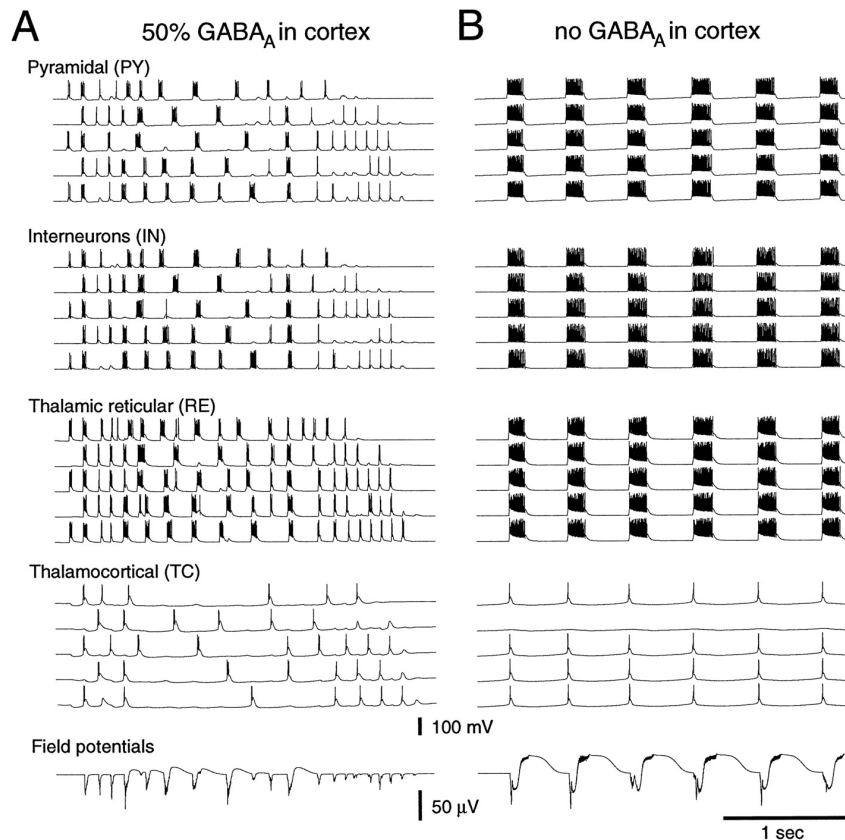


Figure 2.5 Transformation of spindle oscillations (an important feature of thalamic networks of 7 – 14 Hz generated waxing and waning rhythmic waves typical for a sleep) into slow oscillation with spike-and-wave local field potential (LFP) as a result of GABA_A block in cortex with thalamic inhibition intact. A: Spindles with 50 % decreased GABA_A conductances in IN-PY synapse. B: Oscillations after complete GABA_A block in cortical neurons. All neurons discharge in phases separated by silence periods. GABA_B currents were at their peak in TC and PY neurons during silence periods. LFPs displayed spike-and-wave discharges (Source: Destexhe, 1998).

TC neurons in the ventro-lateral nuclei of the thalamus are mainly excited by cerebellar afferents (Sherman, 2016). TC neurons, in turn, excite RE neurons. Axons of RE nucleus provide inhibitory feedback to TC cells. This reciprocal excitatory loop is controlled by local GABA-ergic neurons.

2.1.4 Functions of the cerebellum

Knowing the organisation of the cerebellar microcircuit can shed light on its function. The functions of various brain areas were initially researched by making lesions and observing which areas of the brain became dysfunctional.

There are three distinct functional subdivisions of the cerebellum: vestibulocerebellum, spinocerebellum and neocerebellum. The first one is most important for nystagmus, therefore greater attention will be paid to it.

Vestibulocerebellum

The vestibulocerebellum (Figure 2.5, yellow) is formed by the flocculonodular lobe and its connections to the lateral vestibular nuclei. It is phylogenetically the oldest part of the cerebellum, therefore it is sometimes called archicerebellum. The vestibulocerebellum consists of the nodule and its lateral extension, the paired flocculi. The vestibulocerebellum receives input from the vestibular labyrinth and vestibular nuclei. The output of the cerebellum is organised in a way that the Purkinje cells leave the cerebellum to synapse onto vestibular nucleus and brain stem and bypass the deep cerebellar nuclei. The neurons that receive the terminals of PC are called floccular target neurons (FTN).

The vestibulocerebellum is responsible for the control and regulation of eye movements, and the construction of a body motion estimate. The flocculonodular lobe is also responsible for the balance and muscle tone maintenance. Its damage will result in loss of balance and oculomotor control such as DBN. Monkeys with nodular lesions show downbeat nystagmus (see 2.2.2 Nystagmus) in darkness (Walker et al., 2008). The most common reason for the damage of flocculonodular lobe are tumours, such as medulloblastoma in childhood.

Spinocerebellum (paleocerebellum or archicerebellum)

The spinocerebellum (Figure 2.5, green and blue) is formed by the superior and inferior vermis except the nodule. It receives input afferents primarily from the spinal cord grey matter and vestibular nuclei, making it responsible for muscle movement control, and the sensation of limb position, pressure and touch. Also, as the spinocerebellum sends its efferents to the spinal cord, it makes it responsible for posture and balance control.

The vermis is also involved in the control of rapid eye movements or saccades. Also, together with the lateral part of flocculonodular lobe, the spinocerebellum is responsible for smooth-pursuit eye movements. The vermis is also involved in motor learning, correcting errors during saccades.

Cerebrocerebellum

The cerebrocerebellum (Figure 2.6, red) consists of the lateral cerebellar hemispheres, receiving input exclusively from cerebral cortex. It receives afferents via corticopontine fibres through the pontine nuclei from most of the neocortex, therefore it is sometimes called neocerebellum (Swenson, Review of Clinical and Functional Neuroscience, Chapter 8). The pontine nuclei project to the cerebellum through the middle cerebellar peduncles, where their axons terminate as mossy fibres, forming the largest input to the cerebellum. The neocerebellum sends efferents that reach the thalamus through the dentate nucleus, and hence to the cerebral cortex. The cerebrocerebellum performs cognitive functions (visuospatial perception, a language processing and modulation of emotions), general planning of motor activities and procedural motor learning, such as learning to ski or riding a bike.

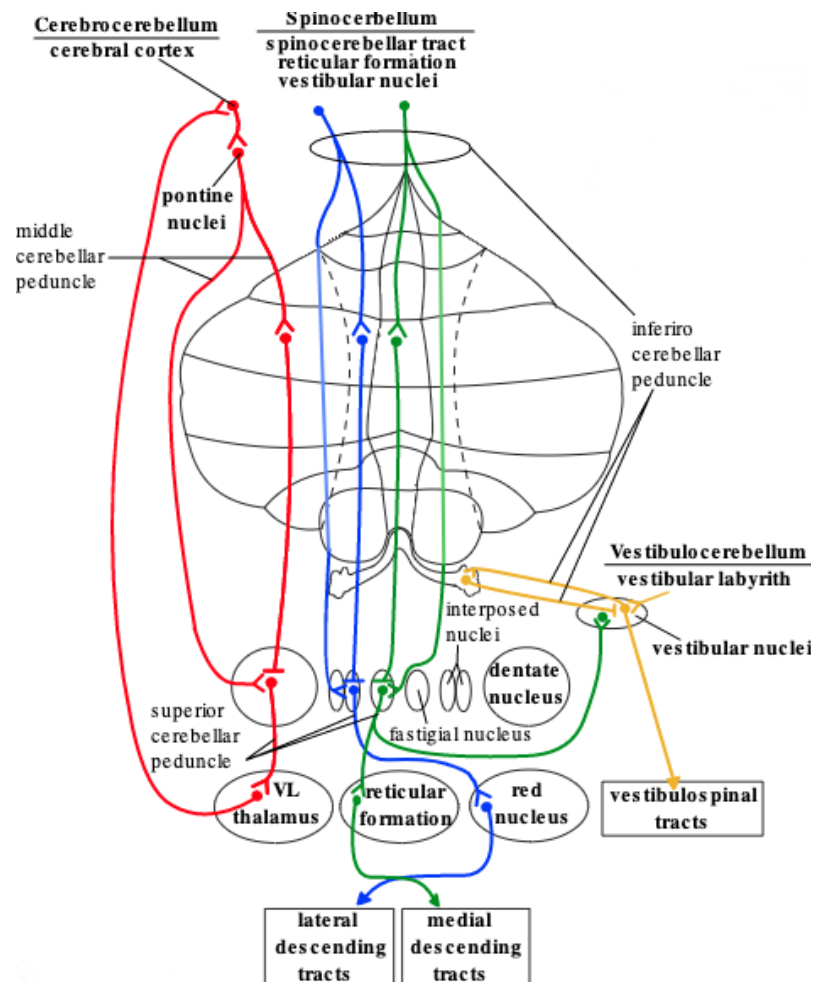


Figure 2.6 The input and output pathways of the three functional subdivisions of the cerebellum. They have specific input and output targets. The vestibulocerebellum is shown in yellow, the spinocerebellum in green and blue, the cerebrocerebellum is red.

(Adapted from Knierim J., Neuroscience online: <https://nba.uth.tmc.edu/neuroscience/m/s3/chapter05.html>).

2.2 Cerebellar contribution to pathologies (experimental background)

2.2.1 Tottering mice, an established model of absence epilepsy and nystagmus

Tottering mice are model mice that have a genetic mutation in a subunit of a Ca^{2+} channel. The Ca^{2+} channels are a large family of membrane proteins that show selective permeability to Ca^{2+} ions. They can be activated in response to the membrane voltage (voltage-gated channels). Here the focus will be on the voltage-gated Ca_v channels which play various roles within neurons, such as gene expression and neurotransmission by mediating Ca^{2+} influx through Ca_v channels in response to neuronal membrane depolarization.

There are six types of Ca_v channels which are called R, T, L, N, P and Q type. Depending on the type, they consist of either four or five subunits. The largest subunit is the α_1 subunit, which consists of the voltage sensor, conduction pore, gating apparatus and sites of channel regulation by drugs, toxins and second messengers (Catterall et al., 2003). The Ca_v channels contribute to increased depolarization and neuronal excitability, which contributes to a greater predisposition to oscillatory disorders such as epilepsy and episodic ataxia type-2, which is associated with central ocular motor and vestibular dysfunction, mainly downbeat nystagmus (DBN) (Strupp et al., 2004).

The mechanisms behind absence epilepsy, as well as mechanisms underlying downbeat nystagmus, remain elusive. Therefore, the animal models are crucial for investigation of the above-mentioned conditions. Both pathologies occur in the same mouse model, which carries a CACNA_{1A} gene mutation in a pore-forming α subunit of the P/Q voltage-gated $\text{Ca}_v2.1$ channel – the tottering mouse model (*tg/tg*). These channels are mainly expressed in the cerebellar Purkinje and granule cells, as well as in some other locations across the nervous system. The function of $\text{Ca}_v2.1$ is reduced in *tg/tg*, leading to a significant reduction of the $\text{Ca}_v2.1$ current density in Purkinje cells (Wakamori et al., 1998) and therefore to synaptic transmission deficits. The *tg/tg* mutation appears due to the change in a single nucleotide base, which cause epilepsy (Fletcher et al., 1996) and abnormal eye movements (Hoebeek et al., 2005; Stahl et al., 2006). The *tg/tg* mutants exhibit ataxia, cortical spike-and-wave discharges (SWD) and absence seizures. They are widely used to study pathophysiology of vestibulocerebellar diseases, including DBN. In fact, ataxic mice exhibit DBN rarely, and with

no magnitude relation to head tilt as observed in humans. Only tilt- and gaze-independent component of human DBN is in common with the properties of ataxic mice nystagmus during yaw rotation. The mutant *tg/tg* exhibit upward deviation of the eyes at rest. This, along with hyperactivity of otolith may serve as surrogate for DBN in rodent model (Stahl et al., 2012).

According to some sources, absence epilepsy (*petit mal*) has also been linked to mutations of the T-type calcium channel gene $CACNA_{1H}$ (Heron et al., 2004) as they produce firing that drives the thalamocortical network into slow oscillations during non-REM sleep (Llinás and Steriade, 2006). Such oscillations engage pyramidal, reticular and thalamic cells into SWD-like oscillatory events in mutant mice (Felix, 2002). Normally the activity of GABA-ergic reticular thalamic neurons activates T-type Ca^{2+} currents, which is elevated in tottering mutants and might synchronise them into bursting mode. This can happen as a result of decreased excitatory synaptic transmission in thalamus. (Felix, 2002). Also, abnormal Ca^{2+} conductance in the *tg/tg* is not only linked to the mutation in T-type ($Ca_v2.1$) channels, but with the elevated expression of N-type ($Ca_v2.2$) and L-type ($Ca_v1.2$) Calcium channels (Campbell and Hess, 1999; Qian and Noebels, 2000; Zhou et al., 2003; Leenders et al., 2002; Matsushita et al., 2002). Such a compensatory mechanisms leads to neurological dysfunction, which was shown in experimental studies with application of $Ca_v1.2$ antagonists and agonists, which used to alleviate or induce stress-related attacks respectively (Campbell and Hess, 1999) in *tg/tg*.

2.2.2 Nystagmus

Nystagmus is an involuntary repetitive movement of the eye. When the whole body is rotated in space the physiological nystagmus occurs. It consists of a slow velocity component, which stabilize the eye on stationary objects, and a fast phase which resets the eyes to the middle of orbit.

Pathological nystagmus is a common eye movement complication of cerebellar disease, which is characterised as a disorder of the mechanisms that underly the interactions of the cerebellar cortex and cerebellar nucleus (CN). In fact, it can be evoked by stimulation of the semi-circular canals or floccular-nodular lobe lesion. This happens when the head is in a fixed position. Patients with DBN usually complain of unsteadiness of gait and vertical oscillopsia (illusion of movement of visual word due to loss of stability of image on retina). Nystagmus can affect one or both eyes. It can be either induced physiologically, such as infantile nystagmus of new-borns, optokinetic and vestibular nystagmus, or be acquired.

Physiologically-induced nystagmus happens during self-rotation as an effort to hold a steady image on retina. Either optokinetic or vestibular nystagmus can be induced by self-

rotation. Optokinetic nystagmus occurs involuntarily when the person gazes into a large moving field and generate 2-3 Hz oscillations driven by cortical and subcortical pathways (Abadi, 2002).

Acquired nystagmus could be caused by neural pathologies. Some of them are cerebellar pathologies (floccular in particular) and associated with the mutation in the P/Q-type voltage-gated calcium (Ca^{2+}) channels (Fletcher et al., 1996). These include downbeat nystagmus (DBN), the most frequent form of acquired nystagmus characterized by an upward gaze drift.

2.2.2.1 Aetiology

DBN is a disorder of the mechanisms that keep the eyes still during fixation (vestibular system). The upward eye movements occur due to the inputs from the anterior canals of the vestibular labyrinth over the projections through the superior vestibular nuclei to motoneurons that supply elevator muscles (Figure 2.7).

The vestibulo-ocular reflex should generate an eye movement equal and opposite to that of a head movement to keep the eye in the same position in space and stabilize the retinal image.

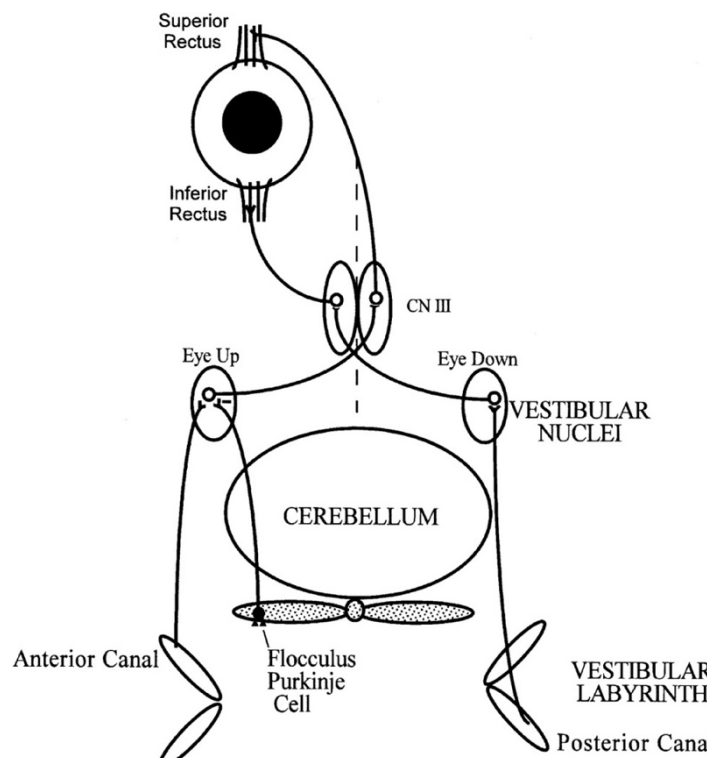


Figure 2.7. Diagram represents the structures involved in the appearance of DBN. Source: (Leigh, 2003).

The upward eye movements evoked by the inputs from the anterior semicircular canals of the vestibular labyrinth projecting through the superior vestibular nuclei to motoneurons that supply elevator muscles, in particular the superior rectus (CN III is oculomotor nucleus in Figure 2.6). The downward eye movements evoked by the inputs from the posterior semicircular canals projecting through the medial vestibular nuclei to motoneurons that supply depressor muscles, in particular the inferior rectus. The cerebellar flocculus inhibits anterior (but not posterior) canal projections in the vestibular nuclei. In case of impaired inhibition from the flocculus, the eyes will drift upward, causing downbeat nystagmus. It is postulated that 4-

diaminopyridine enhances Purkinje cell activity in the flocculus and restores inhibition of anterior canal pathways to normal levels (Glasauer et al., 2005; Kalla et al., 2004; Kalla et al., 2007).

In DBN the slow upward eye drift is composed of two components, a gaze-direction independent bias component and a gaze-dependent component. The upward drift of the eye might be a direct consequence of the asymmetric distribution of on-directions of the floccular (FL) – PCs: the great majority of these inhibitory cells increase their firing rate for downward visually evoked eye movements. Accordingly, damage to the FL would cause a decrease in overall firing rate, which is the cause of disinhibition of floccular target neurons (FTNs) in the vestibular nuclei, which leads to the upward drift of the eye (gaze-independent component of the nystagmus slow phase velocity). The gaze-dependent drift is a consequence of a decrease in efficacy of the neural integrator function, which critically depends on the FL drift with gaze-independent component; 4-AP on the average improved neural integrator function, i.e., gaze-evoked drift, regardless of aetiology (Leigh, 2003).

It was previously believed, that the reason for DBN is a lack of inhibition (Leigh and Zee, 2006), therefore the treatment targets GABAergic PCs receptors. It is believed that DBN could be alleviated by an increase of the PC firing rate in vestibular cerebellum and as a consequence to decrease in firing rate in vestibular nuclei. Therefore the effect of the aminopyridines was researched in several studies. Thus, Kalla et al. (2004) found that 4-AP improved DBN, gain of VOR, smooth pursuit and gaze-holding. It works particularly well when DBN is caused by cerebellar atrophy, but show no effect in case of a structural lesion.

The theory, where the underlying mechanism behind DBN is a lack of activity and excitability of PCs, has been disproved by electrophysiological experiments on the tg/tg mice cerebellum slices, showing that the therapeutic concentrations of K^+ channel blockers do not increase the inhibitory drive of cerebellar Purkinje cells (Alvina and Khodakhah, 2010). On the contrary, the 4-AP restores the regularity of PC firing by prolonging the action potential (AP) and increasing the AP afterhyperpolarization.

Prompted by these experimental results, Glasauer and colleagues performed a series of computer simulations to investigate the potential effect of changes in the regularity of Purkinje cell spiking on the activity of floccular target neurons (Glasauer et al., 2011). Using a simple conductance based model of an FTN, they found that changes in the regularity of the Purkinje cell input only affected the FTN spike rate when the Purkinje cell input to the FTN model was synchronized. Moreover, in the presence of synchronized Purkinje cell input, an increase in the regularity of the Purkinje cell spiking resulted in larger temporal gaps in the inhibitory input to

their FTN model and in an increased spike rate of the FTN. These results predict that the increased irregularity in the Purkinje cell activity in DBN should lead to a decreased activity of the FTNs, rather than the increased activity that is found in experiments, and they are therefore also unable to explain the therapeutic effect of 4-AP.

The most biologically realistic and commonly used model of DBN is the tottering (*tg/tg*) mouse model (described in section 2.2.1).

2.2.2.2 4-AP Potassium channel blocker

It was shown that in *tg/tg* mice, whose Purkinje neurons display irregular firing due to impaired pacemaking activity because of the Cav2.1 mutation, ataxia and DBN attacks can be alleviated with the potassium channel (K_v) blocker 4-aminopyridine (4-AP) (Weisz et al., 2005). 4-AP is a nonselective blocker of voltage-gated potassium channels, the main function of which is to modulate excitability by opening and closing a selective pore to potassium in response to voltage. The flow of potassium ions gets interrupted by 4-AP, which blocks the potassium channel and prolongs repolarization. These was shown to increase Purkinje-cell (PC) excitability and enhance PC activity which were associated with the restoration of the inhibition provided by the cerebellar cortex to FTN with the result on vertical eye movements during DBN in experimental (Strupp et al., 2008; Kalla, 2004) and modelling studies (Glasauer, 2008).

However, in recent electrophysiological experiments it was shown that the therapeutic concentrations of 4-AP did not increase the spike rate of the Purkinje cells, but that they restored the regularity of their spiking, which is impaired in *tg/tg* mice (Alvina, Khodakhah, 2010). The human patients report significant improvement upon 4-AP administration (Kalla et al., 2004). Moreover, the human participants with confirmed CACNA1A heterozygous point mutation showed no further attacks after 4-AP treatment. When 4-AP administration was discontinued for 1 week EA2 attacks reoccurred. Resumption of 4-AP treatment resulted in no more attacks (Strupp et al., 2004). Therefore, the effects of 4-AP need to be researched further. In this thesis, the possible mechanism of the 4AP action on *tg/tg* mutants is explained (Chapter 4).

Also, 4-AP is reported to be successfully used in rodent modelling of seizures *in vitro* as a stable model able to produce prolonged seizure-like events which are distinct from the interictal intervals (Heuzeroth et al., 2019). 4-AP epilepsy model is showing a seizure's morphology and frequency stability for several hours together with low rate of spreading depolarizations. These advantageous features comes in contrast to other *in-vitro* models of epilepsy, such as high K⁺ and low Mg²⁺ models.

2.2.3 Absence epilepsy

Absence epilepsy is a non-convulsive form of epilepsy, sometimes referred as *petit mal*. Absence seizures are characterized by sudden onset, interruption of activity and stare and sudden termination. The patient is unable to recall the events which occurred during the seizure. Childhood absence epilepsy can be manifested as early as at the age of 2 years old. Absence seizures are recognised on the EEG as bilateral GSWDs at 3 Hz in humans (Destexhe et al, 1999). The mechanisms underlying GSWDs in absence seizures are obscure.

The attack does not last more than 10 seconds but can reoccur multiple times a day (up to 200), which significantly affects the quality of patient's life. About 20% of cases cannot be controlled by specific antiepileptic drugs.

2.2.3.1 Aetiology

The description of the absence epilepsy appeared in the medical literature as early as at the beginning of the 18th century (Tissot, 1783). However, its characteristic symptoms were already recognised by Poupart in 1705 (Temkin, 1971, Loiseau, 1992). Thalamus and cerebral cortex are commonly thought to be the brain structures involved in the GSWDs discharges. Over time, either thalamus or cerebral cortex were thought to have a leading role in the aetiology of absence epilepsy. From EEG studies the Steriade group experimentally demonstrated that cortical SWDs correspond to the bursting of reticular nucleus neurons after each cortical spike, which in turn drives the inhibitory postsynaptic currents in thalamocortical relay neurons (Steriade and Contreras, 1995). It was later experimentally shown that weak stimuli caused spindle oscillations, while strong input evoked synchronised GABA_B-mediated slow oscillations on the ferret thalamus, which slices were extracellularly stimulated to mimic the cortical input (Blumenfeld and McCormick, 2000; Bal et al., 2000).

It was suggested by pharmacological studies that GABA_B receptors play a key role in GSWD generation which showed that agonists of GABA_B receptors enhance seizures, while their antagonists alleviate them (Snead, 1992). In line with these findings, spindle oscillations have been transformed into slower 3 Hz oscillations in experimental conditions on the ferret thalamic slices (Huguenard and Prince, 1994), which was later replicated in the modelling study of the thalamic network (Destexhe and Sejnovski, 1995, Destexhe et al., 1996a). This study confirms the transformation of spindles into 3 Hz spike-and-wave oscillations by GABA_A receptors block in the cortex, but not in the thalamus. Slow 3 Hz frequency oscillations normally observed in humans (Destexhe 2008) and in model studies with stronger stimuli

(about 5 shocks per action potential), where 7 Hz oscillations are observed in rodents and in model studies (Destexhe 1998) with weak stimuli (1 shock per stimuli). After the suppression of GABAA-mediated inhibition Thalamic reticular neurons display bursting activity and elicit GABAB-mediated currents in thalamocortical neurons. This leads to synchronised inhibitory postsynaptic currents (Destexhe et al., 1996).

2.2.3.2 Neuromodulation

Direct stimulation of cerebellar surface disrupts thalamocortical oscillations

Neuromodulation is a relatively new therapy for various neurological diseases. The most established neuromodulation application is in the treatment of Parkinson's disease. It also found its application in the epileptic patients.

Both applications of neuromodulatory approach are already approved: extracranial and intracranial. Extracranial, vagus nerve stimulation, is conventional. Intracranial deep brain stimulation (DBS) is very promising.

The most common region for intracranial stimulation is the anterior thalamic nucleus, which is already established. Unfortunately, the effect is limited and not durable (10 % of recipients were seizure-free for more than 2 years and 16% for over 6 months). Overall for all patients seizure frequency decreased by 40 % after continuous application (Fisher et al., 2010).

Other regions have currently been researched in terms of the possibility of giving the higher percentage of complete seizures control and frequency reduction (Fschwind and Seeck, 2016).

Direct stimulation of thalamic nuclei and CN stimulation

Absence epilepsy is one of the various forms of the epileptic syndrome. The possible reason of absence epilepsy, the most common form of generalized epilepsy among children, is excessive cortical activity. By the means of electrocorticogram, it could be described as generalized spike-and-wave discharge (GSWD). Therefore excessive cortical activity leads to the potent bisynaptic inhibition through cortical axonal collaterals to the inhibitory reticular thalamic nucleus. This kind of excessive inhibition in thalamus may contribute to absence seizures, and also is commonly thought to be the cause of cortical oscillatory activity. Oscillatory cortical activity, on its turn, has the dual excitation-inhibition effect on thalamus. Thus, thalamocortical network oscillation occurs (Kros et al., 2015).

Based on the possible explanation of the absence epilepsy occurrence explained above, our collaborators from Erasmus MC, Rotterdam hypothesized that the different firing patterns of CN neuron should affect the GSWD occurrence. They pharmacologically affected CN firing patterns by gamma-aminobutyric acid (GABA)_A neuromodulators and also produced a closed-loop detection system for the on-demand optogenetic stimulation to stimulate CN-neurons. Both experimental approaches had different dynamics but lead to the converging deoscillating effect – termination of absence seizures. Pharmacological manipulations had slow but long-term effect, while optogenetic stimulation of CN neurons had fast but short-term effect. So the authors concluded that CN neuron firing can control the balance of excitation and inhibition in the thalamus and therefore modulate GSWDs occurrence. Moreover, a number of CN neurons were shown to be co-modulated with GSWDs. These neurons during the interictal periods had burst-like firing patterns with more irregular and frequent rates. Such a feature of GSWD-modulated CN neurons was utilised to predict whether their oscillation will be phase-locked to GSWDs during seizures. Also, it was shown that the effectiveness of the stimuli displays phase dependence on the spike-and-wave cycle. Thus, the GSWDs termination success rate as a result of the optogenetic stimulation of CN neuron depends on the phase of the thalamocortical oscillations and was lowest when the stimulus was applied before the peak of the spike. (Kros et al., 2015).

2.3 Chapter conclusions

In this chapter, the cerebellum and its structures are described in terms of their functions and contribution to the nervous system global circuit with particular focus on the cerebello-thalamo-cortical networks. Cerebellar nuclei neurons are described as the only cerebellar output providers. Cerebellum dysfunction may lead to certain pathologies, such as nystagmus

and absence epilepsy. In order to find the cures for these pathologies in laboratory conditions mutant rodents can be used. The commonly used animal model which is appropriate to imitate both absence epilepsy and nystagmus are the tottering mice mutants. The Purkinje neurons of the tottering mice show an irregular firing pattern due to the Cav2.1 mutation. It has been shown by various sources that non-selective voltage-gated potassium channel blocker 4-AP can alleviate this situation by restoring excitability of Purkinje cells. Nystagmus and absence epilepsy were described as pathologies originated from cerebellum dysfunction and their aetiology and possible treatment was discussed.

3

Methodology

3. Methodology

In this chapter the models used for the simulations of the two projects (downbeat nystagmus and absence epilepsy, respectively) will be discussed in detail: these models are the biophysical model of a neuron in the cerebellar nuclei (CN) and its depressing synapses, and the AdEx model for neurons in the neocortex and thalamus with their alpha-function synapses. Also, as the choice of the model for absence epilepsy simulations followed some research and model trials, some preliminary models will be also discussed in this chapter. Finally, the simulation packages used will be presented, along with the tools used for data processing.

3.1 Downbeat nystagmus model

To study the effect of the regularity of the spike times of a Purkinje cell (PC) on the activity of a neuron in the cerebellar nuclei (CN), a biologically detailed conductance-based multi-compartmental model of a single CN neuron was used. This model had been implemented in GENESIS by Steuber and Jaeger, and its dendritic morphology was derived from a rat CN neuron recorded by the same authors (Steuber et al. 2011). Subsequently, this model had been translated into NEURON by Johannes Luthman and provided with inhibitory synapses exhibit short-term depression (STD) (Luthman et al. 2011). The version of the CN NEURON model I used for my simulations is the one uploaded by Ovsepian et al. (2013) on the public ModelDB repository (senselab.med.yale.edu/ModelDB/ShowModel.cshtml?model=150024).

3.1.1 CN neuron model

The single-neuron model consists of 517 compartments and include a large soma (diameter 22 μm) and eight Hodgkin-Huxley-type ion channels: 1) fast and persistent sodium currents, 2-3) high and low-voltage-activated (HVA and LVA) calcium currents, 4) a tonic non-specific cation current that provides an inward current to allow spontaneous activity, 5) a purely calcium-gated potassium (SK) current, 6) a hyperpolarization-activated cyclic nucleotide gated (HCN) h-current, and a mixture of 7-8) fast and slow delayed-rectifier (Kdr) currents (Steuber et al. 2011). The intracellular concentration of free ionized calcium was modelled as a sub-membrane shell with calcium influx from the HVA current and an exponential decay with a time constant of 70 ms. To replicate *in vivo* conditions, the simulation temperature was set to 37 °C. The model neuron's spontaneous firing activity in the absence of synaptic input was at 26 Hz.

The CN neuron model (Steuber et al. 2011) was used to model a floccular target neuron (FTN). By the means of targeted intracellular recordings in brain slices, it was revealed that FTNs spontaneously fire at high rates with the mean firing rate of 47 Hz and exhibit dramatic

postinhibitory rebound firing after the offset of membrane hyperpolarisation. Such an intrinsic firing properties were exceptional among brainstem vestibular nucleus neurons but remarkably similar to neurons in the deep cerebellar nuclei (Sekirnjak et al, 2003). These justify the use of the CN neuron model (Steuber et al. 2011) as an FTN model. In tg/tg mice, greater irregularity of Purkinje cells was observed (Hoebeek et al, 2005), which leads to faster CN or FTN neurons firing (Luthman et al, 2015).

The synapses of the model are located in both the soma and the dendrites. One synaptic mechanism is added to the soma and 400 are randomly attached to the dendritic compartments, providing GABA-ergic synapses originating from Purkinje cells. AMPA, fast and slow NMDA channels are the components of the excitatory inputs to the DCN neurons, where one excitatory synapse is on the soma, and 100 are randomly allocated along the dendritic compartments.

Physiologically the number of synapses that reach the much larger soma is greater than the number of synapses that reach individual dendrites. This was modelled by providing input to the somatic synapses of the original DCN neuron model at a 50 times higher frequency than to the dendritic synapses. This results in soma receiving one-third of all excitatory and one-ninth of all inhibitory synaptic inputs of the DCN neuron model.

3.1.2 CN synapse models

The model CN neuron received two types of synaptic input: excitatory from 150 mossy fibres and inhibitory from 1 to 450 Purkinje cells (PCs). The most biologically plausible value for the convergence ratio (CR) of PCs to a single CN neuron is 90 (Person and Raman, 2011). Therefore, all my experiments were performed with three different CRs: 1, 90 and 450. Fifty of each type of synapses were put on the soma, the others onto randomly chosen dendritic compartments.

There is an assumption that the reason for the synaptic depression is a change in neurotransmitter release probability (R_n), which is described by the formula (Shin et al. 2007)

$$R_n = R_{n-1} + (R_{ss} - R_{n-1})(1 - \exp(-\frac{ISI_n}{\tau})), \quad (3.1)$$

where R_{n-1} is the release probability at the previous spike time (dimensionless);

ISI_n - the interspike interval between current and previous spike, ms;

R_{ss} - the release probability at steady state (dimensionless);

τ - the depression time constant in ms.

The latter two parameters are updated at the time of each spike n (Shin et al., 2007):

$$R_{ss}(r) = 0.08 + 0.60e^{-2.84r} + 0.32 e^{-0.02r} \quad (3.2)$$

$$\tau(r) = 2 + 2500e^{-0.274r} + 100 e^{-0.022r}, \quad (3.3)$$

where r is the instantaneous firing rate in Hz, computed as the inverse of the last ISI .

For values of tau significantly larger than ISI_n , the release probability of the current spike would be the same as the release probability of the previous spike. The value of tau(r) is adapted for every spike, not every millisecond. In such a conditions if the depression is ongoing, than there would be no recovery from it. Recovery from depression will be ongoing only in case when the term $\frac{-ISI_n}{t}$ is not close to 1.

Equations (3.1) and (3.2) can be fitted to the data (and example and the accuracy of this can be seen in Figure 1 of Shin et al., 2007).

To assess how sensitive the results are to the time constant of recovery from depression, the model was tested for different factor values of $\tau(r)$, formula 3.4:

$$\tau(r) = (2 + 2500e^{-0.274r} + 100e^{-0.022r}) * \text{factor} \quad (3.4)$$

The time course of recovery from depression $\tau(r)$ ranges widely, depending on the interspike intervals. $\tau(r)$ was computed for all values of r for different factors (Figure 3.1).

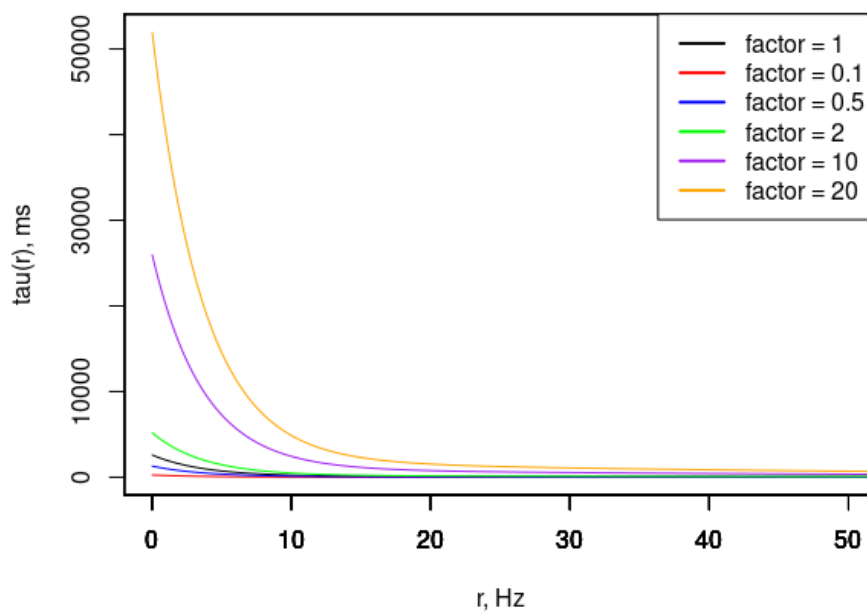


Figure 3.1 Recovery from depression $\tau(r)$ encountered in the PC-FTN simulations for different $\tau(r)$ scaling factors. $\tau(r)$ ranges from 2 to 2,595 ms. When $\tau(r)$ is increased with the factor of 20, it can reach 51,900 ms.

For the better understanding, the range of $\tau(r)$ values, they are shown in the Table 3.1.

Factor	1	0.1	0.5	10	20
Min r, Hz	0.01				
Max r, Hz	500				
Min $\tau(r)$, ms	2.002	0.200	1.001	20.017	40.033
Max $\tau(r)$, ms	2595.137	259.5137	1297.569	25951.37	51902.75
Min ISI, ms	2				
Max ISI, ms	100,000				

Table 3.1. The corresponding values of minimal and maximal $\tau(r)$.

As seen from Table 3.1, the values of $\tau(r)$ are several orders larger than the ISIs.

To assess how similar the $\tau(r)$ is to the ISI intervals, it was plotted against ISI, Figure 3.2.

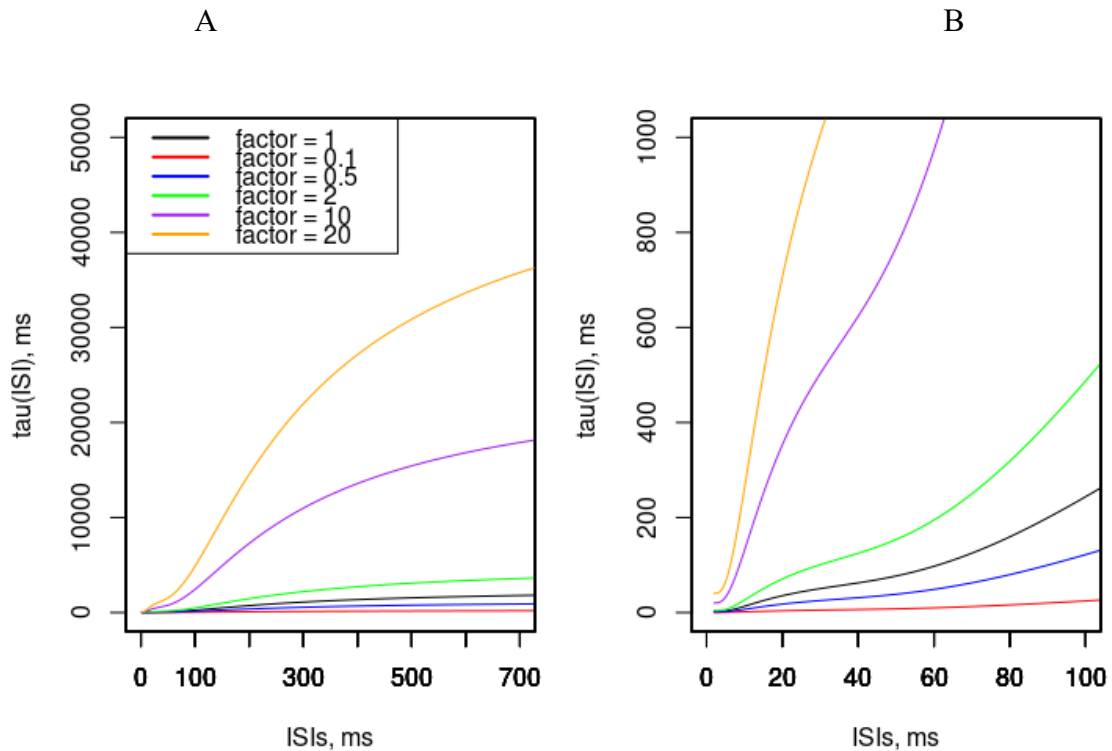


Figure 3.2 A: recovery from depression time constant depends on the ISIs. B: zoom in of A, showing physiological values of ISIs. For the factor 1, ISI of 20 ms would correspond to $\tau(r)$ of about 20ms, for the ISI of 100 ms the $\tau(\text{ISI})$ reaches 200 ms. With the increase of the $\tau(\text{ISI})$ factor, it rises dramatically.

The noise doesn't affect $\tau(r)$, so it would be the same for both regular and irregular PC spike trains.

All synapses were modelled as changes in double-exponential postsynaptic conductance Eq. (3.3) with rise and decay time constants as described in Steuber et al. (2011).

$$G_{syn}(t) = A \frac{g_{max}}{\tau_{decay} - \tau_{rise}} \left(\exp\left(-\frac{1}{\tau_{decay}}\right) - \exp\left(-\frac{t}{\tau_{rise}}\right) \right), \quad (3.5)$$

where A is the normalization constant needed to scale $G_{syn}(t)$ in a way that it reaches a maximum value of g_{max} ;

g_{max} is the maximum synaptic conductance (Luthman et al., 2011);

The GABAergic inhibitory synaptic current

$$I_{inh}(t) = G_{GABA}(t)(V - E_{GABA}), \quad (3.6)$$

where $\tau_{riseGABA} = 0.25$ ms (from Dieter Jaeger's code *cn6c_const_dj4.g*);

$\tau_{decayGABA} = 5.1$ ms (Telgkamp et al., 2004);

E_{GABA} - reversal potential which was between -70 and -90 mV.

The rise and decay time constants were chosen by (Steuber, 2011) to fit their experimental data.

For the other nondepressing synapses, the synaptic current comprises AMPA, fast NMDA and slow NMDA components:

$$I_{exc}(t) = (G_{AMPA}(t) + f_{fNMDA}(V)G_{fNMDA}(t) + f_{sNMDA}(V)G_{sNMDA}(t))(V - E_{exc}), \quad (3.7)$$

where $E_{exc} = 0$ is the excitatory reversal potential;

f_{fNMDA} and f_{sNMDA} factors describe the voltage dependence of the fast and slow NMDA conductances :

$$f(V) = \frac{1}{1 + P_1 \exp(-P_2 V)}, \quad (3.8)$$

where P_1 and P_2 were set to 0.002 and 0.109 for f_{fNMDA} and to 0.25 and 0.057 for f_{sNMDA} component. The parameters of NMDA inputs were set to match the data of Anchisi et al. (2001).

To estimate the plasticity effect of PC synapses on CN neurons I performed simulations with and without STD. The length of synaptic transmission delay *gabaTransDelay* was set to 2 ms.

3.1.3 PC-CN network model

In my simulations, the PC-CN circuit was not modelled explicitly, but instead, the CN neuron was provided with random synaptic input from synthetic PC spike trains. The spike trains were generated using a custom-made variant of NEURON's *NetStim* object (*GammaStim*, implemented by Johannes Luthman) to provide input to the CN neuron model. This generator allowed the irregularity of PC spike trains to be set from 0 to 1.

Since the DCN NEURON model was translated by J. Luthman from GENESIS, it was necessary to use some presynaptic mechanism to reproduce gamma-distributed input spike trains, because the NEURON built-in synaptic input generator, NetStim, generates Poisson-distributed input spike trains. Therefore, the corresponding code was translated to NEURON and added as a new mechanism, GammaStim. As NetStim, GammaStim generates a train of presynaptic stimuli and serves as the source for a NetCon. With the arrival of the positive weighted event in the on = 0 state, the simulator changes to the on = 1 state and goes through its burst sequence before changing back to on = 0 state. During that time it ignores any positive weight events. If the simulator receives a negative weight even in the on state, it receives a negative weight event and change to the off state. In the off state, it will ignore negative weight events. A change to the on state immediately causes the first spike (neuron.yale.edu).

Addition of noise randomises the first spike, so on average it occurs at $\text{start} + \text{noise} \cdot \text{interval}$, where start t0 is the start of the first spike in ms, interval is the interval between spikes in ms, and noise is the amount of randomness. Noise can be assigned with a value fraction from 0 to 1, which means that the ISI consists of a fixed interval of duration $t_0 = (1 - \text{noise}) \cdot \text{interval}$ and a variable interval. After NetStim generates an event, it is guaranteed to remain silent for at least t0 ms. Only when $t > t_0$ ms, the probability of generating another event become nonzero.

The output events were changed to follow the gamma distribution of order from 1 to 6 (parameter a in the formula 3.7). A gamma distribution of order 1 corresponds to the Poisson distribution originally modelled by NetStim. When the ISI distribution of a spike train is modelled with a gamma probability density function, the probability p of an ISI to be of length x ms can be computed as:

$$p(x) = \frac{1}{b^a \Gamma(a)} x^{(a-1)} e^{-\left(\frac{x}{b}\right)} \quad (3.9)$$

where a is the order parameter and b is the scale parameter. $\Gamma(a)$ is the gamma

function with order a and is calculated as:

$$\Gamma(a) = \int_0^{\infty} e^{-t} t^{a-1} dt, \quad (3.10)$$

Another change implemented by Johannes Luthman was the output length, which is now determined by duration in ms instead of the number of events. Also, a refractory period has been added.

Suppose there is a Poisson input spike train with spike times $\{t_1, t_2, t_3, t_4, t_5, t_6, \text{etc.}\}$, Then the interval distribution is a decaying exponential, which is equivalent to a first-order gamma distribution. If the selected spikes to generate a new spike train will be the spikes $\{t_1, t_3, t_5, \text{etc.}\}$, then the interval distribution of this new spike train will be a second-order gamma distribution. By selecting $\{t_1, t_4, t_7, \text{etc.}\}$ the third-order gamma distribution will be generated. In this way, Gamma order determines the CV of ISI distribution.

The degree of irregularity is measured using the coefficient of variation (CV), defined as the ratio of the standard deviation (SD) to the mean of the inter spike intervals (ISIs). A random Poisson process has a CV of one, i.e., the SD is equal to the mean, whereas an entirely regular spike train would have no variability and therefore a CV of zero. Control simulations were run to define the values of the irregularity (noise) parameter needed to obtain the experimental CVs measured by Alvina and Khodakhah (2010). Thus, a CV of 0.07 (typical of wild-type PCs) was obtained with an irregularity parameter of 0.138; whereas a CV of 0.18 (typical of PCs in the *tg/tg* mutant) was obtained with an irregularity index set to 0.354. The spike rates of inhibitory PC spike trains were set to 60 Hz, the excitatory spike trains represent input from mossy fibres were set to spike at 20 Hz.

The outputs of the simulation are presented as means over 92 seconds, from 1 to 93 seconds into the simulations. The first second was truncated in order to equilibrate simulations. In real neural systems the network will be running for essentially longer time. So, there is no need to reach an equilibrium stage. However, a computer simulation needs to start from some (arbitrary) but plausible initialization. So it needs some run time before a steady-state is achieved, which is the so-called the equilibration period. The set-up of simulation occurs in the first second of runtime. Initially the total runtime was 9 seconds, so one second could have a big impact on the whole result if it is just 9 seconds long. In the process of my work, it was necessary to increase the runtime to make the graphs smoother. And in this case one second out of 93 has no impact on the resulting data. It is good practise to make an equilibration.

3.2 Absence epilepsy model

3.2.1 Choosing the network model

At the beginning of the project, there was a final goal in mind, to be able to model the thalamocortical network and be able to research the mechanisms behind GSWD termination. I therefore first searched the literature for candidate circuit models.

3.2.1.1 A single column thalamocortical network model (Traub et al., 2005)

The first model of possible choice was a single-column thalamocortical network model (Traub et al., 2005). This is a biologically detailed network model with 3,560 multicompartment neurons (Figure 3.3), designed to show the network behaviour of neuronal ensembles. Apart from chemical synapses, gap junctions were modelled for fast synaptic responses.

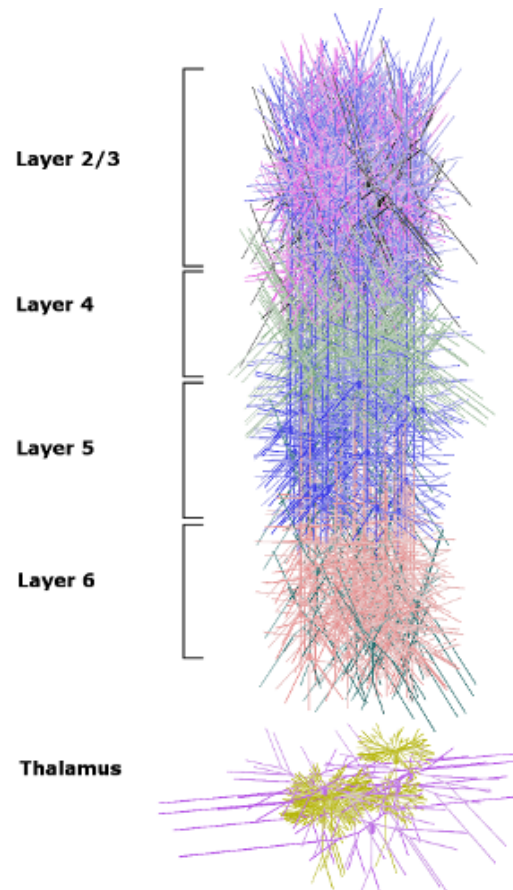


Figure 3.3. The single-column thalamocortical network model of cortex and thalamus (Source: Traub et al., 2005)

After some trials and discussion the choice was not in favour of Traub's model due to its unnecessary big (for the purpose) cortical column and excessive complexity.

3.2.1.2 Birdno model

During the discussion with one of the collaborators I was advised to pay attention to the model designed by Grill's research group (Figure 3.4) (Birdno et al., 2011).

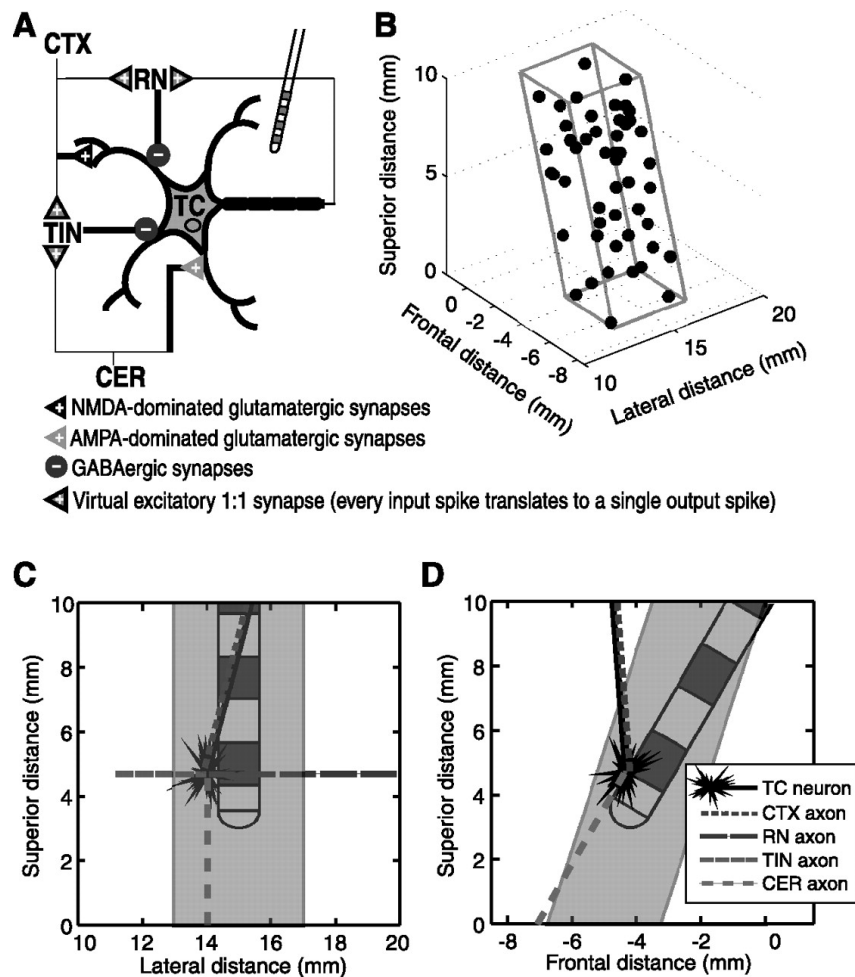


Figure 3.4 Computational model designed to simulate the response of thalamic neurons to DBS.

A. Thalamocortical (TC) neuron with terminating axons.

B. 3D prism representation of 50 somas of ventral intermediate thalamus (VIM).

C, D. VIM thalamus with DBS electrode, drawn under different angle. Source: (Birdno et al., 2011)

The model required some changes regarding peculiar anatomical properties of human thalamus. The experimental results obtained by our collaborators were made on laboratory rodents, therefore I aimed to model rodent anatomical network. Rodents have no ventral intermediate (VIM) nucleus of thalamus, and our model aimed to represent rodent anatomy. Also, the main reason to continue with model search was that the article describing Birdno's

model has invalid link to the source and the model was not published on the *ModelDB* (<https://senselab.med.yale.edu/modeldb/searchFulltext.cshtml?g=birdno+et+al+2011>) and it was impossible to find the source files, as for most of the models.

3.2.1.3 Thalamocortical and thalamic reticular network (Destexhe et al., 1996)

The next model of possible choice was Alain Destexhe's single-compartmental-neuron network model aimed to simulate different types of oscillations between interconnected thalamocortical (TC) and thalamic reticular (RE) cells (Figure 3.5) (Destexhe et al., 1996).

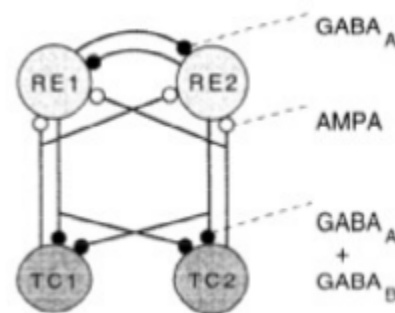


Figure 3.5 Diagram of interconnected thalamocortical (TC) and thalamic reticular (RE) cells. Open circles represent excitatory α -amino-3-hydroxy-5-methyl-4-isoxazolepropionic acid (AMPA) mediated synaptic connections; dark grey circles – inhibitory GABA-ergic synapses. RE and TC represent inhibitory and excitatory neurons respectively. (Source: Destexhe, 2009).

This model might be the model of choice due to the optimal level of complexity and ability to simulate oscillatory behaviour of neurons. Some changes were required. The first was to change the code in order not to use NEURON graphical interface for plotting and for storing the output to file. Those changes were successfully implemented. The second correction was to provide the synaptic input to the model. At this stage I temporarily stopped working on the model in order to continue after the computation neuroscience CNS 2016 conference. At CNS after conversation with the author of this model, Alain Destexhe, another model was selected upon his advice – a network of adaptive exponential integrate-and-fire (AdEx) neurons (Destexhe, 2009; Brette, Gerstner, 2005). This model is based on features of the exponential integrate-and-fire model (Fourcaud et al, 2003) and the 2-variable model of Izhikevich (Izhikevich, 2003).

3.2.2 Epilepsy model: single-neuron AdEx model

The leaky integrate-and-fire (LIF) model is the oldest of the simplified models that show spiking behaviour and described with two coupled non-linear differential equations. To model the patch of the membrane with the spike generation and rest mechanism as a switch, the RC representation of the neurons is used (3.11):

$$C_m \frac{dV}{dt} = -\frac{V-E_m}{R_m} + I, \quad (3.11)$$

where C_m is the membrane capacitance;

R_m is the membrane resistance;

I is the total injected current flowing into the cell.

Time-constant representations could also be used:

$$\tau_m \frac{dV}{dt} = -V + E_m + R_m I, \quad (3.12)$$

where $\tau_m = R_m C_m$.

There are different modifications of the model developed by adding some components in order to make the model more biologically plausible at the level of channel dynamics.

One of the various subtypes of integrate-and-fire models is the quadratic LIF neuron model, which models the ionic current close to the threshold better than the linear LIF model (Hansel and Mato, 2000; Latham et al., 2000). For the LIF model to be able to produce a wide range of realistic behaviours a recovery variable w was added to the quadratic LIF model by Izhikevich (Izhikevich, 2003; Izhikevich and Edelman, 2008):

$$\begin{aligned} \frac{dV}{dt} &= k(V-E_m)(V-V_{thresh}) - w + I \\ \frac{dw}{dt} &= a(b(V-E_m) - w) \end{aligned} \quad (3.13)$$

if $V \geq 30mV$, then $\begin{cases} V \text{ is reset to } c \\ w \text{ is reset to } u + d \end{cases}$

where w is the recovery variable, meant to track the difference between all inward and outward voltage-gated currents;

k , a , b , c , and d are the model parameters (Sterratt et al., 2011).

The adaptive exponential integrate-and-fire model (AdEx) model was first described by Brette-Gerstner (Brette, Gerstner, 2005) and derived from the two-variable LIF model by Izhikevich (Izhikevich, 2004) and exponential LIF model by Fourcad-Trocme (Fourcaud-Trocme et al., 2003). Brette and Gerstner combined the integrate-and-fire (IF) model by Izhikevich (2004) with exponential nonlinearity, which describes the process of spike generation and the upswing of the action potential. The model is able to produce adaptation, bursts, delayed spike initiation, fast spiking, regular spiking etc, same as LIF, but its performance in the spike trains prediction in the model is 96% on average (coincidence factor was 0.96) with 2-ms precision, while LIF model with adaptation predicted only 88% of spikes (Brette, Gerstner, 2005). The model consists of differential equations system (linked):

$$C_m \frac{dV}{dT} = -g_L (V - E_L) + g_L \Delta e^{(V - V_T)/\Delta} - \frac{w}{S} \quad (3.14)$$

$$\frac{dw}{dt} = \frac{1}{\tau_w} [a (V - E_L) - w],$$

where C_m - the specific membrane capacitance;

g_L - resting (leak) conductance;

E_L - the resting potential (which is also equal to the reset value after a spike);

Δ - the steepness of the exponential approach to threshold;

V_T - the spike threshold;

w - adaptation variable;

S - the membrane area;

τ_w - adaptation time constant;

a - dynamics of adaptation;

b - strength of adaptation, which is the amount that w is incremented by after each spike (Destexhe, 2009).

The point neurons in this model display complex intrinsic properties, depending on their parameters as a response to 0.25 nA depolarising or - 0.25 nA hyperpolarising stimulus. To confirm the validity of the model I have started from replication of the individual neuron's properties (Destexhe 2009, Figure 1) in Chapter 5.

I have listed parameters of the single neuron given in the paper (Table 3.1) and applied them to the single-neuron model I developed, as there was no code for it available online.

Parameter description	Parameter notation	Value	Unit
Membrane time constant	tau_m	20.0	ms
Duration of refractory period	tau_refrac	2.6	ms
Resting membrane potential (Leak reversal potential)	v_rest	- 60 (thalamic neurons)	mV
		- 70 (cortical neurons) *	
Reset value for membrane potential after a spike	v_reset	- 60	mV
Spike initiation threshold	v_thresh	- 50	mV
Slope factor	delta_T	2.5	mV
Adaptation time constant	tau_w	600	ms
Capacity of the membrane	cm	0.200	nF
Dynamics of adaptation	a	Depends on the neuron type **	nS *** (Nest)
Strength of adaptation	b	Depends on the neuron type **	nA

*The difference in the value of the resting membrane potential for the cortical neurons is not described in the article (Destexhe 2009). In the description to the Figure 1 (Destexhe 2009) it is written that the resting potential is -60 mV in all cases. Nevertheless, this difference (-60 mV and -70 mV) is clear from the Destexhe 2009, Figure 1. Also, the close replication is impossible if the resting potential of all cortical neurons is not set to -70 mV.

For ** see Table 3.3

For *** the explanation about units difference of dynamics of adaptation parameter *a* in between of Nest and NEURON see Table 5.2 in paragraph 5.2.4 Clarifying Adaptation Units.

Table 3.3 Parameters, their description, notation, value and units used in Single Neuron Model.

Neuron type	Units	RS with strong adaptation	RS with weak adaptation	FS	LTS	TC	RE	RE**
a	nS * (Nest)	1	1	1	20	40	30	80
b	nA	0.04	0.005	0	0	0	0.08	0.03

* for the explanation about units difference of dynamics of adaptation parameter a between Nest and NEURON see Table 5.2 in paragraph 5.2.4 Clarifying Adaptation Units.

Table 3.3 Dynamics and strength of adaptation values for different neuron types.

3.2.3 Epilepsy model: synapse model (exponential, alpha-function)

In a first phase, the thalamocortical model neurons were modelled as exponential integrate-and-fire neurons with spike-triggered and sub-threshold adaptation currents and exponential synaptic conductances – *EIF_cond_exp_isfa_ista*. With this model configuration I aimed to achieve such behaviour pattern of thalamocortical model as spike-and-wave discharges, where “spike” is associated with the synchronous firing of all cortical neurons. Such a firing activates GABA_B-mediated K⁺ currents, and hyperpolarization in pyramidal neurons. This stops the discharges and generates a positive slow "wave" (Steriade, 1974; A.Destexhe, 1999). Unfortunately, the model behaviour showed spikes only, with no waves. In order to enable the model to produce the “wave” component of GSWDs I needed to implement the mechanism responsible for the slow inhibition. In the model, only GABA_A-mediated fast inhibition was incorporated, with only fast exponentially decaying inhibition possible. In order to be able to model the effect of GABA_B, the synaptic mechanism in the model was changed for *EIF_cond_alpha_isfa_ista*, where the synaptic conductance change is described by a gamma function commonly known as “alpha function”, introduced by Rall (1967) (Formula 3.15). The alpha function is a good tool to implement synapses with a slow component such as GABA_BR-mediated synapses, because an alpha-function with a time-constant of 15 ms reaches its peak conductance also after 15 ms. The total inhibition of the alpha synapse (its integral over time) scales with the square of tau.

$$g(t) = \sum_{i=1}^k \frac{(t-t_i)}{\tau} \exp \left[\frac{-(t-t_i)}{\tau} \right], \quad (3.15)$$

where t is the current time;

t_i is the time of i -th spike in the presynaptic neuron;

τ – time constant of the synapse.

The GSWDs associated with absence epilepsy can be of different frequency, dependent on the animal model, where they are observed. Thus, in cats they are of 3 Hz frequency (Gloor & Fariello, 1988) and 5-10 Hz in rodents. As here the attempts are made in order to replicate and explain the experimental results obtained in mice, the target frequency of GSWD would be around 7 Hz, and this could be achieved by the increase in the inhibitory time constant τ from its default value of 5 ms to 15 ms.

3.2.4 Network model for absence epilepsy

The network model is the general case of the single neuron model, extended for some number of neurons, with added terms for synaptic interactions. It is represented by the formula (3.16):

$$\begin{aligned} C_m dV_i / dt &= -g_L (V_i - E_L) + g_L \Delta_i \exp [(V - V_{Ti}) / \Delta_i] - w_i / S - \sum_j g_{ij} (V_i - E_j) \\ dw_i / dt &= (1 / \tau_{wi}) [a_i (V_i - E_L) - w_i], \end{aligned} \quad (3.16)$$

where V_i is the membrane potential of neuron i . All other parameters are listed in the equation below. Indexing shows variation of neuron type.

The term $\sum_j g_{ij} (V_i - E_j)$ indicates synaptic inputs, where g_{ji} is the conductance of the synapse of type j onto neuron i and E_j is the reversal potential for synapses of type j .

Excitatory and inhibitory peak conductance values were used as in the paper (Destexhe et al., 2009), 6 and 67 nS respectively.

In Destexhe (2009) several network configurations are described. They are:

- Cortical single-layer
- Thalamic single-layer
- Two-layer cortical: 2000 neurons in cortical layer A and 500 neurons in cortical layer B (see Figure 3.6)
- Thalamocortical: 2000 neurons in cortical layer and 200 neurons in thalamic neurons

(see Figure 3.7).

95% of the pyramidal (PY) cells were regular spiking (RS), and 5% were low-threshold spiking (LTS). Interneurons (IN) were of fast spiking (FS) type. The interlayer connection was only excitatory, with a connection probability of 1%.

The main difference of thalamic layer B is the replacement of 500 cortical neurons with 200 thalamic neurons and the absence of connections between excitatory cells.

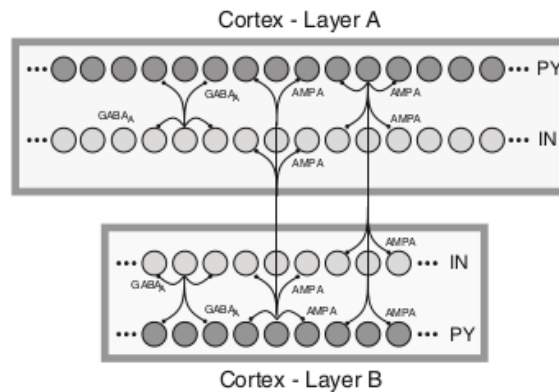


Figure 3.6 Schematically represented 2-layer cortical network model architecture of 2500 neurons, 80% of which are excitatory and 20% are inhibitory. The model consists of 2 layers. Each layer consists of interconnected cortical inhibitory interneurons (IN) and cortical excitatory neurons (PY). There are 10% of low-threshold spiking (LTS) neurons in layer B. (Source: Destexhe 2009).

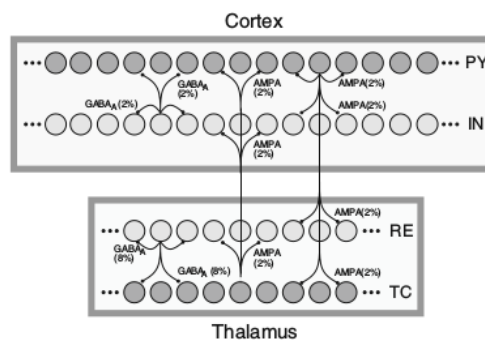


Figure 3.7 Schematically represented thalamocortical model of 2200 interconnected neurons, organised into 2 layers. Layer A: same as in 2-layer cortical model. Layer B: 200 TC and RE cells, 1:1. TC neurons are not interconnected. (Source: Destexhe 2009).

LTS cells are present in amount of 10% for 2-layer cortical model, but it is not mentioned in the article (Destexhe et al., 2009) about their presence in thalamocortical configuration. I

referred to the literature to find out about the presence / absence of LTS cells in thalamus. It was shown, that one of the response type of thalamic relay cells is bursting activity, when the neuron hyperpolarised. During this hyperpolarization neurons typically respond with LTS. Different neurodegenerative disorders are associated with LTS bursting activity in thalamus, including absence epilepsy (Jeanmond and Morel, 1996). Therefore, I decided to leave LTS cells in thalamocortical model as it is in two-layer cortex.

3.3 Simulation software

All simulations were performed with the NEURON simulation software (Hines and Carnevale, 1997), PyNN (Davison et al., 2008) and NEST (Peyser et al., 2017).

3.3.1 NEURON

NEURON is a neural simulation tool designed to model single neurons as well as neuronal networks (Hines and Carnevale, 2001). It can be used either to deal with the complex biologically realistic models with detailed membrane properties or with the large-scale networks where the individual morphology is neglected to reduce the computational cost (like AdEx). Though, it is most computationally effective for the parts of single cell or small networks (Hines and Carnevale, 1997). The default integrator used by NEURON is the backward Euler method, which is suitable to provide the user with good qualitative results even with considerable time step. It is proved to be numerically stable. There is an option to change to the Crank-Nicolson integration method, which is the combination of both backward and forward Euler, where the numerical error is proportional to the square of the time step size.

NEURON is written in two languages, the interpreted (hoc) and compiled (mod). The interpreter is written in hoc, a floating-point calculator (Keringhan and Pike 1984) with added object-oriented syntax. It can be used for example to execute simulations or update parameters. The compiled model description language (NMODL) is used in NEURON to customise and expand the library of biophysical mechanisms for particular models (Hines and Carnevale, 2000).

3.3.1.1 P. Gleeson's implementation (the reason for a change from NEURON to Nest)

Padraig Gleeson raised the issue about the fact that when the alpha function is used instead of the exponential, it produces different results when run on NEURON (<https://github.com/NeuralEnsemble/PyNN/issues/559>).

Apparently, NEURON is very sensitive to the time step when using the alpha function, which is not the case for Nest and Brian simulators.

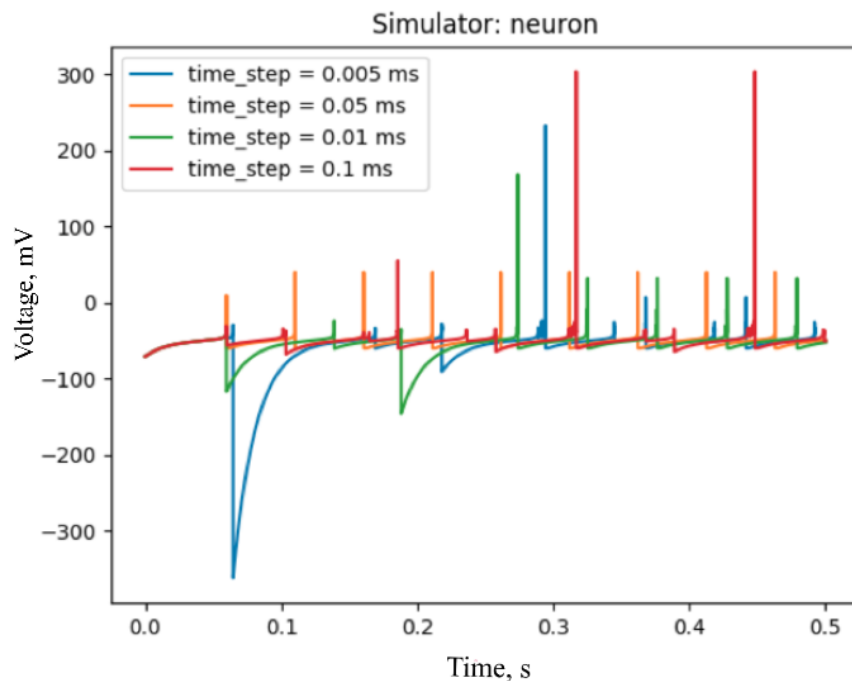


Figure 3.8 is taken from github *NeuralEnsemble* issue #559, reproduced by Appukuttan-Shailesh (<https://github.com/NeuralEnsemble/PyNN/issues/559>). Time is plotted on the horizontal axis in s, and voltage is plotted on the vertical axis in mV. The figure shows NEURON time-step dependency. For each time-step the voltage traces are different, while they should be exactly the same.

The issue #559 was closed as it duplicates another issue risen earlier, #266. Andrew Davison had some suggestions on the possible ways to solve this issue, like checking the .mod file where the AdExp mechanisms for NEURON is implemented. Thus, the issue #266 was opened on the 23 October 2013, and was still not solved on the 13-th of June 2019.

To consider the current issues with the NEURON numeric integration time-step, the decision to use PyNN with NEST, rather than PyNN with NEURON was made.

3.3.2 PyNN

PyNN is an open-source software package (<http://neuralensemble.org/PyNN>). It is a common application programming interface (API) for various simulators (NEURON, NEST, PCSIM, Brian and the Heidelberg VLSI neuromorphic hardware). It allows building neuronal network models, using the Python language once and running it on any of the above-mentioned simulators without modifications (Davison et al., 2009). PyNN provides a library of standardized synapse and neuron models, as well as connectivity algorithms. In order to be able to run the model written in PyNN on different simulators it is required to use standard cell models (single-compartment or point neuron models). The only simulator for multi-compartmental models supported with PyNN is NEURON.

For the thalamocortical network simulations the *EIF_cond_exp_isfa_ista* neuron model was used initially. This is the conductance-based exponential integrate-and-fire (IF) neuron with a spike triggered and sub-threshold adaptation currents (Brette and Gerstner, 2005). Later it was replaced with the alpha function model *EIF_cond_alpha_isfa_ista*.

3.3.2.1 Neo object model

The recording is done from many channels, which makes the datasets very large. Therefore, computation-efficient handling of data method is required. For this purposes, Neo package is utilised by PyNN as a data model to provide the common format for output data.

When the simulation is finished, the `get-data ()` method returns a *NeoBlock* object. This object serves as a top-level data container which contains *Segments* with data objects inside (Garcia et al., 2014).

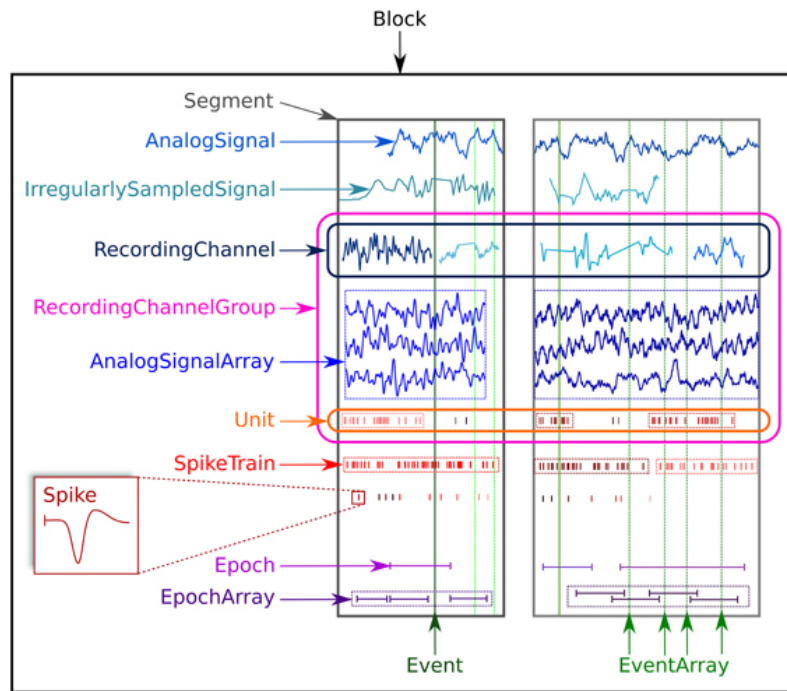


Figure 3.9 Neo data type containers: data objects, container objects and grouping objects (Garcia et al., 2014).

Container objects are implemented in Neo as hierarchical groups of data. Neo data objects contain numerical data and concomitant metadata (for example units). In a *Block* the *Segments* group together any data object types with a common recording time (http://neuralensemble.org/docs/PyNN/data_handling.html). The data objects were used here are described below. *AnalogSignals* (recorded membrane potential in this case) and *SpikeTrains* (array of spikes) are stored within Segments. These data objects can be further recorded (with `record()` method) and stored, processed and analysed same as any neurophysiological data.

3.3.3 NEST

NEST is a one of the most commonly used simulators of the Human Brain Project (R. A. Tikidji-Namburyan et al., 2017) and was designed to model large networks of point spiking neurons or neurons with small numbers of compartments (<http://www.nest-initiative.org>).

Nest is written in C++ and it has a user interface PyNEST which allows to use Python as simulation language for network description, but not for individual neurons (Eppler et al., 2009).

3.4 Data analysis tools

In the project, data analysis is conceptually separated from data acquisition, as it is easier to write a robust lightweight analysis code if it is focused on analysis only. For this reason, MATLAB r2015a (The MathWorks) was used to analyse the output of the DCN model, and R (R Development Core Team, 2008) was used to analyse the thalamocortical model output..

3.5 Chapter conclusions

Since the thesis addresses cerebellar pathologies, we built detailed models to explore the mechanisms underlining downbeat nystagmus and absence epilepsy. Two different models were used to solve them, each with a suitable level of complexity and details: a single-neuron conductance-based multicompartmental model of a FTN neuron with incoming synapses from Purkinje cells, and a thalamocortical network model with AdEx point neurons, where intracellular morphology is neglected. Both models were implemented in NEURON, but the epilepsy model was later translated into PyNN (and run using NEST) to avoid some issues, including time step sensitivity.

4

Modelling Downbeat Nystagmus

This chapter starts with a brief introductory description of the two models which aimed to explain the alleviating effect of 4-aminopyridine (4-AP) on DBN. Afterwards, the role of cerebellar short-term synaptic plasticity in the pathology and medication of downbeat nystagmus is shown. Short-Term Depression is the lacking component of the previously considered models. The conducted research aimed to investigate the role of short-term synaptic plasticity (hundreds to thousands of milliseconds) in the pathology and medication of downbeat nystagmus. This was done using the morphologically-realistic conductance-based model of a cerebellar nucleus neuron as a floccular target neuron. The parameter choice for Purkinje cell input is explained here. The influence of irregularity/regularity, asynchrony/synchrony, STD and a potassium channel blocker 4-AP as a remedy for DBN in a mouse model of episodic ataxia (mutation of P/Q Ca^{2+} channels) will be discussed.

4.1 Experiment 1: Modelling downbeat nystagmus

Reviewing the literature about Potassium channel blocker 4-aminopyridine (4-AP), I have found one model study (Glasauer and Rossert, 2008) which was able to partially explain the beneficial effect of 4-AP on DBN found experimentally (Kalla et al., 2007). Based on two previous models, a multicompartmental model of a Purkinje cell (PC) (Miyasho et al., 2001) and a system-level model of ocular movements (Marti et al., 2005) they were able to show that 4-AP improves a gaze-dependent component of DBN but the effect was less prominent than in experimental studies. These results are only partially in line with the experimental studies, where 4-AP significantly improved a gaze-dependent component of DBN but had less effect on the spontaneous drift.

To achieve these results, Glasauer and Rossert (2008) modelled cerebellar degeneration as a decrease in Ca^{2+} P-type channels (CaP) conductance to 80%, which lead to a decrease in average firing rate in response to Poisson-distributed spike trains and delay in response onset, mimicking the mutation in a gene encoding $\alpha_{12.1}$ subunit. The effect of low concentrations of 4-AP was modelled by lowering the conductance of low-threshold potassium channels – D-type potassium channels (ID) to 60%, which had no effect on firing rate. The effect of low concentrations (1-10 μM) of 4-AP on guinea pig PCs shortened slowly depolarizing potential. This, in turn, reduced the latency of Ca^{2+} spikes in response to intracellular current pulse (Etzion and Grossman, 2001). Eventually, Glasauer and Rossert (2008) modelled the effect of DBN and 4-AP all together by reducing CaP and ID conductances at the same time (Figure 4.1). Eventually, by superimposing the single Purkinje cell's (PC's) response of 2000 neurons

they constructed a population response, which served as an input to the system-level model (Marti et al., 2005) (Figure 4.2).

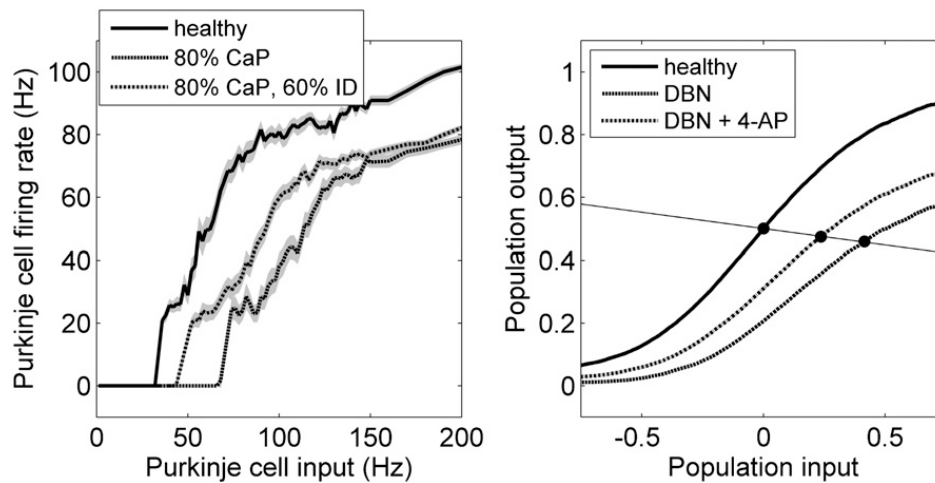


Figure 4.1. Comparison of the simulated single neuron (multicompartmental model, left) and population response (right) constructed from single-neuron responses, which served as the input to the system-level model. Left: The lines show the average firing rate in response to Poisson-distributed spike trains with varying mean frequency. Grey areas are defining the 95% confidence intervals. Right: black dots - activation functions. Their intersections with the solid line give fixed points of the systems model for gaze-independent component. The x-coordinate of the fixed points is proportional to the nystagmus slow phase velocity in gaze-straight ahead. The slope of the activation function determines the overall integrator time constant. Source: (Glasauer and Rossert 2008).

The authors were unable to explain completely the beneficial effect on 4-AP in DBN treatment. They speculate that 4-AP apart from its beneficial effect on single PCs might have some positive effects on the population level. They conclude that additional simulations are needed to explain the difference between experimental and modelling results.

Later, inspired by new experimental results which showed that 4-AP has no effect on PC firing rate, but rather restore their regularity (Alvina and Khodakhah, 2010), they conducted another modelling study using a mathematical model of the ocular motor and cerebellar circuitry (Glasauer et al., 2011). The aim was to investigate the potential effect of changing the regularity of cerebellar PCs on their target neurons in the vestibular nuclei in a modelling study in health and during episodic ataxia type 2 (EA2). To reach this aim, the authors asked how synchronized regular firing effects a realistic number of PCs and as a consequence a potential target neuron in vestibular nuclei. Synchronization of spikes from several excitatory neurons

may lead to the spiking of the postsynaptic neuron due to summation of the excitatory postsynaptic potentials (EPSPs). However, this is clearly not the case for inhibitory input, since the summation of inhibitory postsynaptic potentials (IPSPs) normally does not evoke an action potential.

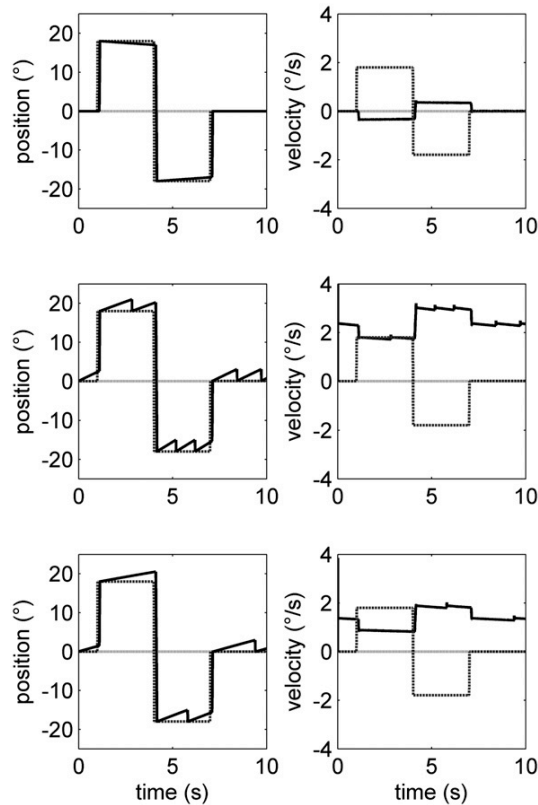


Figure 4.2. Simulation of two DBN components: vertical saccades and gaze holding by the means of activation function (shown at the Figure 4.1, right as a block dots) corresponding to a healthy (upper row), DBN (middle row) and DBN together with applied 4-AP cases. Left column: target position is shown as a grey dashed line, and eye position – as a black line. Right column: phase eye velocity – black solid, target position – grey dashed lines. The gaze-independent nystagmus significantly decreases, while gaze-evoked component is almost unchanged. Source: (Glasauer and Rossert 2008).

	Synchronous regular		Synchronous irregular		Asynchronous
CV	0.07 wild	0.18 tg/tg	0.07 wild	0.18 tg/tg	Synchronous trains randomly shifted in time between 0 and 1/F
ν	70 Hz		70 Hz		
g_{pace}	25.2 nS		25.2 nS		
g_{e0}	30.2 nS		31.6 nS		
σ_e	3.12 nS		7.30 nS		

Table 4.1 Summary of the data being used by (Glasauer et al., 2011). CV – the mean coefficient of variation, g_{pace} – pacemaker cell conductance, g_{e0} – PC conductance, σ_e – noise standard deviation, F – the mean PC output frequency.

200 integrate-and-fire PCs were modelled together with one additional pacemaker PC connected using inhibitory alpha synapses to synchronise other neurons, driven by constant excitatory input. They generated regular firing patterns as in wildtype mice (CV = 0.07) and irregular firing patterns as in tg/tg mice (CV = 0.18). The coefficient of variation (CV) of interspike interval (ISI) is the measurement of regularity. It calculates as ratio of the standard deviation to the mean inter-spike intervals (ISI) (CV = σ /mean ISI). The case when the standard deviation is equal to the mean ISI describes the completely irregular process with CV = 1, while CV = 0 describes a completely regular process. CV values were taken from the experimental study (Alvina and Khodakhah, 2010) and summarised in Table 4.1. According to their initial assumption about the joint effect of regularity and synchrony, they simulated 4 inhibitory input configurations: irregular synchronised, regular synchronised, irregular unsynchronised and regular unsynchronised (Figure 4.3).

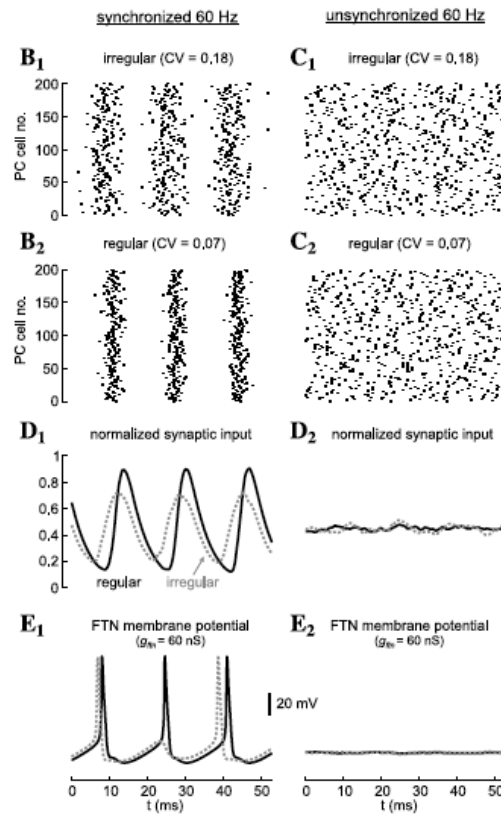


Figure 4.3. Simulated effects of regularity on synchronised and unsynchronised inhibition. B: Raster plot of 200 synchronised integrate-and-fire (I&F) PCs with regular (CV = 0.07 (B1)) and irregular ((B2) CV = 0.18) spike times. C: Raster plot of 200 unsynchronised PCs, but the response of each neuron is randomly shifted to create unsynchronised responses with irregular (C1) and regular spike times. The CV values are the same as in B. D: Normalised synaptic input generated from synchronised and unsynchronised spike trains (as in B) with regular (black solid) and irregular (grey dashed lines) spike times. E: Membrane potential response of floccular target neuron (FTN) as a result of synchronised (E1) and unsynchronised (E2) synaptic inhibitions using the input shown in D with regular (solid black) and irregular (dashed grey lines) spike times. Source: (Glasauer et al., 2011).

As a result, synchronised PCs with regular firing (Figure 4.3 B2) showed higher overall synchrony than with irregular firing (Figure 4.3 B1), which resulted in higher conductance (Figure 4.3 D1). When the synchrony was removed from generated spike trains (Figure 4.3 C1 and C2), the effect on regularity was also annihilated (Figure 4.3 D2). Interestingly, the synaptic strength and thus the mean synaptic inhibition remained the same in all four cases, but synchronised regular inhibition led to high spiking activity, which resulted in less effective

inhibition on the output. Note, one spike is missing in regular synchronised configuration (Figure 4.3 E1, dashed grey line). Therefore, in the presence of synchronized Purkinje cell input, the regularity of the Purkinje cell spiking resulted in larger temporal gaps in the inhibitory input to their floccular target neuron (FTN) model and an increased spike rate of the FTN. These results predict that the increased irregularity in the Purkinje cell activity in DBN should lead to a decreased activity of the FTNs, rather than the increased activity that is found in experiments. Therefore, these results were unable to explain the therapeutic effect of 4-AP.

Importantly, the model by Glasauer and colleagues does not take short-term depression (STD) at the synapses between Purkinje cells and FTNs into account. We hypothesized that this absence of STD could explain the apparent contradiction between the experimental (Alvina and Khodakhah, 2010) and computational (Glasauer et al., 2011) results. Our assumption was based on previous results obtained by our research group (Luthman et al., 2011), showing that FTN neuron firing rate acceleration with input irregularity depends on STD (Figure 4.4). In the absence of STD, the irregularity dependent increase in firing rate disappears. The STD effect on the FTN firing rate is largest when PC firing is completely irregular.

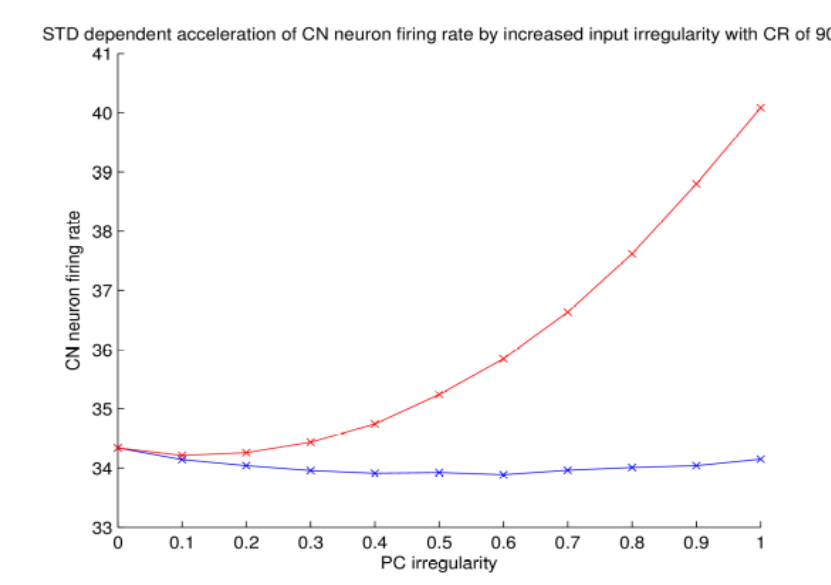


Figure 4.4 Change of the model CN neuron as FTN model firing rate in response to different degree of irregularity in the presence (red curve) or absence (blue line) of synaptic depression at the PC – FTN synapse. Reproduced from (Luthman et al., 2011).

To simulate the effect of irregular versus regular Purkinje cell input in the presence or absence of STD in the pathology and 4-AP treatment of DBN, I used a morphologically realistic conductance-based model of a cerebellar nucleus neuron (Steuber et al., 2011; Luthman et al.,

2011) as an FTN model to simulate the effect of irregular versus regular Purkinje cell input (Figure 4.5).

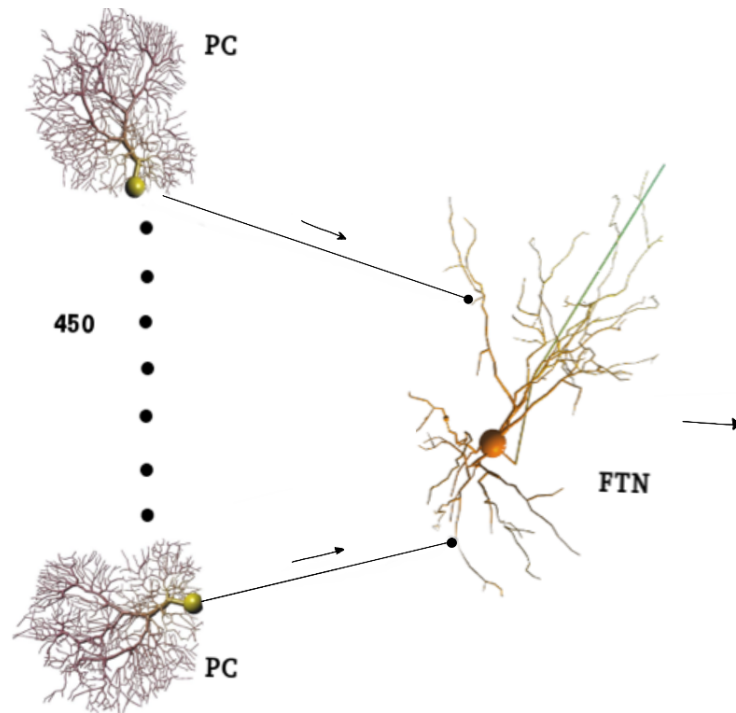


Figure 4.5 Diagram representing the structure of the morphologically realistic conductance-based model of a CN neuron as an FTN model. It is constructed of 450 PC which can fire with different degrees of synchronicity (0 - 450). PCs are connected by double-exponential synapses with CN neuron – the model of FTN, where the input irregularity converts to the output firing rate. The input provided at 60 Hz with regularity presented via CV of 0.34 and 0.66 for the regular wild-type and irregular *tg/tg* input respectively and in the presence and absence of STD at the Purkinje cell – FTN synapses.

To run the simulation in NEURON, the CV values should be transformed to a degree of regularity or “noise”. By default in the current model, Gamma order, which is the order parameter in (Formula 3.10), was set to 3 and all simulations were performed with this setting. Gamma order could be varied from 1 to 6, with 1 for pure Poisson process generated by *NetStim.mod*.

The transformation from CV to noise was performed with the help of Figure 4.6, green line. This gave us the satisfactory results, as the noise calculated from the CV values taken from (Alvina et al., 2010) (0.07 and 0.18) is 0.138 and 0.354, which is in the reasonable range (0 – 1).

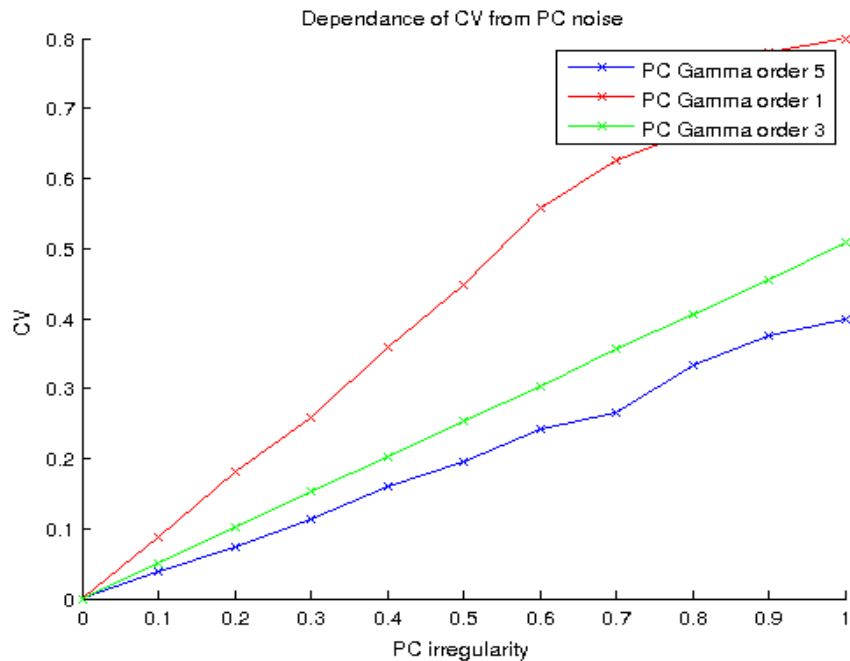


Figure 4.6. Dependence of Purkinje spike trains CV from noise levels for 3 different Gamma orders. There is inverse relationship between Gamma order and CV (The smaller the Gamma order the higher CV).

The relationship between CV and noise, which is the irregularity setting (both terms are used interchangeably) was determined empirically, using Figure 4.6 above. I am not aware of a way of doing this analytically.

The data from (Alvina et al., 2010), especially for *tg/tg* mice was still too regular. According to my assumption, it should represent less regularity to be able to cause such severe repercussions, such as episodic ataxia type 2 (EA2) and nystagmus as its symptom. Therefore, I referred to other experimental data, taken from our collaborator Dr Freek E. Hoebeek, Department of Neuroscience, Erasmus Medical Centre, Rotterdam, The Netherlands, and his research group. The inter-spike-interval coefficient of variation (CV) values from wild-type and tottering (*tg/tg*) mice was taken from Luthman et al. (2011) and were 0.34 and 0.66 respectively. This data was different from (Alvina et al., 2010), especially for *tg/tg* mice: CV = 0.66 vs 0.18 previously. But the new *tg/tg* CV value became out of range (greater than 1) after transformation to noise. In order to transform the new CV value to noise, the Gamma order was changed in Gammastim.mod file. In Figure 4.4 the CV(noise) dependency represented for different Gamma order values. It could be easily concluded, that Gamma order of 1 (the

minimal value) is the best option for the transformation of CV values to noise. The respective ISI distributions of input spike trains are shown on Figure 4.7.

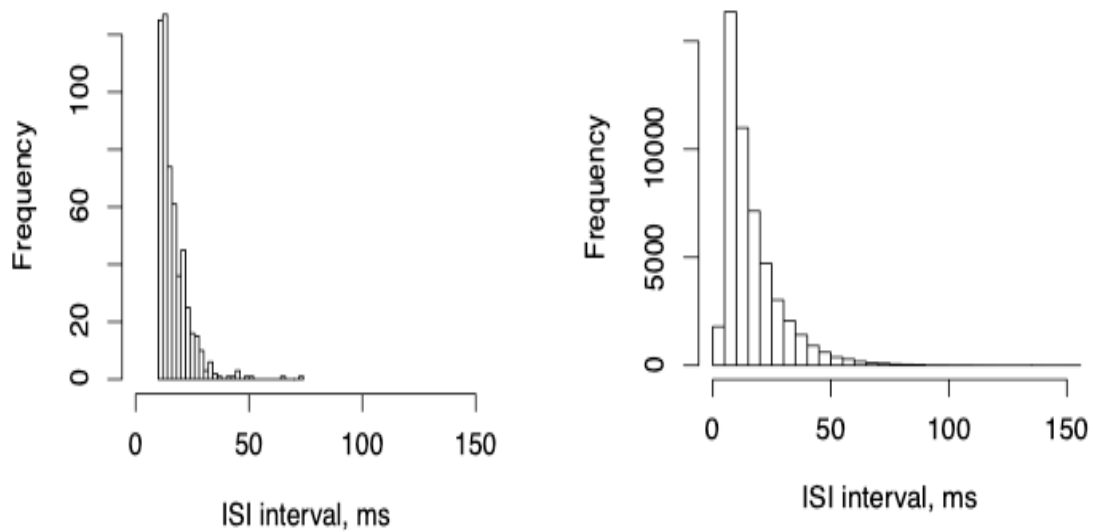


Figure 4.7 ISI distribution of input spike trains from wild-type mice with irregularity settings of 0.425 (on the left) and *tg/tg* mice (on the right) with irregularity settings of 0.825. The average ISI is around 16ms for wild-type and approximately 10 ms for *tg/tg*, making the wild-type input frequency to be 62 Hz and the *tg/tg* - 100 Hz.

The respective values for noise can be found in Table 4.2. More demonstrative presentation of output firing rate is in the Figure 4.8. Table 4.1 and Figure 4.8 demonstrate the difference in output from FTN firing rate between wild-type and *tg/tg* mice with the presence of STD and without it. Modulation of the signal occurs in FTN neuron, where the signal is transformed from an input irregularity to an output firing rate. The difference in firing rate for different levels of synchronicity (1 /90/ 450), which will be called here convergence ratio (CR), was estimated with both noise levels, which is applicable to both wild-type and *tg/tg* mice.

At the CR of 1 (four bars on the left, figure 4.8), when the FTN neuron receives an input from a single PC or completely synchronised PCs, irregular Purkinje cell input led to an increase in the FTN spike rate of 16% compared to regular input in the presence of STD and to a 13.95% increase in the absence of STD. Thus, for CR = 1, the FTN output increases in STD-independent way. At a CR = 90 (four bars in the middle), which is the most realistic among represented (De Zeeuw, et al., 1994; De Zeeuw et al., 1995; Palkovits et al., 1977), the FR acceleration is significant only for the case where STD is switched on. The difference between regular and irregular distribution of spike times occurrence is 17.83%. In the case where FTN neuron receives an input from 450 PCs, representing completely desynchronised

PC input, the FTN neuron output is recorded also in STD-dependent way. The difference between *tg/tg* irregular and wild-type more regular responses is 15%. Therefore, for higher convergence ratios of 90 and 450, an input irregularity based FTN spike rate increase only occurred in the presence of STD.

CR	90			
CV(input)	0.34		0.66	
Noise(input)	0.425		0.83	
STD	+	-	+	-
CV(output)	0.34	0.34	0.37	0.39
Noise(output)	0.425	0.425	0.46	0.49
Firing Rate (Hz)	38.7	36.2	47.1	36.6
CR	450			
CV(input)	0.34		0.66	
Noise(input)	0.425		0.83	
STD	+	-	+	-
CV(output)	0.32	0.31	0.34	0.34
Noise(output)	0.4	0.39	0.43	0.43
Firing Rate (Hz)	38.4	35.8	45.2	34.8
CR	1			
CV(input)	0.34		0.66	
Noise(input)	0.425		0.83	
STD	+	-	+	-
CV(output)	0.85	0.88	0.99	1.03
Noise(output)	1.063	1.1	1.24	1.29
Firing Rate (Hz)	64.6	62.9	76.86	73.1

Table 4.2 Output firing rate in Hz (as mean \pm *stdev*) from wild type and *tg/tg* mice's FTN neurons, which were completely synchronised or unsynchronised with or without the presence of STD.

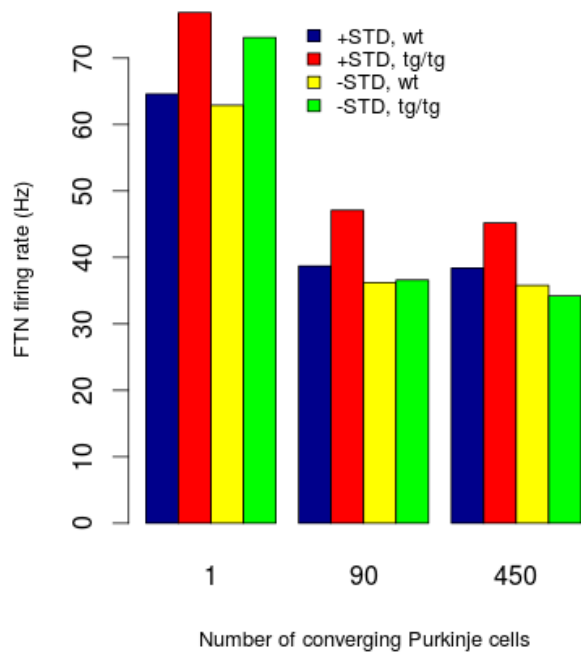


Figure 4.8 FTN neuron model firing rate response to spike trains from tg/tg and wild-type PC in the presence and absence of STD at the Purkinje cell – FTN synapses for a different number of PC converging onto FTN model.

Based on the above, I proposed a mechanisms of STD contribution to the translation process of input irregularity into output spike rate. For this I reconstructed individual PC synaptic conductance traces onto FTN (Figure 4.9 A,B) as well as a population conductance trace (Figure 4.9 C,D) (sum of all 450 PC – FTN synaptic conductance traces). Then in the model I recorded voltage traces from FTN neuron and found that in the presence of STD, the short inter-spike intervals in the irregular input lead to increased depression of the synaptic conductance (red), a decreased total inhibitory conductance injected into the FTN model, and an increased output spike rate (note the presence of 6 versus 4 spikes with and without STD in panel E). Our results are in line with experimental research results (Alvina and Khodakhah, 2010).

4.2 The robustness of the results

The robustness of the results against scaling tau up or down was estimated. The changes in the recovery time constant were made by using formula 3.4, applying different scaling factors to see whether or not the mapping of input irregularity on output firing rate is affected. The model was not sensitive to the changes in tau(r) values for tottering (0.425 noise) irregularity settings. For the wild-type (0.825 noise) irregularity settings it showed remarkable stability for the factors increasing tau(r), but there is some variation in the firing rate for the factors 0.1 and 0.5, slightly decreasing the output firing rate. More sensitivity is observed at the completely irregular cases (noise 1) for small tau(r) values.

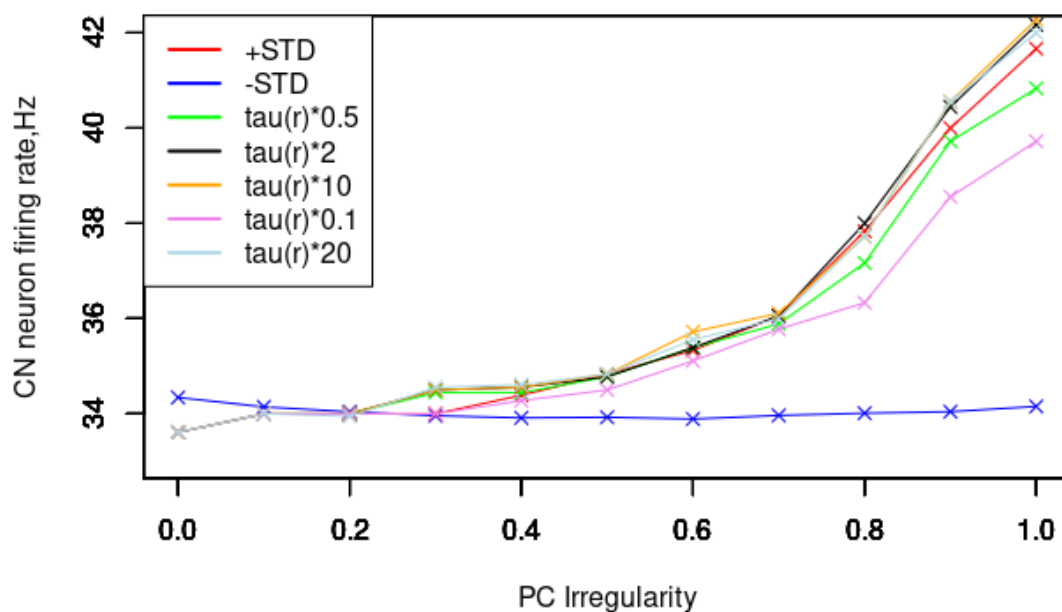


Figure 4.9 The CN neuron firing rate in response to different degrees of irregularity in the PC input spike trains with. Different values of tau(r) are evaluated.

For small tau values the recovery from depression is fast, and the depression does not build up. The depression builds up for large tau values, where recovery is not so effective – that is why the CN neuron firing rates are higher in this case. For small tau values the CN firing rates are lower as the depression disappears faster between spikes and the inhibitory synapses stay stronger. The model appeared to be very stable, because for all tau(r) it still shows robust results. Therefore, the results are not very sensitive to the parameters of recovery from depression.

4.3 The mechanism of the translation of input irregularity into the output firing rate

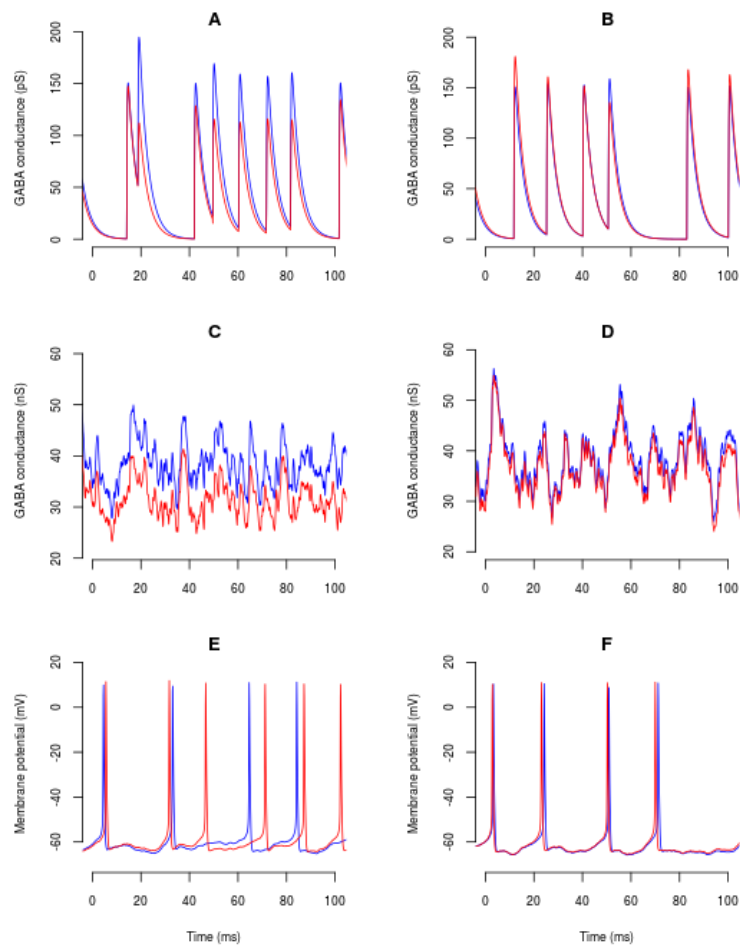


Figure 4.10 The mechanism of the translation of input irregularity into the output spike rate by STD. Response of the FTN model to irregular (*tg/tg*, left) and regular (*wt*, right) Purkinje cell input at 60 Hz and a convergence ratio of 90. The presence (absence) of STD is indicated in red (blue). A and B show the conductance trace of a single Purkinje cell synapse, C and D show the sum of conductance traces of all Purkinje cell synapses onto the FTN model, E and F are voltage traces recorded in the FTN soma. In the presence of STD, the short inter-spike intervals in the irregular input lead to an increased depression of the synaptic conductance (red), a decreased total inhibitory conductance injected into the FTN model, and an increased output spike rate (note the presence of 6 versus 4 spikes with and without STD in panel E).

4.4 Chapter conclusions

Our results provide a potential explanation for the pathology and 4-AP treatment of pathological nystagmus. DBN happens as a consequence of the mutation in the CACNA1a gene, which results in Cav2.1 P/Q channel channelopathy. This alters intrinsic firing properties of GABAergic PCs, making it irregular. For both synchronized and unsynchronized Purkinje cell input, irregular (DBN) input trains result in higher FTN spike rates than regular (4-AP) ones. In the presence of unsynchronized Purkinje cell input, the acceleration of the FTN spike output during simulated DBN and the corresponding deceleration during simulated 4-AP treatment depended on STD at the Purkinje cell synapses. Acceleration of the FTN firing rate lead to nystagmus and motor deficit, while 4-AP treatment restored PCs regularity and alleviated nystagmus.

5

**Replication of the
Thalamocortical
Models**

Chapter 5 is focused on the results of the various model replications on the way to a thalamocortical network model, suitable to display complex ictal behaviour. In this chapter, I show the results of the replication of the single neuron model, single-layer model, two-layer cortical and thalamocortical model. Along with the replication results I explain the discrepancies in the model description in the paper (Destexhe, 2009) and the model code and plots, which were identified and fixed. Also, some historical misunderstandings in parameters are also clarified.

5.1 Experiment 2: Single neuron model replication

I aimed at finding a thalamocortical model, which can display epileptic behaviour. As a starting point, I replicated the behaviour of different single cortical and thalamic neurons, out of which the thalamocortical model was built. If the single neuron model is built accurately following the description in the paper (Destexhe 2009), one would notice that regular spiking (RS) and fast spiking (FS) cortical neurons reset to the resting potential value like thalamic neurons, which is not the case for Figure 1 (Destexhe, 2009). This crucial difference in behaviour of the cortical and thalamic neurons is not described in the above-mentioned paper, but is clearly shown on the Figure 1 of the paper. After a change in the resting potential of cortical neurons to -70 mV (from -60 mV) and setting the reset value to -60 mV, it became possible to replicate the behaviour of the individual neurons qualitatively, but not quantitatively, due to differences in the simulation software and its versions. It is clearly seen, that for the thalamic neurons, in response to a depolarising stimulus, the resting potential is equal to the reset value, while it is not the case for cortical neurons (Figure 5.1).

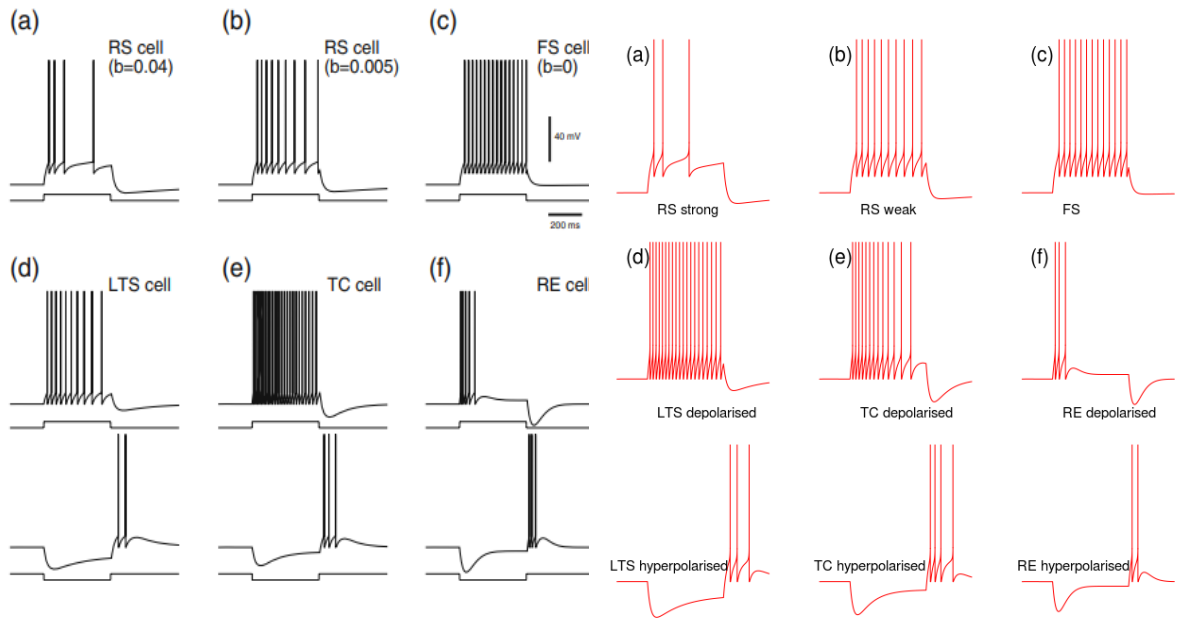


Figure 5.1. Original (left panel in black) and replication (right panel in red) of Figure 1, Destexhe 2009: intrinsic properties of the single neurons, utilized in the model. From (a) through (c) and the upper panel of (d) to (f) the single neuron activity is shown as a response to a depolarizing stimulus of 0.25 nA; lower panel of (d) – (f) – a single neuron response to a hyperpolarising stimulus of -0.25 nA.

(a) Regular spiking cortical neuron with strong adaptation: $a = 1$ nS, $b = 0.04$ nA; (b) Regular spiking neuron with weak adaptation: $a = 1$ nS, $b = 0.005$ nA; (c) Fast spiking cortical neuron without adaptation show tonic firing $a = 1$ nS, $b = 0$ nA; (d) Low threshold spiking neuron: $a = 20$ nS, $b = 0$ nA; (e) Thalamocortical relay neuron: $a = 40$ nS, $b = 0$ nA; (f) Thalamic reticular neuron: $a = 30$ nS, $b = 0.08$ nA.

The b parameter of the AdEx model denotes the strength of spike-triggered adaptation and regulates it. The resultant adaptation is strong for $b = 0.04$ nA and weak for 0.005 nA (Figure 1, a ($a = 1$ nS, $b = 0.04$ nA), b ($a = 1$ nS, $b = 0.005$ nA); Figure 2 RS weak) (Table 2). This behaviour is similar to RS cortical neurons (Connors and Gutnick 1990). For $b = 0$ there is no visible adaptation for a step-current response (Figure 1, c (Destexhe, 2009): $a = 1$ nS, $b = 0$ nA and Figure 5.1 c and 5.2 FS), the intrinsic behaviour is similar to FS neurons of cortex (Connors and Gutnick 1990), and is utilised to model cortical inhibitory neurons. This state can be described as an absence of spike-triggered adaptation and an adaptation sensitivity to the sub-threshold voltage (Naud et al., 2008).

The dynamics of adaptation parameter a was kept at the same level at the value of 1 nS for all cortical neurons. According to Izhikevich (2004), the further increase in dynamics of adaptation results in bursting activity (Figure 5.1 d, e, f and Figure 5.2 LTS, TC and RE depolarised). The moderate value of a , even with the strength of adaptation of zero, displays spike-frequency adaptation, as in low-threshold spiking (LTS) neuron (de la Peña and Gejjo-Barrientos 1996) (Figure 5.1, d; Figure 5.2, LTS depolarised).

As a response to hyperpolarising step current, both LTS and TC neurons show a strong rebound burst and moderate adaptation.

All thalamic single neuron behaviour is shown as a response to a hyperpolarising (the bottom panel) and depolarising (middle panel) step-current input. The further increase of parameter a leads to a stronger bursting, which is characteristic for the TC neurons. Unfortunately with the given parameter set and with no change to the step current amplitude, the TC dynamics could not be replicated (Figure 5.1 e ($a = 40$ nS and $b = 0$ nA); Figure 5.2 e TC depolarized). Moreover, it looks like the parameter values of the LTS and TC neurons are interchanged: Figure 5.1 e on the right and Figure 5.2 e looks like a replication of the Figure 5.1 d on the left (original), and Figure 5.1 d on the right, Figure 5.2 d looks like the replication of the Figure 5.1 e on the left (original). The possible explanation might be due to the typo in the paper (Destexhe, 2009). Further increase in dynamics of adaptation also leads to bursting behaviour as a response for both depolarising and hyperpolarising stimuli (Figure 5.1f ($a = 30$ nS and $b = 0.08$ nA); Figure 5.2 f RE hyperpolarised). This behaviour type is indicative for the thalamic reticular (RE) neurons (Destexhe and Sejnowski 2003).

Specifying the parameters for the RE single neuron, Alain Destexhe made a typo, where he mixed up the units and values for dynamics and strength of adaptation. The further replications and results are made with the corrections to the parameters (Destexhe, 2009). The values used for single neuron plot are: $a = 30$ nS, $b = 0.08$ nA. Another possibility for these values might be the opposite scenario, where $a = 80$ nS, $b = 0.03$ nA. The trial of both adaptation parameters has shown that higher dynamics of adaptation value displays more prone to bursting behaviour and better replicates Figure 1 (Destexhe, 2009). When the spike occurs, the adaptation variable increments by the value of strength of adaptation b . The layout of the adaptation variable plot (Figure 5.2) is organized to match the Figure 5.1.

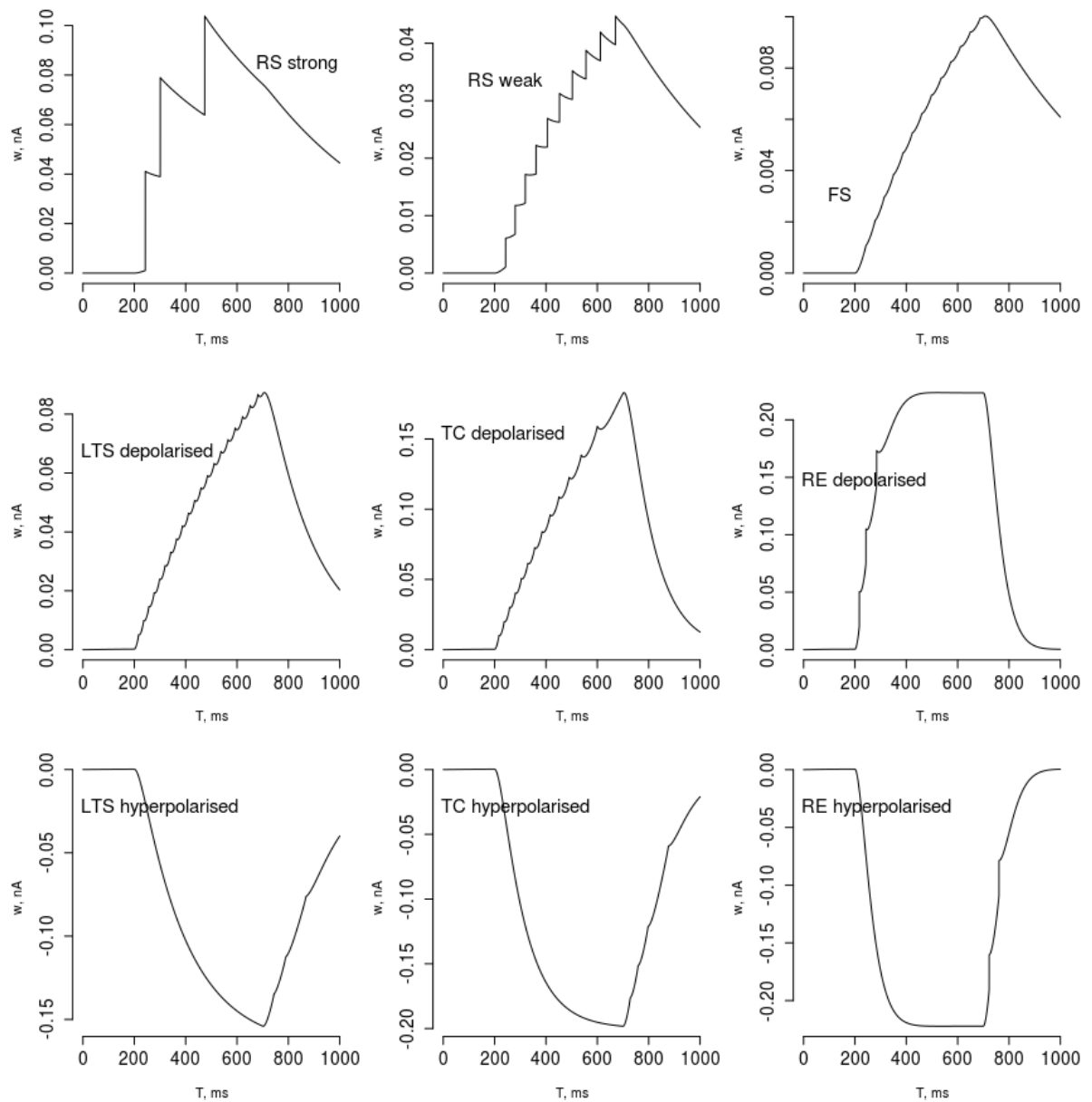


Figure 5.2. Adaptation variable w for neurons with different intrinsic properties as modelled in the AdEx model, plotted against time. RS neuron fired 3 spikes with strong adaptation, and 10 spikes with weak adaptation. FS neuron fired 13 spikes, but they are hardly distinguishable due to the zero strength of adaptation. LTS neuron fired 20 weak adaptable spikes. TC neuron fired 13 spikes. RE neuron fired only 3 spikes. In response to hyperpolarising step current, all thalamic neurons and LTS neurons show rebound bursting.

Visualization of adaptation variable could serve as a confirmation of a single neuron behaviour. I consider the single-neuron replication to be successful in qualitative replication of single neurons behaviour (Destexhe, 2009, Figure 1).

5.2 Experiment 3: Replication of Destexhe 2009

5.2.1 Replication of one-layer cortical model of 500 neurons

The single-layer cortical model available online contains 500 neurons. It is called *demo_cx_lts* and is translated from NEURON to PyNN by Andrew Davison. This model configuration consists of 500 cortical neurons in total, 100 of which are inhibitory FS interneurons (20%), while the rest (80%) are excitatory pyramidal neurons. 5% of PY neurons were LTS spiking, and all the rest are RS.

The 500 neurons cortical model displays up-and-down behaviour, with diminished down states (Figure 5.3). Where not all neurons plotted the up-and-down states are not so clear, and the behaviour looks like asynchronous.

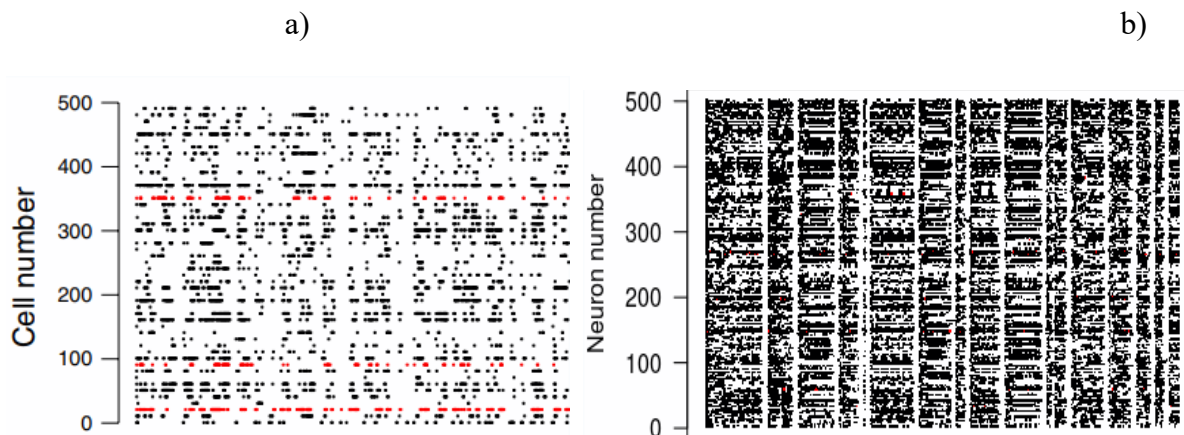


Figure 5.3. Asynchronous irregular activity of small cortical network of 500 neurons. a) Original Figure 7, Destexhe 2009. LTS neurons shown in red, 10% of neurons plotted. b) NEURON replication of the original Figure 7, 100% of neurons plotted.

The mean firing rate was the same for both NEURON and Nest outputs, but the maximal firing rate is higher for the NEURON output possibly due to the differences in integration.

5.2.2 Replication of two-layer cortical model of 2500 neurons

There are two versions of the model available online. Both two-layer cortical configurations can be downloaded from Open Source Brain web site (<http://www.opensourcebrain.org/projects/31>). One is `demo_cxcx01b_N=2500 LTS.oc`, which is originally written in NEURON simulator in hoc and mod languages. Later, the model was written from scratch by Lyle Muller (researcher from A. Destexhe's lab) in PyNN, based on the model description in the article (Destexhe, 2009).

The PyNN configuration of the model, `demo_cx_up-down` configuration consists of 2 layers of cortical pyramidal cells and interneurons, making 4 populations. First layer consists of 1600 pyramidal (PY) neurons and 400 interneurons (IN), and second layer – 400 PY and 100 IN. Cortical neurons in the model display three types of intrinsic behaviour: RS, FS and LTS. The connections are created randomly, with no self-connections, with weights of the synaptic conductances for excitatory and inhibitory projections preserved. The network is excited by an excitatory Poisson stimulus of 50 Hz, lasting for 50 ms. The model was updated to work with PyNN 0.8 in 2016 by Andrew Davison.

Parameters of the two-layer cortical model appeared to be different from the ones described in the paper. The inter-layer connection probability was affected, as its value was 0.7%, in the Table 1 of the paper, and 2% in the text of the paper. The probabilities of connections are specified in Table 5.1.

Also, in the table, the maximal and actual numbers of synapses per neuron are given.

As I am particularly interested in the thalamocortical network, I needed to translate the two-layer cortical model to a thalamocortical model. As a starting point I have replicated the two-layer cortical model (Figure 5.4).

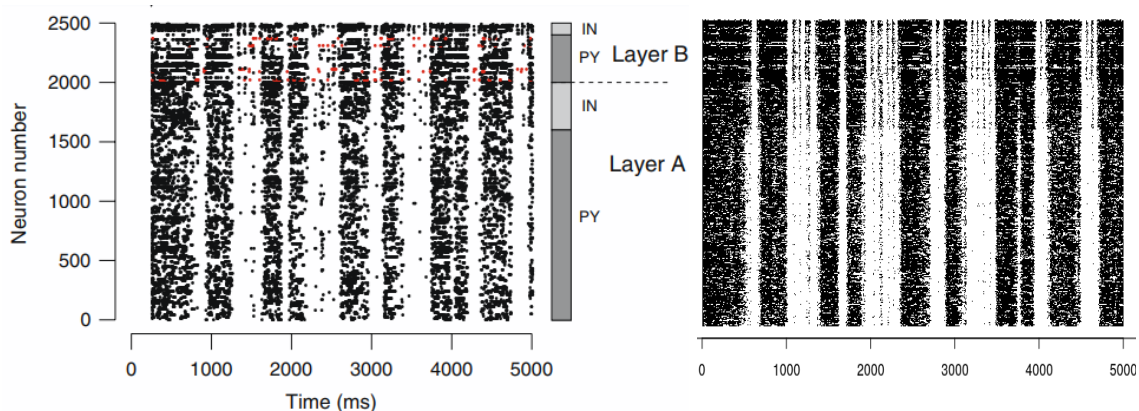


Figure 5.4 The original and the replication of the two-layer cortical model of 2500 neurons. The external input lasts 50 ms.

Also there was a bug in NEURON **.mod* file *IF_BG4.mod* (NEURON Model Description Language, which is used to add new biophysical mechanisms to NEURON). In *IF_BG4.mod* the AdEx parameters and equations are given and spike times are stored as a vector as a result of Euler method application. The refractory period is implemented as variable *reset* inside the *NMODL* function *fire()*, which is decremented by the integration time step *dt* each time *fire()* is called, i.e. each time the *BREAKPOINT* block is executed. NEURON executes the *BREAKPOINT* block twice for every time step, so that *reset* is reduced twice as fast as intended. This means that when *REFRACTORY* = 5.0 ms, the effective refractory period is actually 2.5 ms (A. Davison, Porting a model from NEURON to PyNN: a case study, 2017). Since the *BREAKPOINT* mechanism is not implemented in PyNN, the correction of the error was done by changing the refractory period parameter *REFRACTORY* from 5.0 to be 2.5 [ms] for PyNN. This correction is done across all configurations of two-layer models.

5.2.3 Replication of thalamocortical model

To be able to work with the thalamocortical network model, I had to modify the 2-layer cortex model in order to get a model as depicted in Figure 5.5. The changes were made in layer B, because layer A was identical in both models, and also identical to the single-layer cortex model described in the article (Destexhe, 2009). There were 2 types of connections: inter-layer (vertical) and intra-layer (horizontal). The probability for all inter-layer connections was 2% and they were excitatory only. For all types of neurons in the network the connections to the neurons of a same type were allowed, apart from TC neurons. Self-connections, that is connections of the neuron to itself, were not allowed. All RE-TC connections had 8% probability of connection, all remaining intra-layer connections had a probability of 2% (Figure 5.5).

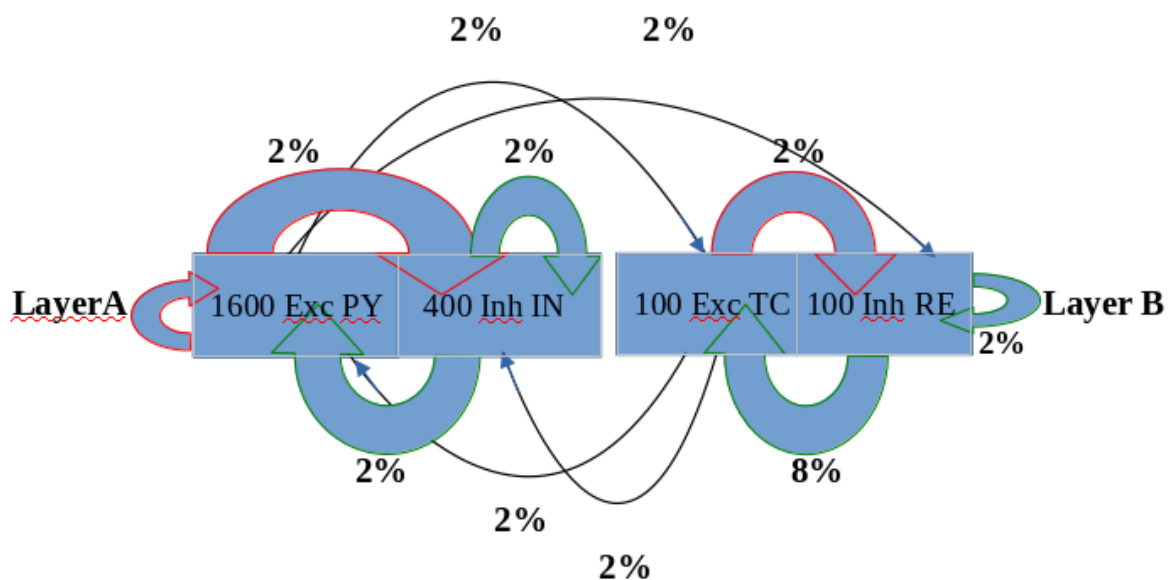
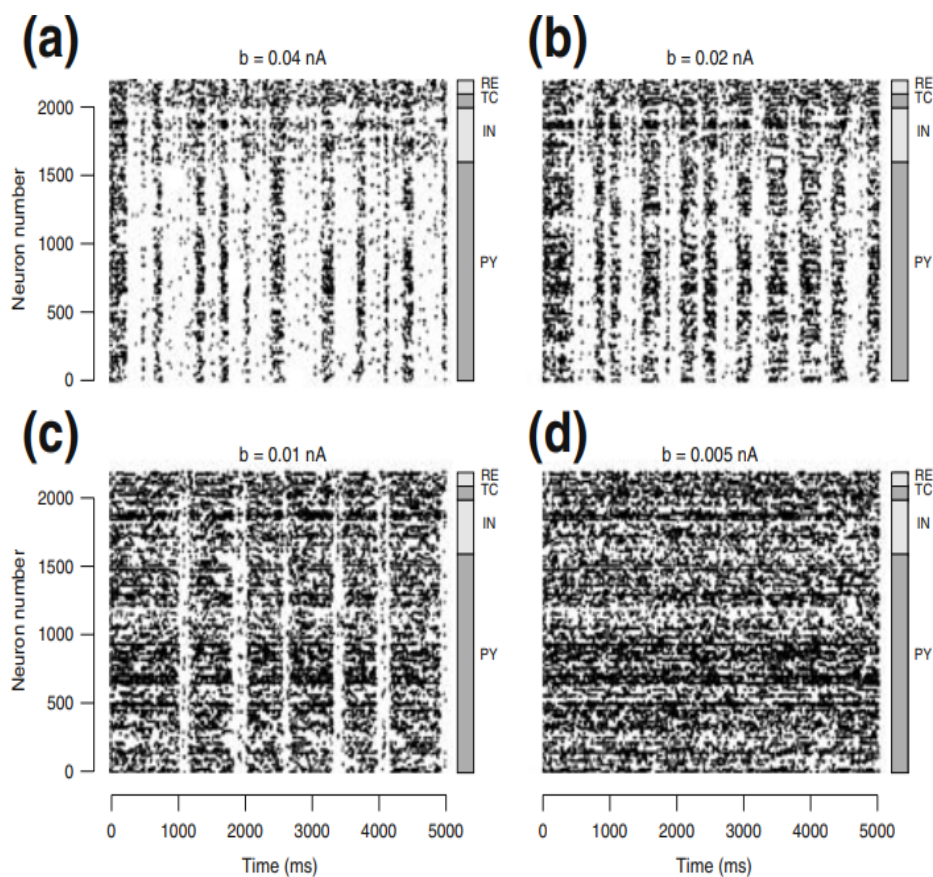


Figure 5.5 Thalamocortical network connectivity diagram. The inter-layer connections of excitatory type are shown in black, the intra-layer connections are shown in blue, with the red outline for excitatory connections, and with the green outline for inhibitory connections.

The thalamocortical model was implemented in both NEURON and PyNN. In NEURON, the model was implemented as one array of limited size, so probabilities of connections should be very carefully adjusted in order not to exceed the given size. It was impossible to increase the inter-layer probabilities of connections from the initial 0.7% to 2% in NEURON and preserve

the mean number of synapses per neuron (Table 1, Destexhe, 2009) at the same time (this is important because it was modelled as an array of a fixed size). Therefore, the decision was made for further use of the version of the model in PyNN as more up-to date and allowing more variability. Also, the replications of the figures from Destexhe 2009 were closer to the original in PyNN (Figure 5.6).

The input to the model was simulated as one external Poisson AMPA-mediated population, which was connected to 10% of the whole neuron population and lasted for 50 ms. The input frequency was 200 Hz. The synaptic weight was strengthened 10 times, compared to a normal AMPA conductance, and was 6 nS.



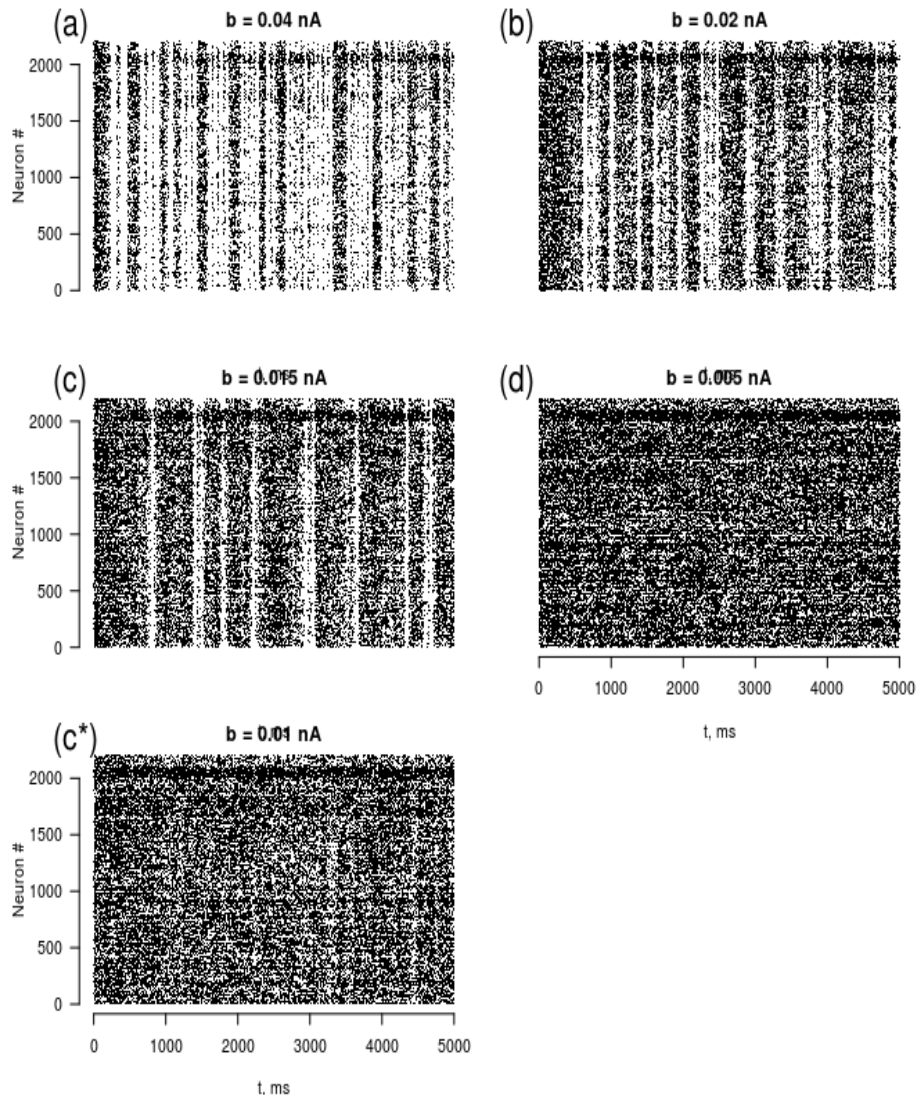


Figure 5.6 Thalamocortical network model replication: the gradual transition from the up-and-down to AI state with decreasing adaptation strength. Top panel: original figure from (Destexhe 2009); bottom panel: PyNN replication. 10% of the whole network activity is shown on the both left and right panels. 10% of the second layer excitatory neurons are LTS neurons. (a), (b), (c) and (d) correspond on the both panels. (a) self-sustained up-and-down activity with strong adaptation $b = 0.04$ nA, 11 up states in original and 12 up states in replication; (b) moderate adaptation with $b = 0.02$ nA, up states are longer, 11 up states in original, and 12 up states in replication; (c) diminished adaptation with $b = 0.01$ nA original, and $b = 0.015$ nA replication; 6 up states original, 9 up states replication; (c*) $b = 0.01$ nA, continuous asynchronous-irregular up state; (d) negligible adaptation with $b = 0.005$ nA, asynchronous-irregular state.

	CV ISI	CC
Original	2.45	0.004
Replicated	3.8036	0.93

Table 5.1 The comparison of CC and CV values of the figure 13 (Destexhe 2009) and its replication.

The assigned parameters correspond to the ones in the paper (Destexhe 2009). The qualitative behaviour of the replicated thalamocortical network also correspond to the paper for all values of the strength of adaptation, apart from diminished adaptation with $b = 0.01$ nA. In the original figure, the thalamocortical network with diminished adaptation is still showing the up-and-down states. It is a transitional state in between of the moderate and negligible adaptation. The up states are getting wider and prevail over down states. With further decrease of the adaptation strength, the down states will disappear completely (Figure 5.6, d). In the replicated figure, this transition from up-and-down to asynchronous irregular (AI) state happens sooner, with higher values of parameter b (Figure 5.6, c*). The close replication of the last up-and-down state, before the network will transit to AI state, is replicated with strength of adaptation of 0.015 nA.

A quantitative measure of the AI state is given in the paper (Destexhe 2009), to compare original plot with replication, the coefficient of variation of inter spike interval (CV ISI) and cross-correlation (CC) was calculated also for the latter one. The results of statistical comparison is given in the Table 5.1.

```

ext = pyNN.Population(1, pyNN.SpikeSourcePoisson,
    cellparams={'start':0.0, 'rate':200., 'duration':50})
ext_prj = pyNN.Projection(ext, neurons, pyNN.FixedProbabilityConnector(0.1),
    synapse_type=pyNN.StaticSynapse(weight=60e-3, delay=0.1),
    receptor_type='excitatory')

```

Figure 5.7 The input to the network: one external population is connected to 10% of the thalamocortical network with 10 times accelerated maximal AMPA conductance (synaptic weight, which initially was $6e-3$ uS). The external neurons firing rate is 200 Hz, and the stimulation lasts for 50 ms.

Since the synaptic connection probabilities in the thalamus, particularly in synapses from RE to TC neurons, are substantially higher (8%) than other horizontal intra-layer network connections (2 %), stronger firing of TC neurons is observed for all strengths of adaptation.

5.2.4 Clarifying adaptation units

Replicating (Destexhe 2009) article I have noticed that the parameter units in the paper are different from the ones in the downloadable codes. Also, the default units in NEURON and PyNN are different. At some point I have noticed, that the units of the dynamics of adaptation a parameter are of different order (nS vs μ S) from conductance units, which are both measured in Siemens. Moreover, in the downloadable code many parameters are normalised, and their values are multiplied by 1000 both in the parameter section and deeper in the code body, which is hidden from first-time user. As I found that the paper had multiple typos, the clarification of units for both NEURON and PyNN was necessary.

I specify the units of b in nA and for a in nS because it is the units used by the Nest simulator, in which my results were produced (Peyser and Alexander et al., 2017).

Some figures were created from the data generated in the NEURON simulator (Hines and Carnevale, 2014), whose default values are in μ S. Alain Destexhe used NEURON simulator while working of the paper (Destexhe, 2009), therefore, in the paper the units for dynamics of adaptation are μ S. In the available Python code, the units are multiplied by 1000 to be converted to nS, as PyNN uses nS for a , and μ S for conductance g . Some confusion arose due to the difference in units, multiple typos in the paper (Destexhe, 2009) and 1000 factors for the a parameter used in the code explained in Table 5.2.

Parameter	PyNN	Nest	Nest translation	NEURON	NEURON translation
a	nS	nS	-	μ S	x0.001
g	uS	μ S	x1000	μ S	-

Table 5.2. Units and variables for the adaptation.

In the source code, PyNN converts the units to the original unit of the simulator (Table 5.2). Thus, the dynamics of adaptation a in nS will be further converted internally by PyNN to

μ S, if the simulator is NEURON. If the simulator is Nest, the units of conductance will be converted from the μ S to nS by PyNN, but the units of a will remain the same.

Connection	Connection type	Connection Probability name	Connection Probability %	Expected Nb.synapses/neurons	Actual Nb.synapses/neurons
Cortical horizontal inter-layer	PY \rightarrow PY	PROB_CONNECT	2	32	29.7815
	PY \rightarrow IN				
	IN \rightarrow PY	PROB_CONNECT	2	8	6.8635
	IN \rightarrow IN				
Thalamo-cortical (L2 \rightarrow L1) vertical intra-layer	TC \rightarrow PY	PROB_CONNECT4	2*	2	1.4685
	TC \rightarrow IN				
Cortico-thalamic (L1 \rightarrow L2) vertical intra-layer	PY \rightarrow TC	PROB_CONNECT3	2*	32	30.13
	PY \rightarrow RE				
Thalamic horizontal inter-layer	RE \rightarrow TC	PROB_CONNECT2	8	8	6.83
	RE \rightarrow RE				
	TC \rightarrow RE	PROB_CONNECT2_EXC	2	2	1.55

Table 5.3. Original probabilities of connections by (Destexhe, 2009). * In the text of the paper, the probabilities of connections are specified as 1%. I use the value of 2% in all simulations, considering that 1% is a typo on the article (Destexhe, 2009).

5.3 Chapter conclusions

The adjustments and calibration of the chosen model (Destexhe, 2009) were performed. In particular:

- The two-layer cortical model was initially implemented in NEURON simulator. As it shows unexpected behaviour which I could not explain (as in Figure 3.6), it was translated to Python and run in PyNN with Nest simulator.
- The original 2-layer cortical configuration was changed in a way that the second cortical layer was transformed to thalamic, so that the model became thalamocortical.
- While doing this, all the intermediate configurations of the model were replicated, such as the one-layer model of 500 cortical neurons and two-layer cortical model.
- In order to confirm that the thalamocortical model exhibited intrinsic neuronal behaviour the single-layer model was created and the single-neuron behaviour was confirmed to be appropriate to the claimed neuron types.

Therefore, after the abovementioned modifications, the thalamocortical model is now suitable for the next step of the experiment – the implementation of the interictal activity and then bursting to model epileptic spike-and-wave discharges.

6

Dynamics of the Interictal Asynchronous State

In this and the following chapters, I modified the thalamocortical model (Destexhe 2009) so as to reproduce electrophysiological data from the Rotterdam group on the response of thalamic neurons to optogenetic stimulation of the deep cerebellar nuclei. First, I tried to reproduce the asynchronous irregular (AI) interictal state. The interictal state considered here is a step towards modelling of epileptiform behaviour, which is characterised by generalised spike-and-wave discharges (GSWDs) as a model of absence epilepsy. Changes applied to the thalamocortical model will be discussed chronologically: the modification of the neuron model following Naud's adaptive exponential integrate-and-fire model, the design of the background input, the investigation of the interictal dynamics and the variety of responses such as increased, decreased and biphasic activity, achieved by application of different types of input from the CN.

6.1 Naud's single neuron model parameters

Initially the parameter fitting was performed for the single neuron model, to track the intrinsic behaviour contributing to epileptiform activity (Chapter 5). The extensive literature search was performed, and the desired pattern of single neuron activity was found in (Naud, 2008), described as regular bursting (Figure 6.1, left).

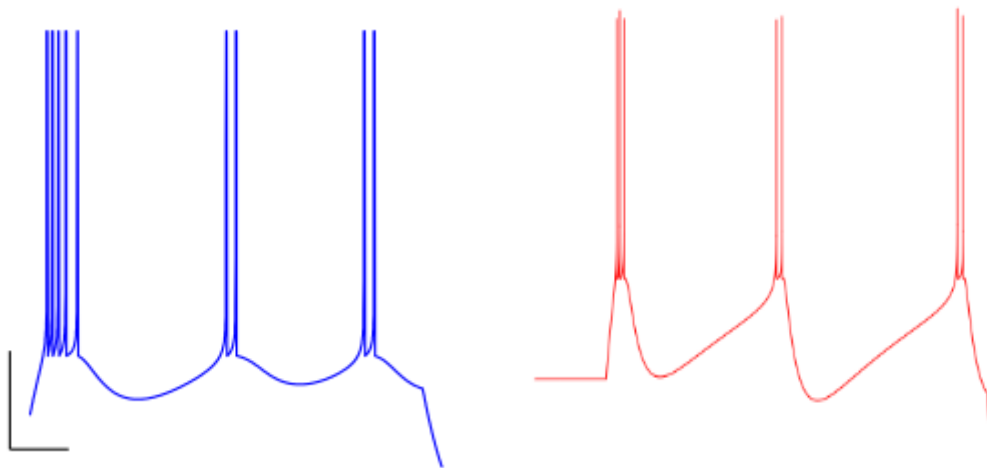


Figure 6.1. Single neuron regular bursting firing pattern. Left panel: (Naud 2008) original, Figure 4d. Right panel: PyNN Nest Replication. The voltage traces are shown with scale bars that correspond to 100 ms and 20 mV.

Not all the parameters were adapted from (Naud, 2008), as I aimed to keep them as close as possible to the Destexhe single-neuron model for consistency. The list of parameters from (Naud, 2008) and replication of its regular bursting behaviour is provided in Table 6.1.

Parameter	(Naud, 2008)	Replication
C total capacitance	200 pF	0.200 nF = 200 pF
g_L total leak conductance	12 nS	10 nS *
E_L effective rest potential	-70 mV	-60 mV
V_T effective threshold potential	-50 mV	-50 mV
ΔT threshold slope factor	2 mV	2 mV
a dynamics of adaptation	2 nS	2 nS
τ_w time constant	300 ms	300 ms
b strength of adaptation	60 pA	0.1 nA = 100 pA
V_r reset potential	-58 mV	-60 mV
I step current	500 pA	250 pA

* g_L is a calculated value, as in single neuron model the τ_m used instead: $\tau_m = C/g_L$

Table 6.1. The comparison of (Naud, 2008) and best-selected parameters to replicate the regular bursting firing pattern of Figure 6.1.

The parameters found to be crucial for regular bursting firing pattern replications were the time constant τ_w (which was decreased by a factor of two from its original single neuron model level) and the dynamics and strength of adaptation a and b respectively. This parameter list was found to successfully replicate the regular bursting single neuron behaviour and was applied to the thalamocortical network (to all neurons of the network, with a cell-specific modification of parameters a and b).

6.2 Synaptic model

I replaced the decaying-exponential synapse model by an alpha-function (see formula 3.11 in Chapter 3). This was crucial for the reproduction of spike-and-wave discharges and will be discussed in the next chapter.

6.3 Background input

In the thalamocortical model, 2-10 % of the network had been stimulated with a strong (200-400 Hz) 50 ms pulse to initiate self-sustained activity. This procedure did not work for the ictal model, as the above-mentioned type of input was too short to lead to self-sustained activity. After some trials, the optimal configuration for background input was found. Random 1 Hz AMPAR-mediated input was provided constantly for all the time of the simulation to 400 excitatory cortical neurons, via 20 synapses onto each of the neurons receiving this input.

6.4 Interictal state dynamics investigation

To investigate the interictal state dynamics, the raster plot and the peri-stimulus histogram (PSTH) were constructed for all neuronal sub-populations in the model (Figure 6.2).

There were 5 populations: cortical excitatory neurons (PY neurons) receiving the background input of 1 Hz, cortical excitatory (PY neurons) who did not receive the background input, cortical inhibitory neurons (IN), thalamic excitatory neurons (TC) and thalamic inhibitory neurons (RE). The firing rates of the above-mentioned populations were compared with the literature sources. Thus, the firing rate (FR) of a subpopulation of pyramidal neurons (so-called chattering cells) is 20-70 Hz (Gray and McCormick, 1996), for the Interneurons – 9-17 Hz (Hyun-Jae Pi et al., 2013), 100 – 200 Hz for the TC neurons (Kim et al., 2001) and 10-30 Hz for the RE neurons (Glenn and Steriade, 1982). The firing rates of the neurons in the present model were much higher (Figure 6.2, right panel). This may be a result of relatively small network size (Destexhe, 2009).

The attempt to lower the firing rates by increasing the inhibitory-excitatory synapses in cortex in between of IN and PY was made (Figure 6.3). As a result, the FR of cortical PY neurons receiving the background 1 Hz input could be decreased from 200 Hz to 35 Hz, and the FR of PY neurons not connected to the Poisson generator was lowered from 150 Hz to 30 Hz. The FR of IN was lowered from 80 Hz to 30 Hz, of TC and RE neurons decreased from 250 Hz to 115 Hz and 90 Hz respectively.

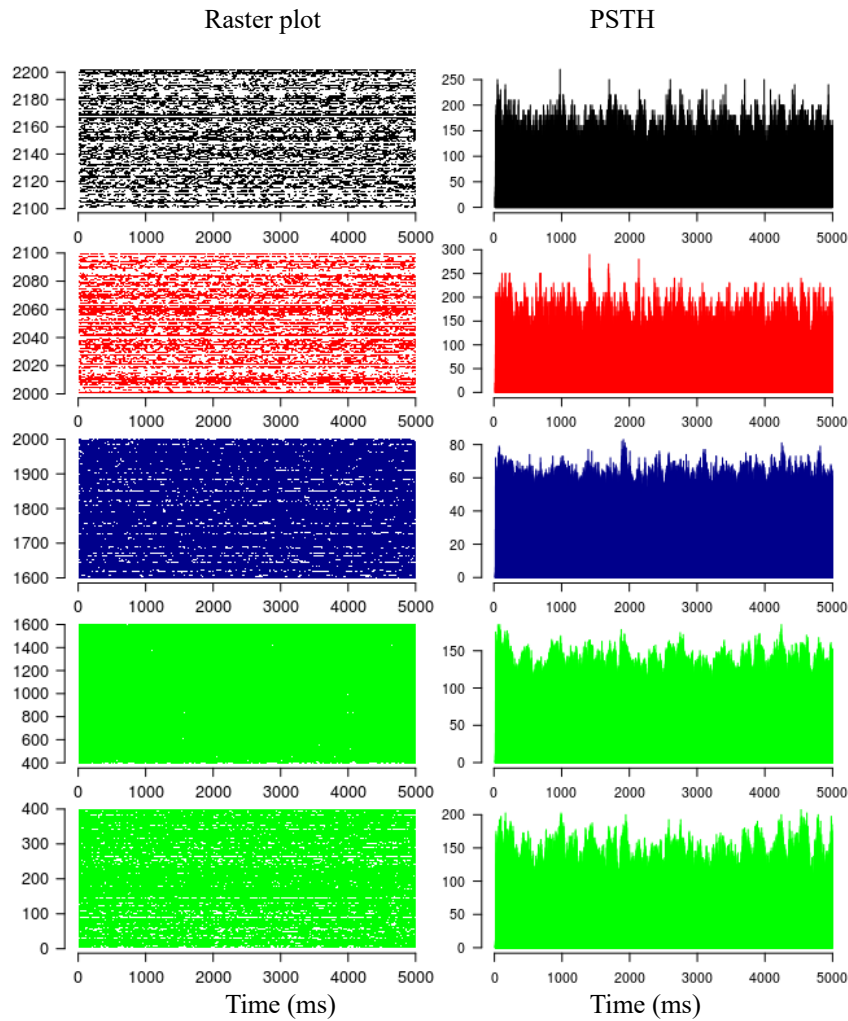


Figure 6.2 Comparison of raster plots (left panel) and PSTHs (right panel) of different (colour-coded) populations contributing to the thalamocortical network model. RE neurons population in black, TC – in red, IN – in blue, PY – in green. The bottom green population is separated based on the fact that the background 1Hz input was provided only to the first 400 neurons. The x axes of all plots measure the time in milliseconds (ms). The y axes of the raster plots show the id number of neurons, while the y axes of the PSTH show the firing rate in Hz.

It may be that in this model of the asynchronous state, the strength of inhibition had been too weak. Initially the Alpha-function was applied to the ictal state, where TAU_I was 15 ms. TAU_I was decreased to 5 ms for the interictal state, meaning TAU_I was lowered 3 times. A corresponding adjustment should have been done to the G_MAX as well, as the area under an alpha-function scales with the square of TAU_I . When TAU_I decreased 3-fold (from interictal to ictal), the G_MAX should relatively increase by a factor of 9. The 9-fold increase to $GABA_G_MAX$ is already lead to a significant drop in FR (Figure 6.3).

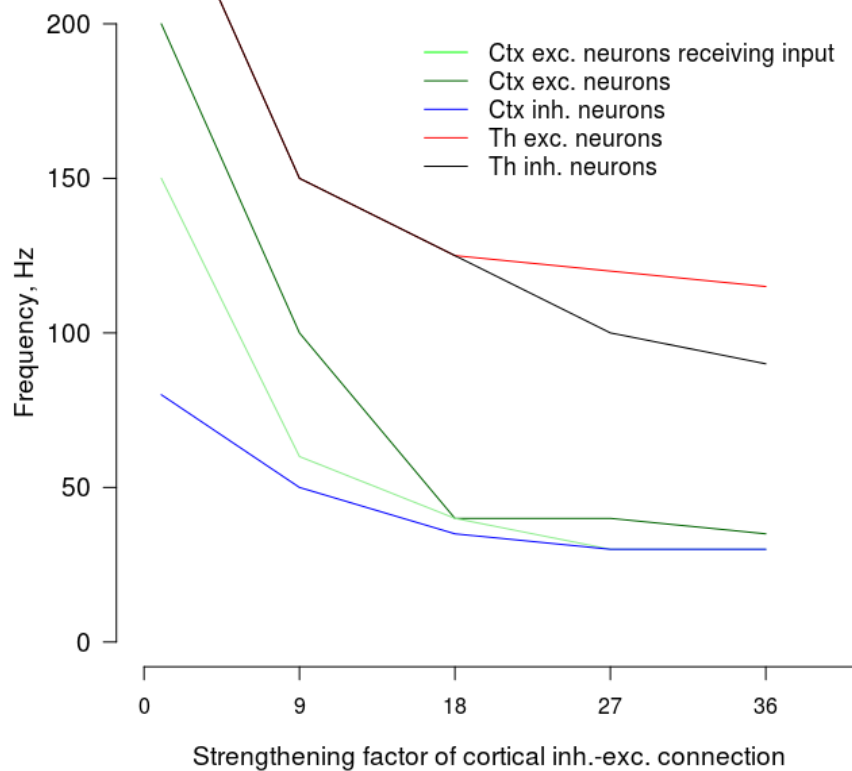


Figure 6.3 Decrease in the firing rate of different modelled sub-populations in response to IN – PY synapse strengthening. The strengthening of the inhibitory synapse is the factor by which GABA_G_MAX has been multiplied, which is displayed on x axes.

All other simulations were made with the model where IN-PY synapses were not strengthened. When applied to the network model, Naud’s parameters and a background input are showing interictal asynchronous irregular behaviour (Figure 6.2, left panel).

6.5 Modelling experimental response types

In *in vivo* experiments several response types of the thalamic neurons to CN stimulation were observed (Kros et al., 2015). To be more specific, with 50 ms optogenetic stimulation of DCN neurons, 61% of thalamic neurons (total n = 165) increased their firing rate, 10.3.% responded in a biphasic manner (initial excitation, followed by inhibition of firing rate), 9.1 % demonstrated a decrease in their firing rate and 11.5% had a delayed sustained response. To further validate the model, I tried to replicate the above-mentioned response types.

To achieve all four response types of thalamo-cortical neurons, different input patterns have been applied to all TC neurons. It is known that the CN projections which synapse onto the TC neurons are glutamatergic (Houck and Person, 2015). In the model the excitation is

modelled as an AMPAR conductance. Also, to achieve the variety of responses, the assumption was made that there is a possibility of CN input being mixed with additional polysynaptic input possibly gated via CN-afferents to TC (for instance disynaptic GABAergic input via thalamic interneurons or reticular cells).

The replication of all response types but the delayed pattern were successful (Figure 6.4).

Theoretically, the closest option to replicate the delayed response (Figure 6.4 D) would be excitatory input with jitter, as it prolongs the response. This response prolongation, however, was not sufficient to reproduce the experimental data. Another possibility would be to apply a strong excitatory pulse to a silent network (as in Chapter 5), so that the network is driven to self-sustained asynchronous irregular activity. In the experimental recording, however, there was spontaneous activity preceding the stimulus.

A possible explanation of the difficulties in replicating the delayed response type may be an absence of the mechanisms which shapes the delayed response in the model. For instance, the thalamus has a cholinergic innervation but acetylcholine receptors were not implemented in this model.

Taking into account the results of the interictal state dynamics investigation (Paragraph 6.3), various patterns of response were modelled with IN – PY synapse strengthened nine times (Figure 6.6).

To summarise, the model could successfully reproduce as many as 80.4% of the TC responses seen in experimental conditions. Delayed response was not possible to replicate because the mechanisms that make this type of response possible are not implemented in the model.

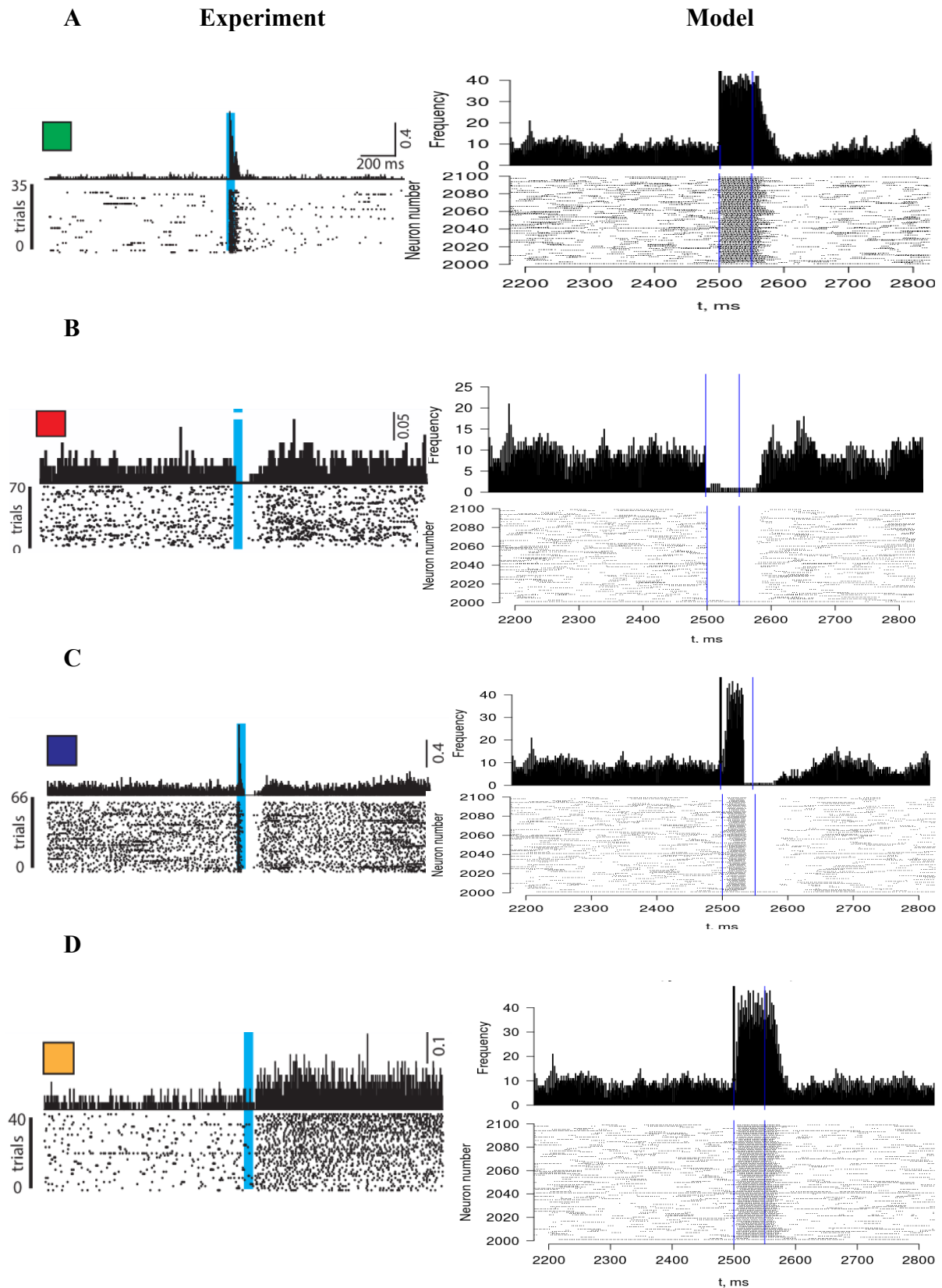


Figure 6.4 Peri-stimulus time histograms (top panels) and raster plots (bottom panels) show variety of TC responses depending on the type of CN stimulation. The input lasts for 50 ms in all cases and was marked with blue line for the experimental results. The left panel shows the experimental results (Kros et al., 2015), and the right panel shows

the replicated modelling results, where the start and termination of the input are marked with a blue lines. A: increased TC response as a result of excitatory AMPAR-mediated CN input; B: decreased TC response as a results of inhibitory GABA_A-mediated CN input; C: Biphasic TC response as a result of biphasic CN input lasting for 50 ms, where first 25 ms of input duration were excitatory, and another 25 ms were inhibitory; D: Delayed TC response. Jitter was modelled as a random delay from -5 to 5 ms. Note different time-axes for experimental and modelling responses.

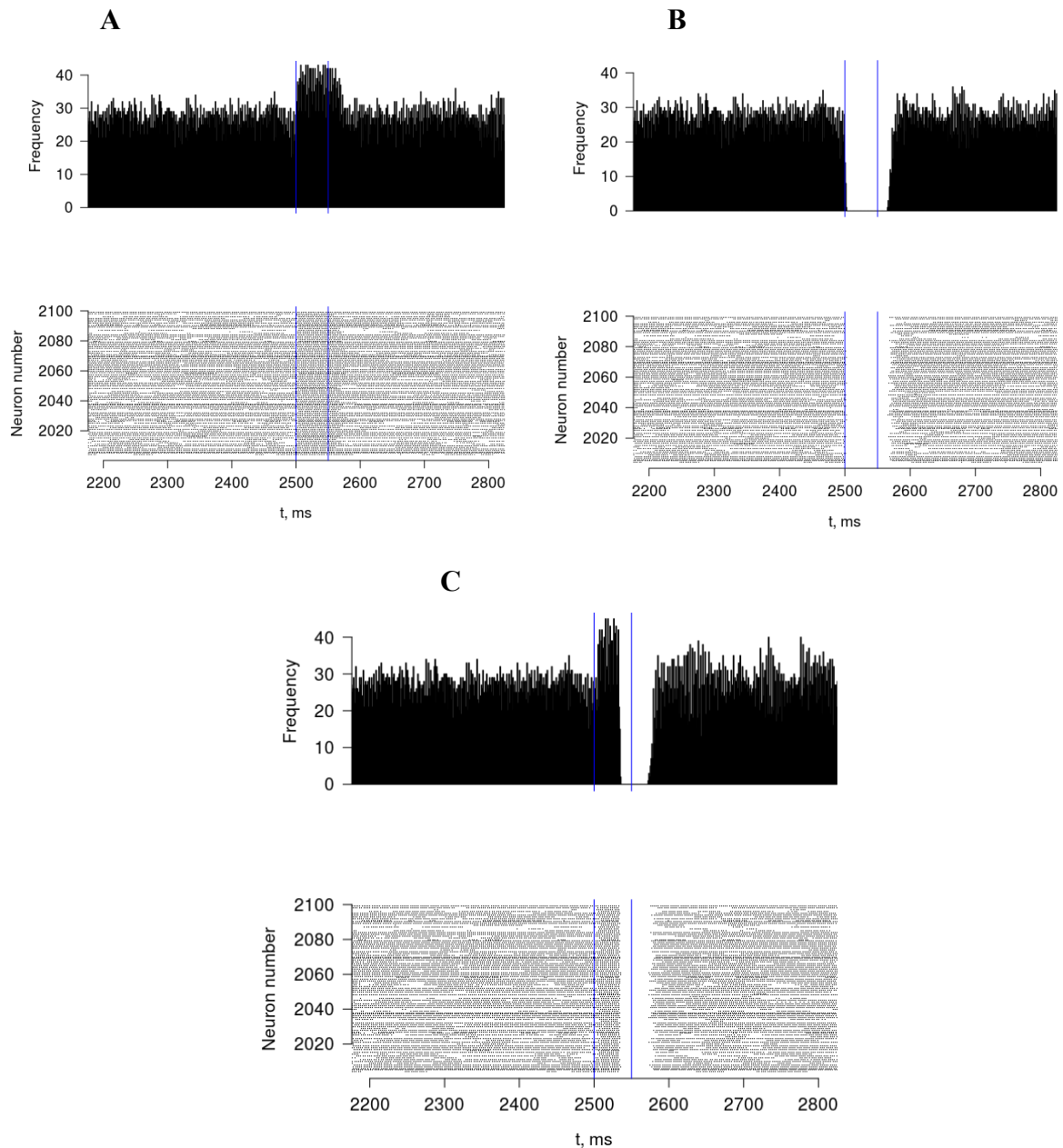


Figure 6.5. Three response types to the different configurations of CN stimulus, when the IN – PY synapse strengthened 9 times. A: an excitatory response type as a result of 50 ms excitatory CN stimulus; B: an inhibitory response type as a result of 50 ms inhibitory CN input; C: a biphasic response type as a result of dual excitatory and inhibitory input, where each part of stimulus lasts for 25 ms, making the total duration of stimulus 50 ms.

6.6 Chapter conclusions

A detailed analysis of the thalamocortical interictal model and parameter validation of this asynchronously irregular spiking model allowed its successful calibration and fine-tuning. One of the crucial points in model development appeared to be the maintenance of self-sustained activity during the model run time. Trials of strong but short stimuli have not resulted in self-sustained activity. Empirically the 1 Hz of continuous AMPA-mediated stimulus was selected as the best option to preserve network activity. To further bring the model closer to the *in-vivo* neuronal networks behaviour the possible amendments were made. Specifically, the simulated neuronal populations firing rates were matched with the values described in literature for the thalamocortical relay neurons. The higher firing rate of simulated neurons could be explained by the relatively small size of the network, it was successfully lowered by strengthening of the IN-PY synapses.

After model validation, the different TC neuronal responses observed in the experimental research after the CN stimulus were attempted to replicate. The interictal state dynamics were investigated. Thus, 80.4% of the TC responses seen in the experimental settings were replicated successfully. The next step of the experiment would be to establish the bursting network and to apply deoscillating CN stimulus to it.

7

The Ictal State: Generalised Spike-and-Wave Discharges and their Termination by Optogenetic Stimulation

The steps towards the ictal state of the model will be discussed in this chapter. They were: model of synapses with alpha-function, adjustment of the inhibitory synaptic conductance, removing model bistability by adjusting the adaptation time-constant τ_w and dynamics of adaptation a .

When the ictal oscillatory state of the model was achieved, the cerebellar nucleus (CN) input to TC neurons was designed to be able to stop seizures and switch neuronal activity from ictal to the asynchronous irregular interictal state (Chapter 6). As I am aiming here to explain the experimental results, all the effort was made to replicate the experimental conditions as closely as possible. The failure rate of the CN input was tested against the phase of the ictal burst at which it was applied (Paragraph 7.2).

7.1 Generalised spike-and-wave discharges (GSWDs) as indication of the ictal state

While I was modifying the 2-layer thalamocortical model which displays up-and-down states to the model able to produce GSWDs, I have been trying to implement the ability of the model to show spike-and wave oscillations. GSWDs are the benchmark of absence epilepsy, and they are measured by means of electrocorticogram (ECoG) at primary motor M1 and sensory S1 cortices. To estimate if the model displays GSWDs or not, the total synaptic current was calculated from the model output as a proxy for local field potentials. If the total synaptic current showed an oscillatory spike-and-wave pattern, then it was concluded, that the model displays the epileptiform behaviour. After the definition of ictal behaviour was clarified, the parameter search was performed.

7.1.1 Outline of the main changes and parameters important for the ictal state

7.1.1.1 Alpha function

After some unsuccessful application of Naud's (Naud, 2008) regular bursting neuron parameters to the network model, an extensive literature search was performed in order to answer the question how to make the thalamocortical model burst. In the thalamocortical model neurons were modelled as exponential integrate-and-fire neurons with spike-triggered and sub-threshold adaptation currents – *EIF_cond_exp_isfa_ista*.

The desired behaviour pattern of thalamocortical model is spike-and-wave discharges, where “spike” is associated with the synchronous firing of all cortical neurons. Such a firing activates GABA_B-mediated K⁺ currents, and hyperpolarization in pyramidal neurons. This stops the discharges and generates a positive slow "wave" (Steriade, 1974; Destexhe, 1999).

Therefore, I am aiming to alternate thalamocortical activity, where all cortical and thalamic neurons are simultaneously active / silent.

To enable the model to produce the “wave” component of GSWDs I needed to implement the mechanism responsible for the slow inhibition, as in the model only GABA_A-mediated fast inhibition was incorporated. Initially the model was described by the *EIF_cond_exp_isfa_ista*, exponential integrate-and-fire model, where only fast exponentially decaying inhibition was possible. In order to be able to model the effect of GABA_B, the synaptic mechanism in the model was changed for *EIF_cond_alpha_isfa_ista*, where the synaptic conductance is described by an alpha function. The alpha function would be a good tool to implement GABA_B-mediated synapses, because an alpha-function with a time-constant of 15 ms reaches its peak conductance also after 15 ms. The total inhibition of the alpha synapse (its integral over time) scales with the square of tau.

The GSWDs associated with absence epilepsy can be of different frequency, dependent on the animal model, where they are observed. Thus, in cats they are of 3 Hz frequency (Gloor & Fariello, 1988) and 5-10 Hz in rodents. As here attempts are made to replicate and explain the experimental results obtained in mice, the target frequency of GSWD would be around 7 Hz.

7.1.1.2 Inhibitory synaptic conductance

A sufficient modification to switch the network from the interictal to the ictal state was an increase by a factor of three of the time-constant of the inhibitory synaptic conductance (τ_i). The original value of the time-constant of the inhibitory synaptic conductance in the thalamocortical model and in the current model of the interictal state, was 5 ms. Its two fold increase to 10 ms did not lead to the ictal state. Values of 15 ms and greater switched the network to epileptiform activity. Also, the magnitude of the inhibitory synaptic conductance defined the frequency of epileptic bursts. Thus, with $\tau_i = 153$ ms only 4 bursts appear over the 5 s period, while a 2-fold decrease of it led to 8 bursts. A further decrease of the τ_i value to 25 ms led to 22 bursts, and decrease in τ_i to 15 ms led to 35 bursts over the period of 5 s, which is approximately 7 Hz frequency. I aimed particularly at such a frequency of 7 Hz because the experimental recordings from rodents made by our collaborators appeared to be at this frequency (Kros et al., 2015).

7.1.1.3 Model bistability and the adaptation time constant τ_w

While testing the ictal state of the model and adjusting its parameters, the model sometimes spontaneously switched to the asynchronous irregular state. Further simulations were set up to investigate the nature of this issue.

In the thalamocortical network model, the adaptation time constant τ_w was 600 ms. This was changed down to 300 ms during parameter search due to Naud's parameters, being the most successful in achieving the ictal state in single neuron model. With this lower value, the model still used to switch spontaneously from ictal to interictal state (Figure 7.1).

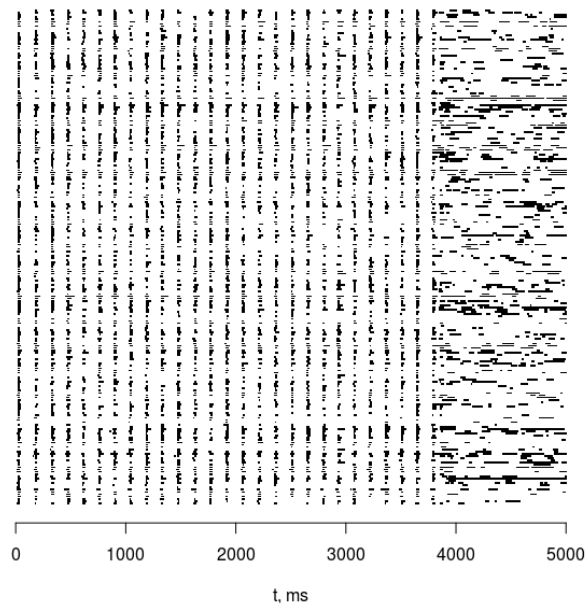


Figure 7.1 Spontaneous phase shift from ictal to asynchronous irregular state in the thalamocortical network of 2200 neurons, where every second neuron was recorded. The model incorporated all above-mentioned changes.

No CN input was provided, only constant 1Hz background input to 400 excitatory pyramidal neurons. Due to empiric tests it was established that model displays bistability only with relatively high levels of adaptation time constant. To avoid spontaneous phase transition the τ_w parameter was again decreased twice to 150 ms, and the ictal state was permanent until the end of the simulation and no bistability observed. Both the cortical and thalamic adaptation time constants were responsible for the model bistability, as it was not enough to set one of them to the lower value.

The experiment was repeated with 5 different seeds for 3 values of τ_w : 600 ms, 300 ms and 150 ms (Table 7.1). The model run time was 5 s.

Here a strong correlation between τ_w and the phase transition pattern can be seen. Formally, τ_w is the time required for the system response. For $\tau_w = 600$ ms, where the response time is high, a phase transition always happens. The moderate $\tau_w = 300$ ms looks like the border value, where a spontaneous phase transition may happen or not, and with $\tau_w = 150$ ms the transition from ictal state to the asynchronous irregular one was never observed. The value of $\tau_w = 144$ ms was deduced as optimal in (Brette, Gerstner, 2005). Therefore from now on, to be sure that the phase transition not occur spontaneously (but simulated on purpose where needed), I will be using the value $\tau_w = 150$ ms for the adaptation time constant. As expected, the phase change happens in general sooner for the high $\tau_w = 600$ ms.

The idea of lowering the τ_w in order to bring the model into the oscillatory state is in line with the Brette-Gerstner model in the Brian simulator, where $\tau_w = 144$ ms for regular spiking, and lowered to $\tau_w = 20$ ms for the bursting mode. All the other parameters (a [nS], b [nA], V_r [mV]) remained the same (Brette, Gerstner, 2005).

The most important finding is that the spontaneous phase transition was never observed for the low value of $\tau_w = 150$ ms, and this value guarantees the stability of the ictal state. Therefore this value is used for all further simulation to ensure the absence of spontaneous phase change.

$\tau_w = 600 \text{ ms}$

Seed	Observation	Time of phase transition, ms
983651	Phase change	780
112233	Phase change	495
702493	Phase change	560
425607	Phase change	640
214853	Phase change	600

$\tau_w = 300 \text{ ms}$

Seed	Observation	Time of phase transition, ms
983651	No phase change	n/a
112233	Phase change	3190
702493	No phase change	n/a
425607	Phase change	3180
214853	Phase change	3800

$\tau_w = 150 \text{ ms}$

Seed	Observation	Time of phase transition, ms
983651	No phase change	n/a
112233	No phase change	n/a
702493	No phase change	n/a
425607	No phase change	n/a
214853	No phase change	n/a

Table 7.1 Comparison of the three values of adaptation time constant τ_w , 5 trials (with five seeds) for each. The pattern of spike times is displayed in the “observation” column. The exact time of the spontaneous phase transition is given in the third column if applicable.

7.1.1.4 A note on the role of adaptation parameter a in the ictal state

The adaptation parameter a (refer to formula) quantifies a conductance that mediates subthreshold adaptation (Ladenbauer et al., 2012; Izhikevich 2003).

As described in Chapter 5, there are two original configurations of Destexhe's model, 500 neurons cortical network and 2200 neurons thalamocortical network models. Each configuration has some code in NEURON and PyNN. As in Alain Destexhe's article (Destexhe, 2009) the dynamics of adaptation a is given in μS , which is the units of the NEURON simulator, there are the same values in the NEURON codes. When the PyNN version for 500 neurons cortical network was created, the a values remained the same in the parameter section. To convert the units from μS to nS (which PyNN accepts), a factor of 1000 was added in the code where the parameters are assigned to the neurons of all types (where the network is created, not in the parameter section of the program), whereas for the thalamocortical model the unit conversion was done in the parameter section. This fact brought some confusion, same as the fact that in PyNN a [nS] has a different units from g [μS] – conductance. In the Brian AdEx model (Brette, Gerstner, 2005) the only way to switch to bursting is to decrease τ_w .

In the later work (Touboul and Brette, 2008), it is claimed that the model can oscillate near the resting potential or produce a damped oscillation, and that “self-sustained oscillations are not possible in this model, nor in Izhikevich model, as is shown in Touboul (2008)”. In order to trigger damped oscillations, in Brian code (Touboul and Brette, 2008), the parameter a was changed gradually from 4 nS for phasic spiking to 8000 nS for oscillatory and again 4 nS for bursting tonic and bursting phasic modes.

As mentioned in section 7.1.1.2, the only parameter needed to switch the model from AI state to ictal (once the network parameters are established) is the inhibitory time constant, and neither a nor τ_w play a role into this process. No tuning of a was required to drive the ictal state.

7.2 GSWDs

The model tuning was considered to be complete when the it was not showing spontaneous phase transitions (bi-stability) and when the benchmark of epileptic behaviour, GSWDs (Figure 7.2) were obtained. This happened after all the changes listed in the above paragraphs, including the change to the background input (see Paragraph 6.2).

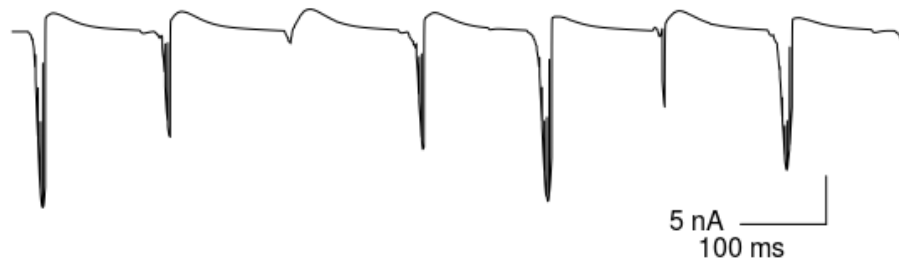


Figure 7.2. LFP approximation of 449 cortical neurons firing with 7 Hz frequency. Negative deflections are due to the synchronous firing of all cortical neurons, and the “waves” reflect the silent period during hyperpolarisation.

In the experimental research, GSWDs are measured as local field potential (LFP) (Destexhe et al., 2001) or electrocorticogram (EcoG) on the primary sensory cortex S1 and primary motor cortex M1 (Kros et al., 2015). LFP is generated by electric currents of the neurons, but synaptic currents are considered to be the main contributor to it (Destexhe et al., 2001). Therefore, the total synaptic current served as LFP approximation and was calculated as a product of voltage and conductance of a subset ($n = 449$) of cortical neurons (Figure 7.3).

To investigate the ictal state, the recordings was made from every 10-th neuron in the network, as this is indicative for the behaviour of the complete network of 2200 neurons.

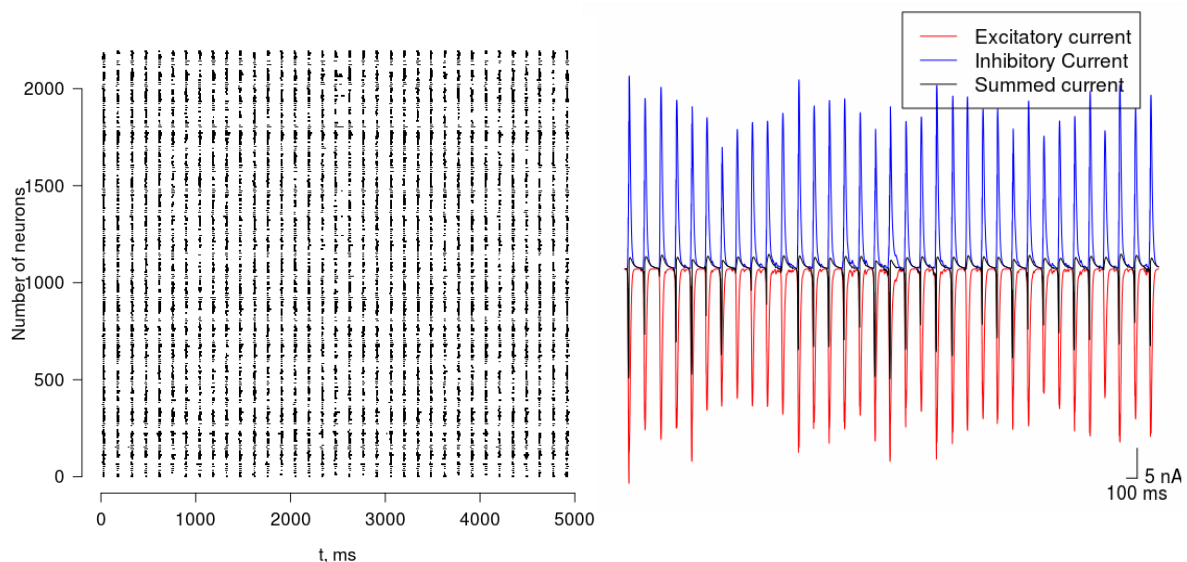


Figure 7.3 Raster plot (left panel) and LFP (right panel, black) of the ictal network of 2200 neurons. The average firing rate is 7 Hz.

7.3 CN input to terminate seizures

The simulated CN input was designed after the CN input found in experimental research (Kros et al., 2015). The CN input consisted of 20 equal populations targeting all (100) TC neurons. The spike times of the abovementioned populations were defined in an external text file, which were read by the PyNN *SpikeSourceArray* function. The text file was created, targeting the particular start time of the input, and provided input for 50 ms, where a spike occurred every second millisecond. The input strength (weight) was defined as maximal corresponding conductance (AMPA, GABA or both for mixed input) x scale. The scale is the factor, which defined how hard it is to get the phase-transition response, the so-called failure rate.

There were three input configurations:

- 1) synchronised exclusively excitatory AMPAR-mediated (Figure 7.7, Figure 7.8 A);
- 2) jitter, where spike times were delivered with some random delay, arriving some time later than the time defined in the array of a text file. Three jitter values were tested, they were 10, 50 and 0 ms, where the last one corresponds to synchronised excitatory stimulus (Figure 7.7);
- 3) mixed input, which aimed to replicate the input from other prethalamic nuclei, such as Zona Incerta (ZI). The input consisted of 1:1 excitatory and inhibitory inputs to TC neurons (Figure 7.7).

The most successful input configuration in seizure termination appeared to be excitatory input from CN (Figure 7.4). The effect of excitatory CN input on the different neuronal populations is shown in Figure 7.5.

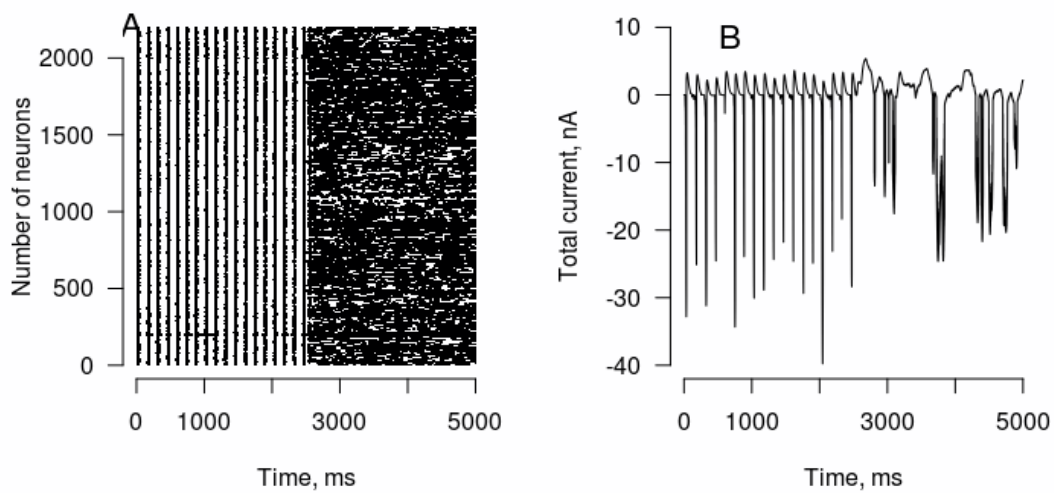


Figure 7.4 Activity phase change in response to CN input to thalamocortical neurons. A: raster plot of 2200 neurons in the network. Spike times of every second neuron are plotted. The ictal bursting activity terminates immediately in response to the CN stimulus applied at 2475 ms. As a result, the network switches to the normal asynchronous state. B: total synaptic current as an approximation of local field potential, indicating oscillatory activity at 7 Hz. Before the CN stimulus application, the local field potential displays generalised spike-and-wave discharges (GSWDs). This type of activity immediately terminates after CN stimulation.

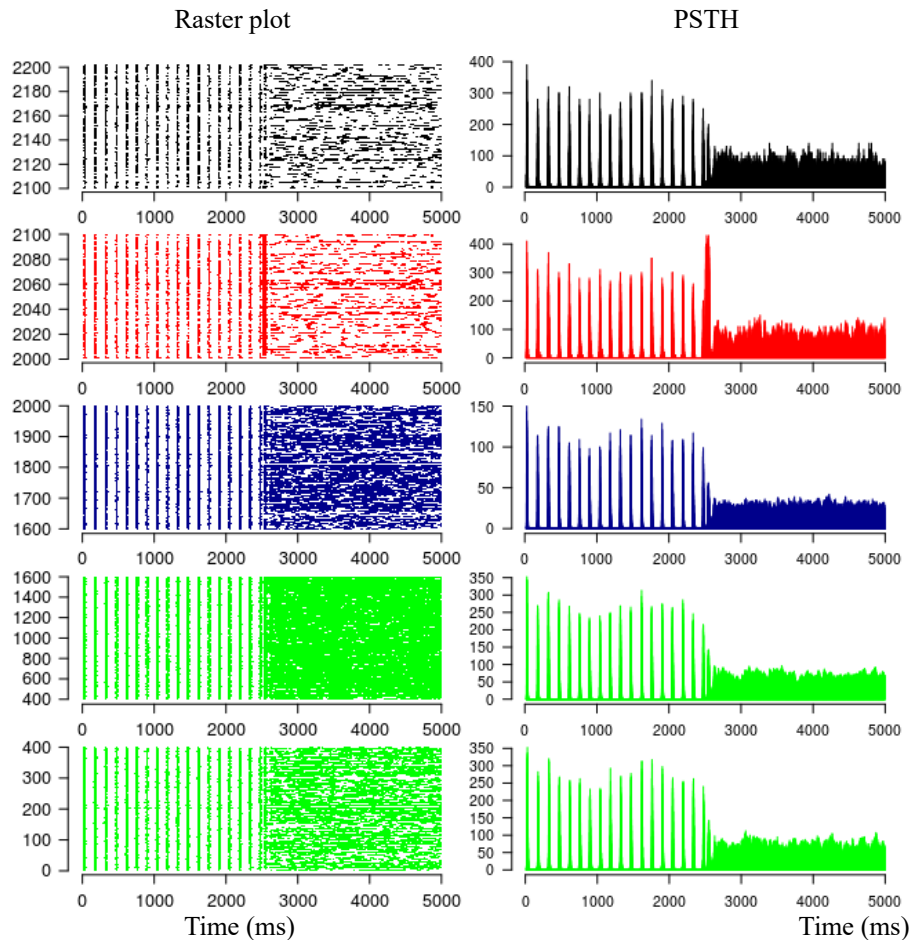


Figure 7.5 Raster plots (left panel) and PSTHs (right panel) of different (colour-coded) neuronal populations in the thalamocortical network model (RE thalamic reticular, TC thalamocortical, IN cortical inhibitory interneurons, PY cortical pyramidal cells). The oscillatory activity during the ictal state is terminated by excitatory AMPAR-mediated CN input to all TC cells (for 50 ms at 2500 ms), which results in earlier spiking in the TC cells and desynchronization of the network.

Stimulation lasted for 50 ms with the scale 20. RE neurons population in black, TC – in red, IN – in blue, PY – in green. The bottom green population is separated based on the fact that the 1 Hz background input comes to the first 400 neurons. The x axis of all plots are measuring the time in milliseconds (ms). The y axis of the raster plots show the id number of neurons, while the y axes of the PSTH show the firing rate in Hz.

It was hypothesised that there could be a difference in the success / failure rate of the CN stimulation, depending on its application time in relation to the phase (at the burst or in between of the bursts). Moreover, such evidence was described in the earlier experimental study (Kros et al., 2015). The peak of the negative deflection on the LFP was accounted for the beginning

of the “wave period” (0°) and the next peak was accounted for its end (360°). The period was also calculated, which was defined as the time between the two adjacent LFP peaks. This “wave period” was shared into sectors so that the time points in between of two negative LFP deflections were considered to be 90° , 180° and 270° , and the CN stimulus was applied at those times. The obtained results were aimed to be compared with experimental results (Kros et al., 2015). The beginning of the “wave period” in experimental study was not at the peak of the ECoG (simulated LFP), but at the peak of PSTH. Therefore, to make the comparison possible the failure rate (Figure 7.9) was plotted for various time points depending on the peak of the peri-stimulus histogram (PSTH). To compare the obtained results with (Kros et al., 2015) the difference between LFP and PHTS peaks were calculated (Figure 7.6). The two adjacent peaks were randomly selected for this purpose. In Figure 7.6 the peaks of the PSTH for cortical neurons were considered to be at 2475 ms and at 2618 ms, accounting for the full cycle, and the period appeared to be 143 ms. While both modelled LFP and PSTH was plotted and compared, the difference in the peak of the burst of LFP and of PSTH appeared to be 8 ms, which accounts for about 20° shift (Figure 7.6). Therefore, one should expect at least 20° difference between modelling and experimental results.

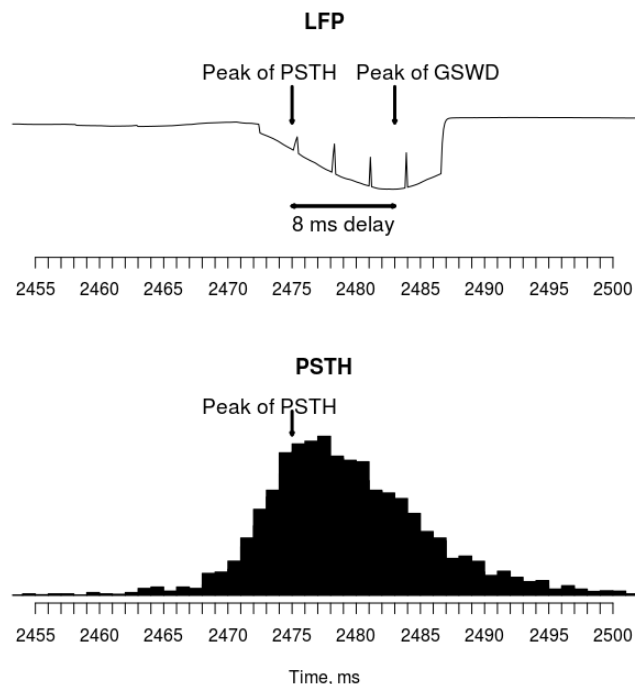


Figure 7.6 Delay in between of the local field potential measured at the superficial cortex and the PSTH recorded from the whole cortex. The delay between PSTH and LFP is 8 ms (about 20°).

As one can see from Figure 7.9, the experimental and modelling results appeared to be shifted for about 30°, which corresponds to the shift of 11.9 ms for the Primary Motor Cortex and twice as much for the Primary Sensory Cortex. 20° difference out of total 30° failure rates discrepancy in modelling and experimental studies are due to the difference in 0° selection (LFP and PSTH). Another 3.9 ms difference might be due to the model approximations.

The irregular input to TC neurons was modelled as jitter (Figure 7.7). Apparently, the excitatory CN stimulus with no jitter was the most successful. Introducing jitter has hardly any effect. It reached the peak of efficiency at 0° and 360°, at the peak of the PSTH bursts. The highest stimulation threshold to terminate epileptiform activity was at 270° (Figure 7.7).

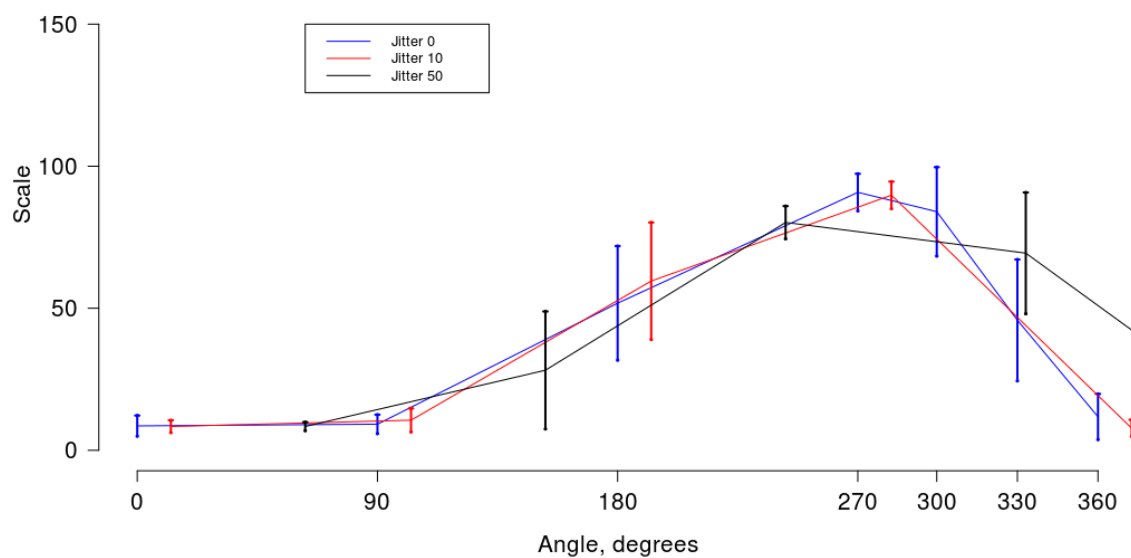


Figure 7.7 The comparison of the stimulation threshold (proportional to failure rate) of inputs with jitter 10 (red line), 50 (black line) and no jitter (blue line), meaning pure excitatory input for different phases from 0° to 360°. The failure rate of seizure termination is the lowest when TC stimulus was applied on the peak of the bursts (the spike discharges). Jitter 10 was shifted to the right of x axes for 5 ms, and jitter 50 was shifted to the right of x axes for 25 ms, so that the centre of the stimulus window coincides with the synchronised input.

When the CN excitatory stimulus was compared with mixed 1:1 excitatory and inhibitory stimulus, which represents the indirect pathways from CN to TC neurons, it showed to be less effective in epileptic seizures termination (Figure 7.8). Excitatory direct CN stimulus with no

jitter appeared to be more successful in comparison to the mixed stimulus (Figure 7.8 A), same with jitter 10 and 50 ms.

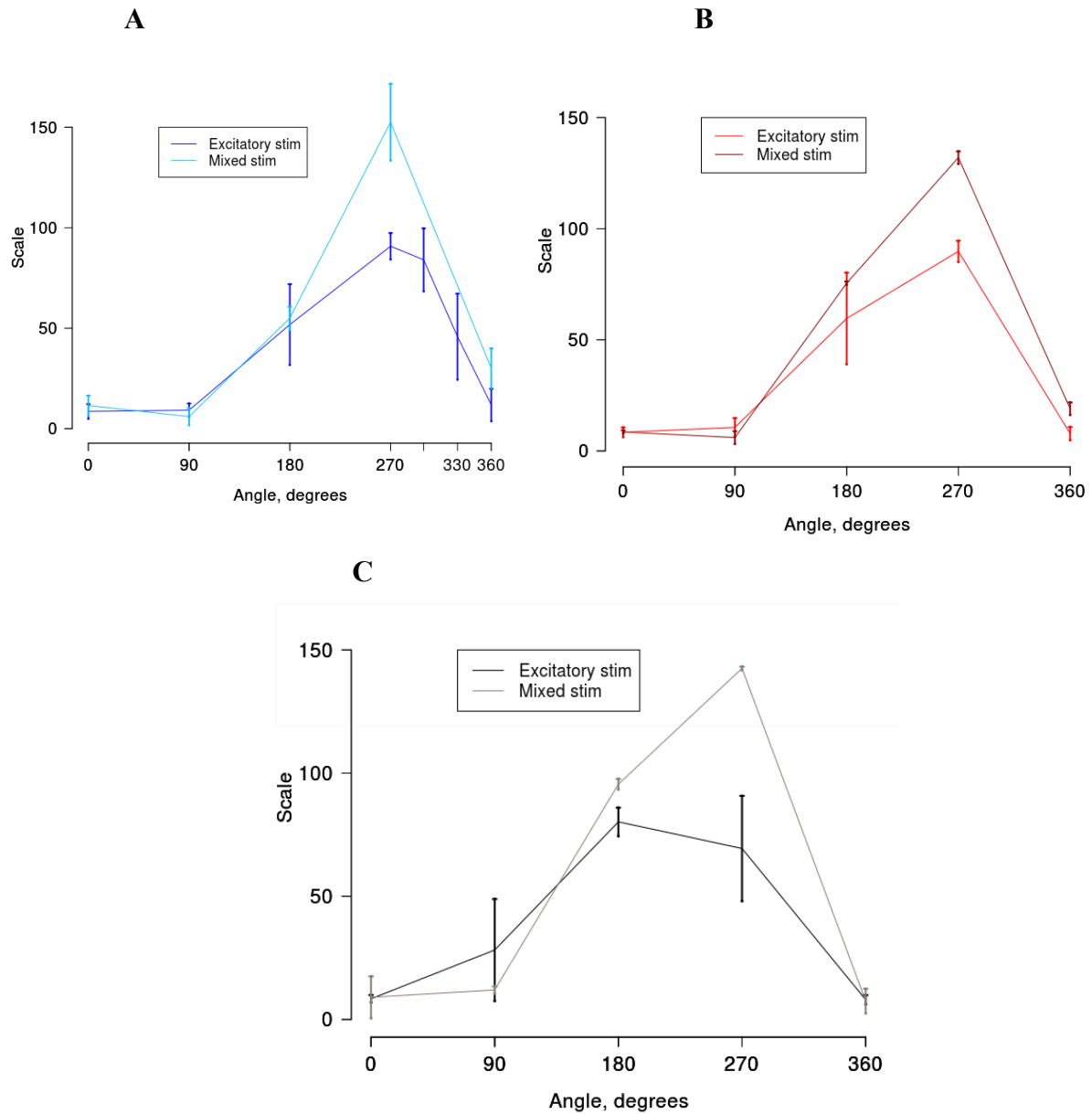


Figure 7.8 Excitatory CN stimulus with various degrees of jitter applied at the peak of the burst of cortical PSTH and after it. The stimulation threshold was measured and plotted for each time point. A: excitatory and mixed stimulus for jitter 0; B: excitatory and mixed stimulus for jitter 10; C: excitatory and mixed stimulus for jitter 50. Excitatory TC stimulus from CN proofed to be more effective then mixed stimulus.

Therefore, I consider that a purely excitatory CN stimulus is more effective in order to terminate seizures than a mixed excitatory/inhibitory stimulus (Figure 7.8 B,C).

7.4 Phase dependence of the CN input in simulations and experiments

After defining the most successful CN stimulus to stop epileptiform activity the comparison of success rates of stimulation with the published experimental results was performed (Figure 7.9). Kros and collaborators (Kros et al., 2015) showed the impact of optical CN stimulation on cortical activity by calculating a success rate of the excitatory stimulus. The modelling output was compared with experimental results for both Primary Motor and Primary Sensory cortices. To make comparison possible, the experimental success rate was converted into failure rate (approximate) based on the figure provided in the paper (Kros et al., 2015; Figure 5C).

The AMPAR-mediated CN stimulus found to be the most effective when applied on the peak of the epileptic burst. It was least effective at 270 – 300 degrees for the modelling study. For the experimental results, the most ineffective time to apply CN stimulus was 300 – 330 degrees for Primary Motor Cortex and 330 – 360 degrees for the Primary Sensory Cortex.

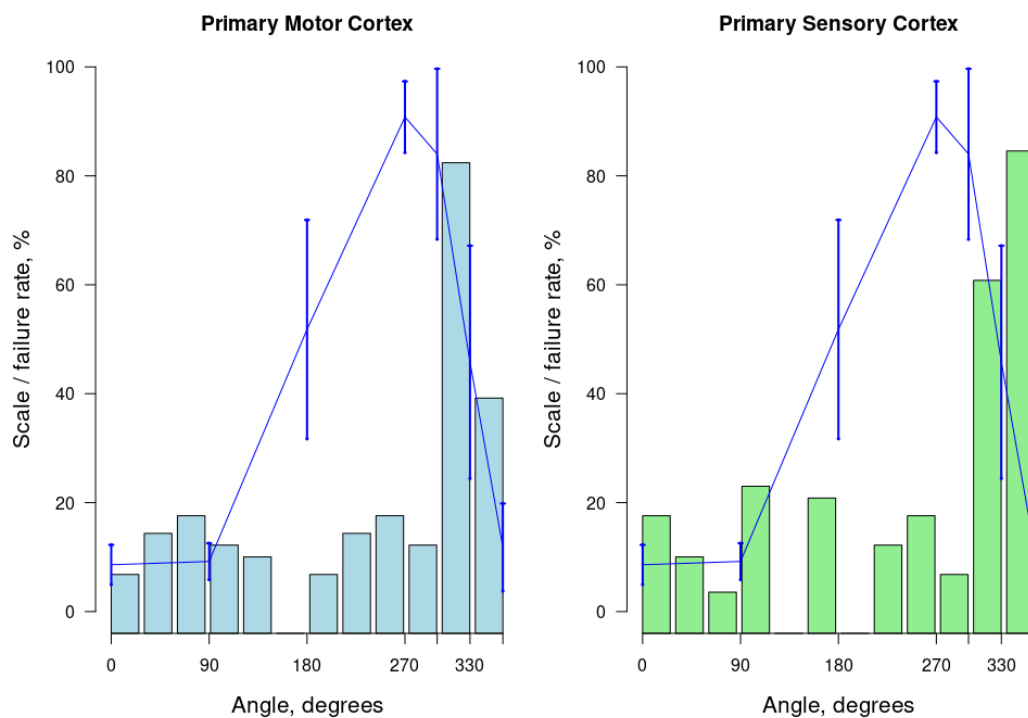


Figure 7.9. Comparison of experimental and modelled AMPA-mediated CN input in seizure termination. CN input proved to be most effective when applied on the peak of the burst for experimental study (lowest failure rate).

To conclude, the ictal state was defined as the state with generalised spike-and-wave discharges. These GSWDs were successfully terminated with the excitatory CN input to TC neurons. The success of the termination was phase-dependent, and depends on stimulus application time relative to the peak of the burst. The most successful termination occurred when AMPA-mediated CN stimulus was applied at the peak of the burst. This result was compared to the experimental study (Kros et al., 2015; Figure 5), which showed very similar, but slightly temporarily shifted results (11.9 ms shift for Primary Motor Cortex). This temporal shift can be explained by the differences of the experimental set-up (8 ms) and by the limitations of the model.

7.5 Phase dependence of spontaneous GSWDs termination as a model of evoked one

A possible approach to study the mechanism underlying the GSWDs termination by CN input is to use a simplified model of this process. One possibility would be to use the spontaneous GSWD termination as a model of evoked termination. For this purpose, the network activity directly preceding spontaneous GSWD terminations was studied. For $\tau_w = 300$ ms, where bistability happens with some probability, the simulation was run a number of times with different seeds. 20 experiments where the GSWDs were terminated spontaneously were considered for further analysis.

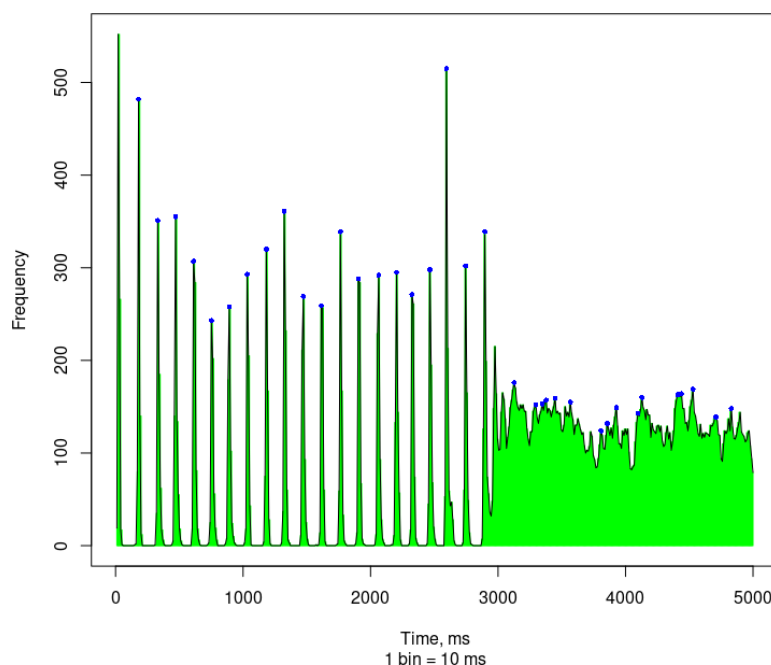


Figure 7.10. ISI histogram of one simulation with a spontaneous GSWDs termination. There are 21 GSWDs before its termination occur. After this point, all blue circles, which are the peaks of GSWDs, are meaningless.

The spike time histogram of each run was plotted, and the peaks of each GSWDs were identified (Figure 7.10, blue circles). The precise time of GSWDs termination was defined as the last spike with the inter-burst-interval of the same duration (normal) as all the previous intervals, where the following interval is of abnormal duration (significantly longer or shorter than the mean of previous intervals).

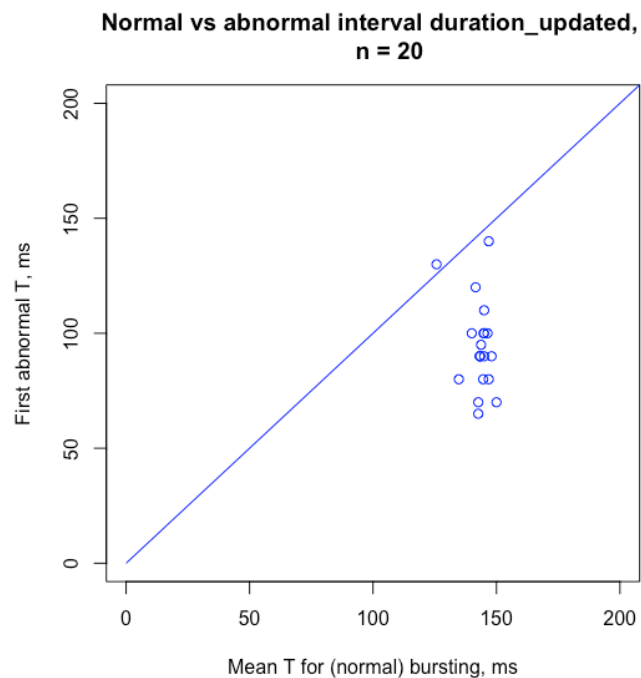


Figure 7.11. First abnormal period as a function of the mean period of normal bursting defining the phase angle of GSWDs, where identity ($y = x$) line is assumed to have a phase of 360 degrees and the x-axis zero degrees.

The phase angle of GSWDs termination can be determined by the slope of the (imaginary) line connecting each data point (Figure 7.11) to the origin, where the identity ($x = y$) line has a phase of 360 degrees (and the x-axis zero degrees). The peaks of GSWDs were stored and the phase of the spontaneous GSWDs termination was calculated. If the data points were arranged on a line through the origin, the phases of spontaneous GSWDs termination would be similar. However, this is not the case here. Therefore, a bar plot was created to further investigate the phase angles of spontaneous GSWDs terminations (Figure 7.12). The pink bars indicate the number of spontaneous GSWDs terminations which occur at a certain phase. In other words, pink bars show a success rate. The blue line is the failure rate from Figure 7.9, showing the required increase in the synaptic weight in order to evoke GSWD termination. The mean phase angle over the all seeds for the spontaneous GSWDs termination is 226.94 degrees

(the most common (successful) time for GSWDs termination. The maximum failure rate for the evoked SGWDs termination is at 270 degrees. Therefore, the two phase angles at peak value almost coincide in time, but they demonstrate opposite scenarios, which makes spontaneous GSWDs termination not a suitable model to study the mechanism of GSWD termination by CN input.

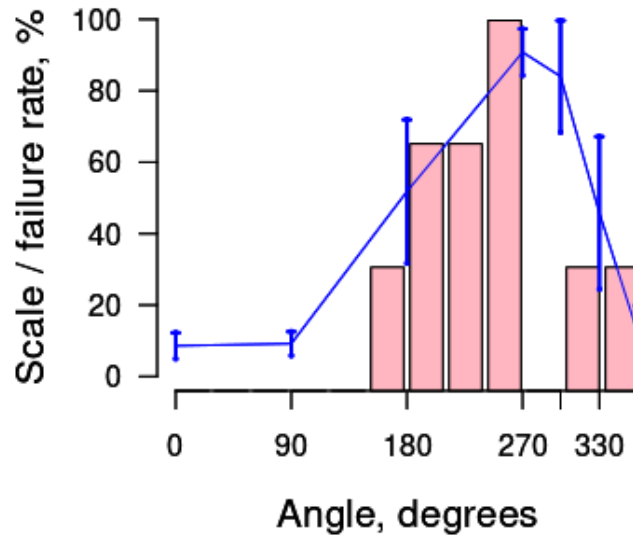


Figure 7.12. Comparison of spontaneous GSWDs terminations and evoked (by AMPA-mediated CN input) GSWD terminations. Same as for Figure 7.9, the CN input is most effective when applied on the peak of the burst, and least effective at 270 degrees, which is the opposite to the spontaneous GSWDs termination.

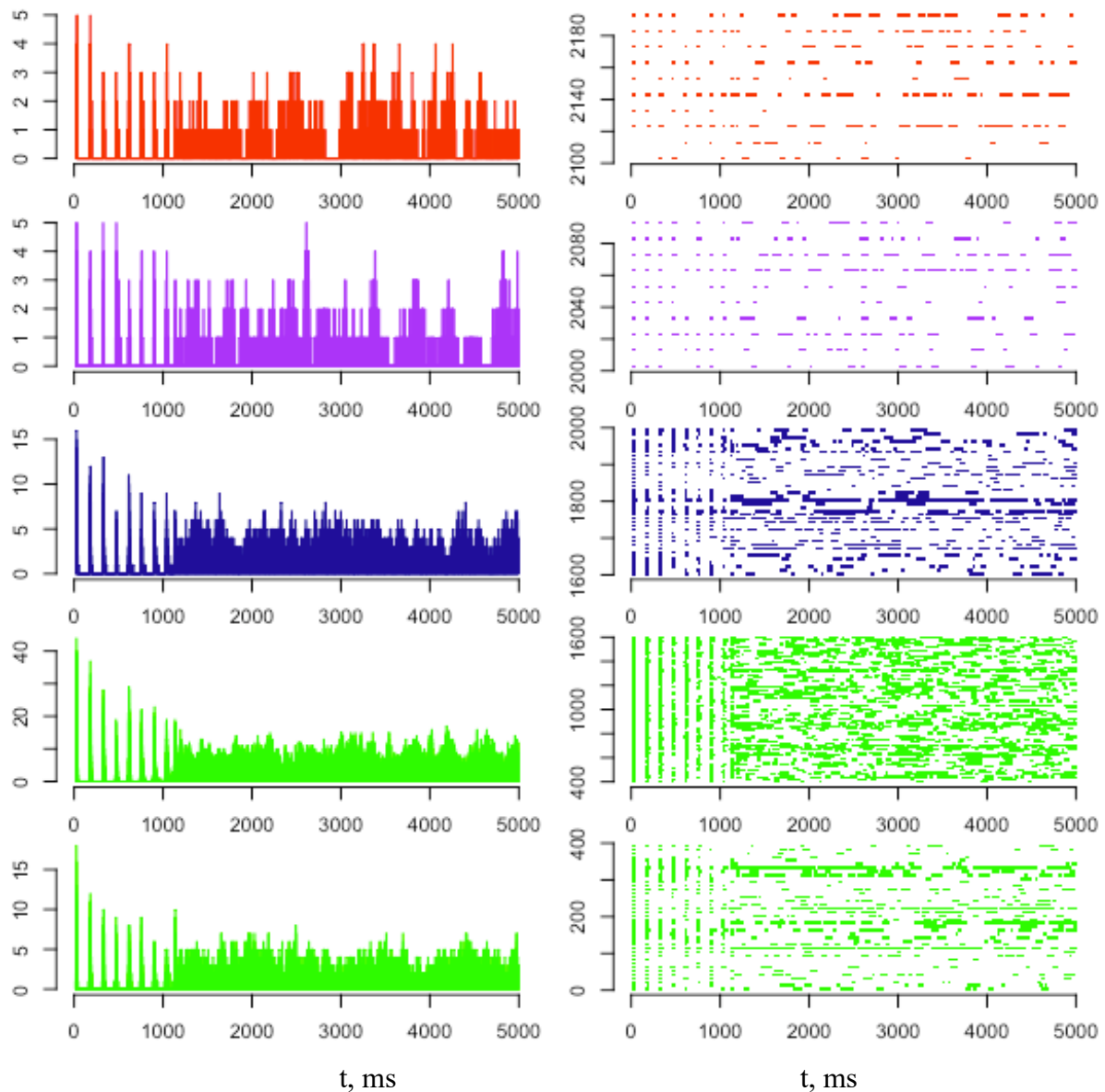


Figure 7.13. PSTHs (on the left) and raster plots (on the right) for each individual population. The spontaneous GSWDs termination occurs after 1000 ms.

In order to explain the mechanism behind the spontaneous GSWDs termination I attempted to plot the PSTHs and raster plots for each individual population (Figure 7.13). The idea was to have a close look at the different neuronal populations to see if the GSWDs termination occurs in all populations at the same time or if one neuronal population is leads and triggers other populations, which might give a clue to the mechanism of this process. Unfortunately, there is no evidence of any neuronal population terminating GSWDs earlier. Further computational studies and experiments should be designed to understand the mechanism underlying both evoked and spontaneous GSWDs terminations.

7.6 Chapter conclusions

Absence seizures can be detected by generalised spike-and-wave discharges (GSWDs) in the electroencephalogram. These GSWDs are based on neuronal oscillations in thalamocortical networks, which can be caused by excessive inhibition in the thalamus or excessive cortical activity.

I simulate a thalamocortical network model with adaptive exponential integrate-and-fire neurons, displaying complex intrinsic properties such as low-threshold spiking, regular spiking, fast spiking and adaptation. The conductance change in the post-synaptic neurons is modelled by alpha synapses. I have driven the network activity to exhibit asynchronous irregular (AI) dynamics, depending on the time constants of the inhibitory synaptic conductance, which are 5 ms (AI) and 15 ms (oscillatory) respectively. An increase in the inhibitory decay time constant reflects a change from GABA_A dominated inhibition to more GABA_B, which can result in GSWDs, given that the “wave” components of GSWDs are related to slow GABA_B - mediated K⁺ currents.

I provide CN input to all thalamocortical neurons to analyse the mechanism of reverting from abnormal oscillatory activity to the normal AI state. The results confirm that input from the CN can control oscillatory activity in thalamocortical networks. Furthermore, they show that the effectiveness of this input exhibits phase-dependence. In our simulations, CN input terminates epileptic absence seizures most effectively when it arrives at the peak of GSWDs, while the least efficiency for seizure termination is observed in between the GSWD bursts. This finding is potentially relevant for therapeutic applications of CN stimulation in closed-loop systems to terminate seizures.

The idea of using the spontaneous GSWDs terminations as a model for evoked ones was considered and researched. Unfortunately, the spontaneous GSWDs termination occur at a phase opposite to the CN-stimulated GSWD termination. Therefore, spontaneous GSWD terminations cannot serve as a model of CN-stimulated GSWDs termination. Further experiments should be designed in order to explain the mechanism underlying the CN-stimulated GSWDs termination.

8

Validation of modelling results using experimental data

Chapter 8 is focused on an analysis of the experimental data from Rotterdam, The Netherlands, and some simulations with experimental data as input that were performed to confirm the results of the modelling study. On top of this, the opposite scenario to absence seizure termination was considered. The attempt to trigger seizures in an interictal network with CN input is discussed.

The initial aim of utilising the experimental data was to answer the following questions:

1. How strong and synchronised should the CN input be to terminate the absence seizures?
2. Could seizures be triggered by CN input?

The raw experimental recordings were originally presented in the form of *.abf file. The program of choice to open these files was AxoGraph. The files contained the spike times in response to the optogenetic stimuli, where the stimuli were time-stamped. There were 39 data files overall (Appendix ii).

When the activity after the stimulus is increased the response type is identified as “excitatory”, when the activity is decreased as “inhibitory” response. The “delayed” and “biphasic” responses are also possible, but will not be considered here for simplicity.

For easy comparison of the modelling to the experimental results, the length of the simulation and the stimuli start times were adjusted. The experimental data were cut 2500 ms at both sides of the stimuli, so that the onset of the optogenetic stimulus was around 2500 ms.

To address the **first aim**, to evaluate the response to the optogenetic stimuli and test the current model by comparing its predictions to the real data, the excitatory (increased) response type was used because it was shown to be the most effective in terminating seizures in the model study. Therefore, the excitatory response from the real data served as CN input to the thalamocortical model and was applied to the TC neurons.

To address the **second aim**, the raw recordings were used as input to the interictal model. As the purpose was to evaluate how strong and synchronized CN neuron input should be to **trigger** seizures in the thalamocortical network, the recordings should be in the “bursting mode”, which is the case for the recordings before the optogenetic activation (as optogenetic activation switches the bursting to asynchronous irregular state). Various factors (scales) applied to the synaptic conductance were tested.

8.1. Experiment 1: modified pre-recorded input to all TC neurons in the ictal network

The factor multiplying the weight of the input from CN to TC is called “scale” in analogy to the modelling study. The minimal possible scale which evokes the phase transition is used. To prove that the scale in use is actually the minimal one, two plots will be shown for each input type: the input with the scale which is high enough to switch off the ictal state, and the one with the scale which is just below the effective one. The CN input is verified to be excitatory.

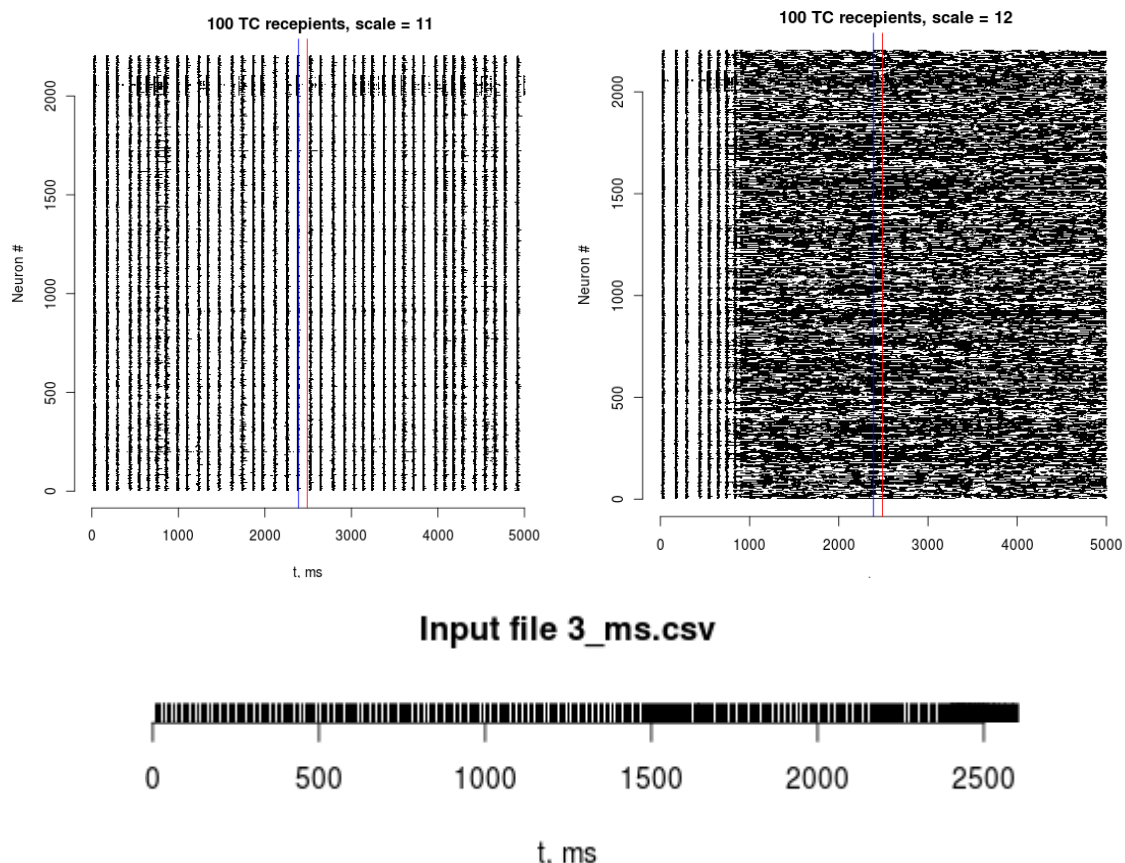


Figure 8.1. Top panel: Evaluation of the required synaptic weight between the CN and TC neurons. Blue and red lines marking the beginning and the end of the optogenetic stimulation.

Please note, that the CN stimulus at the time of the optogenetic activation can not be seen as prominent one at the neurons #2000 – 2100 on the left figure.

The phase shift happens exactly where CN stimulus leads to prominent TC activity (wide densely black lines around 700 ms on the left). Bottom panel: input spike trains from the file 3.1_ms.csv. Optogenetic stimulation occurs at 2408.35 ms.

In the Figure 8.1, the top panel on the left shows the model response to the stimulus with a scale of 11. The output is in the ictal state, and no effect of the input is observed. On the right of the top panel in Figure 8.1, the scale is set to 12, and the phase shift occurs before the optogenetic stimulus arrives (also, it is a response to the elevation of CN activity, which can be seen as dense black lines in TC neurons). The input profile can be seen in Figure 8.1, bottom panel, where a prominent activity around 700 ms is shown. To further evaluate this effect, Figure 8.2 was created.

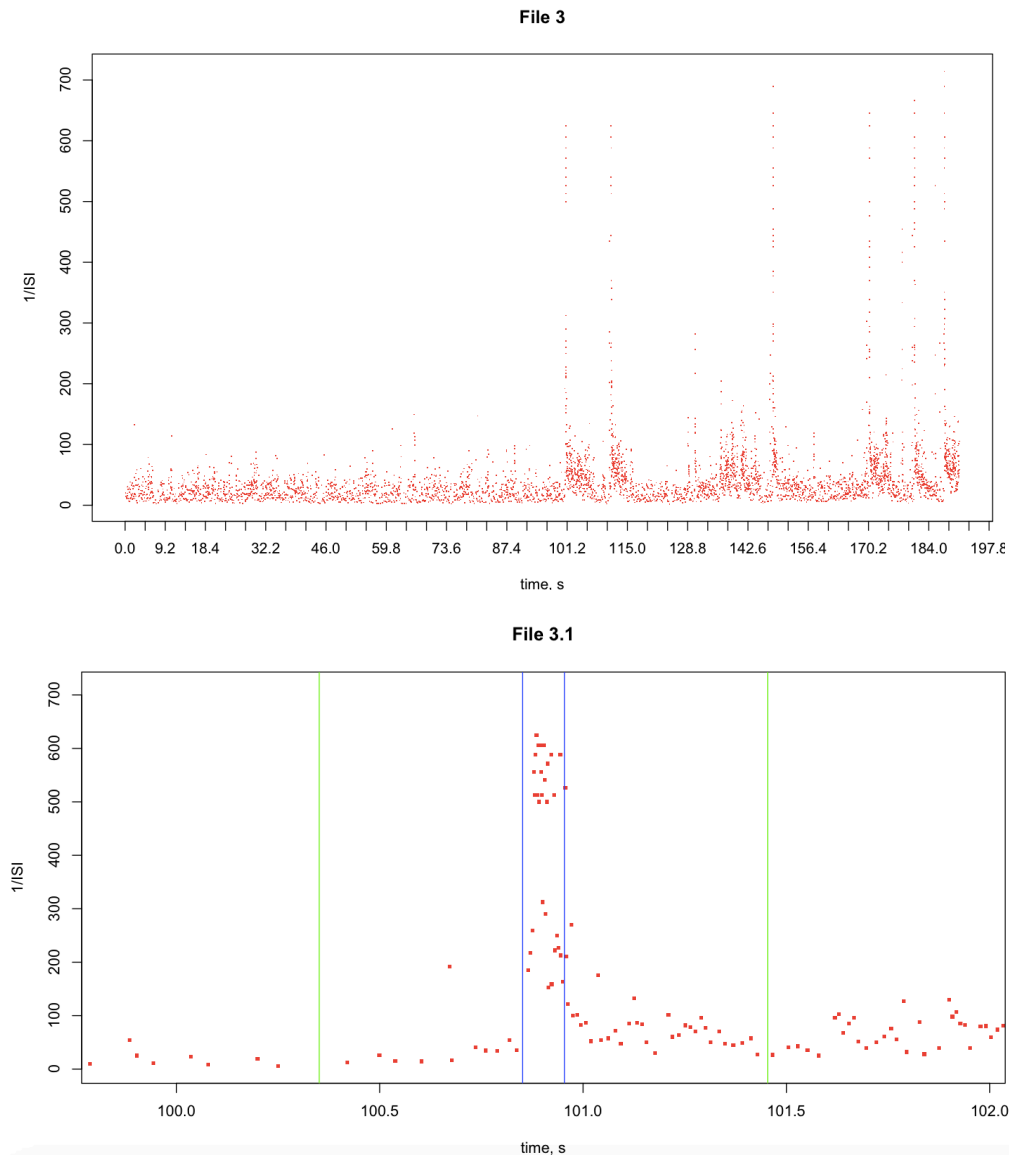


Figure 8.2. Top: the complete recorded real data input file (from *.abf). Bottom: zoom in on the bottom plot. Optogenetic activation is marked with blue vertical lines as part of the input provided to TC neurons.

It was concluded from Experiment 1, that any significant fluctuation in the input, even though it is much smaller than the response to optogenetic activation, can possibly cause the phase transition before the activation occurs. For this reason, the raw data was analysed further in order to find a suitable input which features a strongly increased CN response with a flat baseline activity with minimum fluctuations, so that the phase transition occurs as a response to the optogenetic activation rather than random input fluctuations (Figure 8.3)

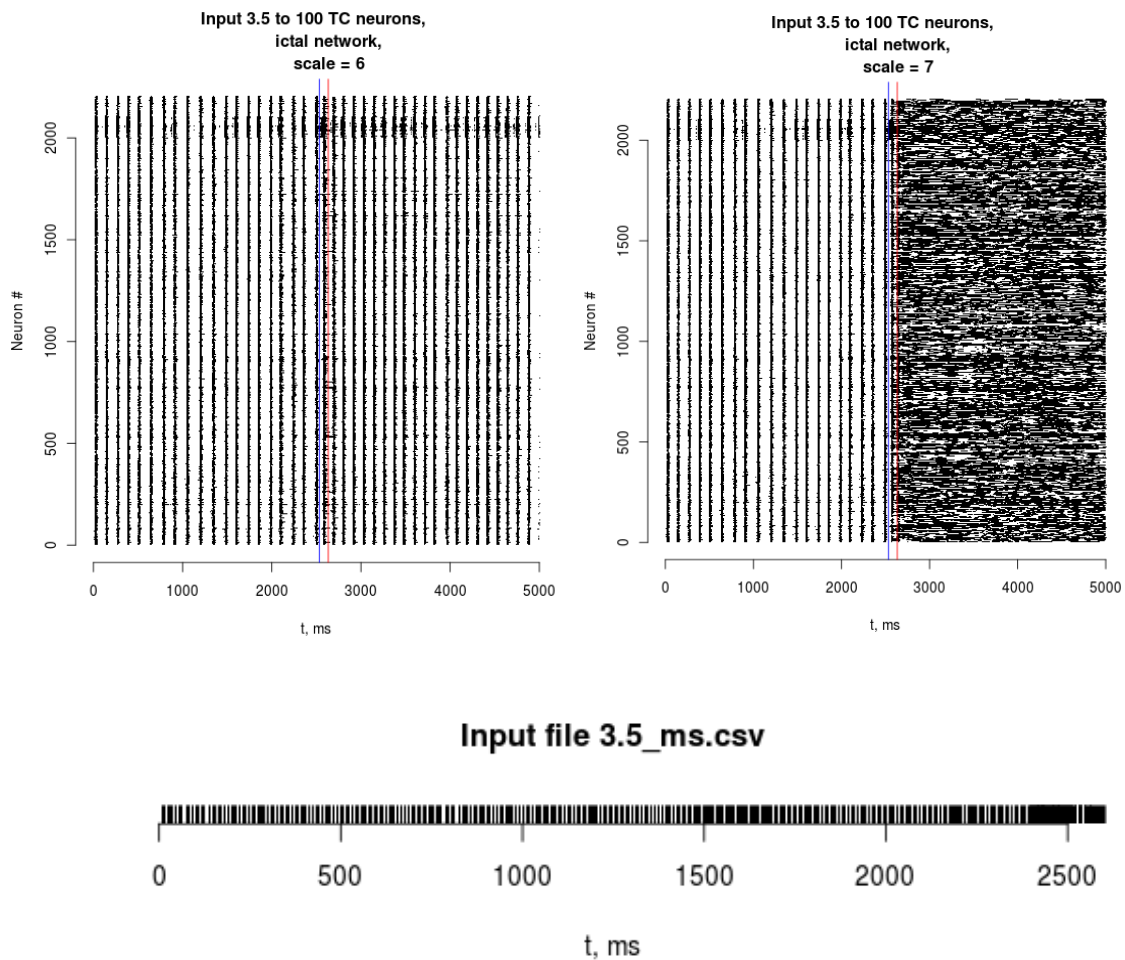


Figure 8.3. Top left: no termination of the ictal activity as a response to the optogenetic stimulation. Please note the strength of CN input at the time of optogenetic activation (dense black line at around 2500 ms). Right: with the increase in scale / stronger input the phase transition happened exactly at the time of the optogenetic stimulation. Bottom panel: input spike trains. Optogenetic stimulation happens at 2532.9ms.

In the previous modelling studies, a constant 1 Hz input was provided to the model throughout the simulation in order to support continuous activity. In these simulations,

the CN input was a strong input applied during 50 ms on top of the background input. The real (experimental) data is not so uniform, because stronger spontaneous activity may occur, which is significantly higher than the baseline activity level. Such real data fluctuations are strong enough to evoke the phase transition. If the aim is to investigate the effect of optogenetic activation, the data before the optogenetic activation should as uniform as possible, without strong spontaneous activity. With the limited number of recordings available it was challenging to find a suitable data file of certain length to match with the modelling settings for easy comparison. However, as shown in Figure 8.3, an excitatory CN stimulus evoked by the optogenetic activation can terminate the simulated absence seizures, which confirms the results of the modelling study. Therefore, further experiments was set up to evaluate if the success of seizure termination depended on the number of the TC neurons receiving CN input.

8.2 Experiment 2: varying the number of TC neurons receiving CN input

Number of TC input recipients	Scale
100	7
50	5
75	7
25	6.5 – 7 *

* Depends on which set of 25 TC neurons is selected.

Table 8.1. Comparison of the scale values required to terminate the ictal state in the thalamocortical network receiving input to a different number of TC neurons (input file 3.5).

The results shown in Table 8.1 are counter-intuitive, because the more neurons receive the input, the easier it should be to elicit an effect. In this case, it was easier to terminate the ictal state by stimulating only half (50) of the TC neurons.

To address the second question set at the beginning of this chapter (could seizures be triggered by providing CN input?), an experiment using the interictal network was performed.

8.3 Experiment 3: could seizures be triggered by CN input?

The experimental recordings of the spike times before the optogenetic stimulation were applied to the network model for 5 s. Different CN-TC synaptic weights (scale) were tested.

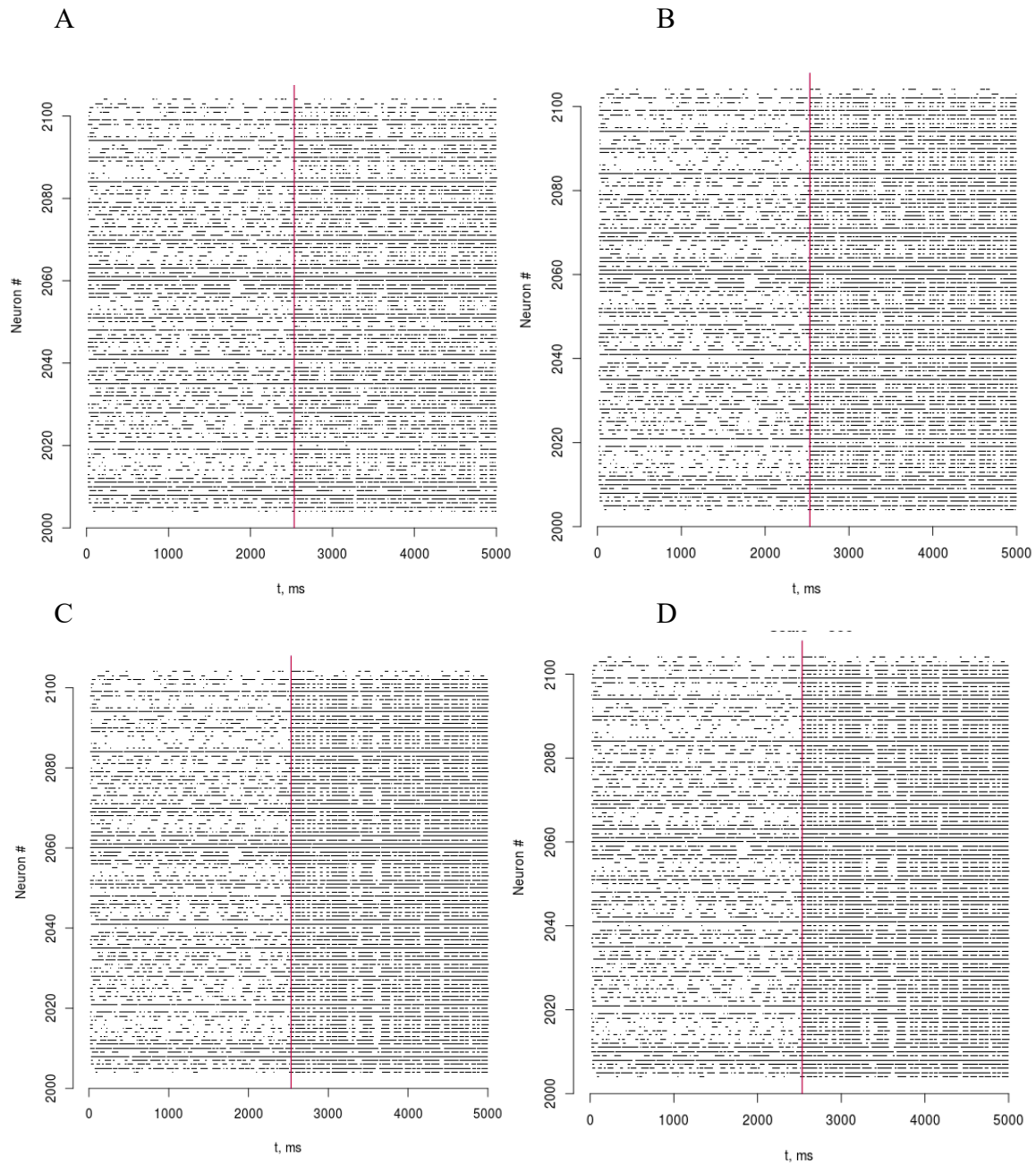


Figure 8.4. Interictal network behavior in response to ictal CN input. The weights of synaptic connections are progressively increased in order to investigate if it is possible to trigger absence seizures with the CN input of some strength. A: scale 50, B: scale 100, C: scale 200, D: scale 500.

From Experiment 3 it is clear that ictal CN input, even very strong one, does not trigger absence seizures. Instead, an entrainment of the network activity to the CN spike trains occurred for all values of synaptic weights tested.

8.4 Chapter Conclusions

- The thalamocortical network is very sensitive to any CN activity fluctuations and resultant TC neuron activity.
- The susceptibility of the network to the CN activity depends on the synaptic conductance scale.
- Pre-recorded excitatory CN input can terminate absence seizures, which confirms the modelling results.
- When evaluating the number of CN – TC connections required to terminate absence seizures, preliminary conclusion would be that the network does not require a stronger CN - TC synaptic weight (a higher scale) to terminate seizures when a smaller number of TC neurons receive CN input (see Table 8.1). For all number of TC neurons receiving CN input apart from 50, the scale required to switch the ictal activity off (scale 7) is roughly the same. There is a drop in the 50 neurons, which might be due to an artefact and might be improved with the number of trials (seeds). This requires further investigation.
- Further work should be done to evaluate the relationship between the phase and the required strength of the recorded CN input.
- Recorded CN input cannot trigger absence seizures, but can entrain the network instead.

9

Discussion

The cerebellum plays an important role in organising the functions of other brain structures. Its nuclei integrate the inhibitory inputs from Purkinje cells and excitatory inputs from mossy and climbing fiber collaterals and provide the main outlet to the rest of the brain, in particular to the thalamus, which serves as a bottleneck for information flow to the cortex, where it relays sensory inputs. However, the mechanisms of information processing in the cerebellum and its contribution to a number of pathologies remain to be elucidated. In this thesis, I have used computational modelling to investigate the contribution of the cerebellum to pathologies, in particular to downbeat nystagmus and absence epilepsy, and attempted to describe the mechanisms underlying them, in order to be able to propose possible treatment.

To understand the mechanism underlying downbeat nystagmus, a biologically detailed conductance-based model of a floccular target neuron (FTN) was used. The FTN neuron response to spike trains from tottering (tg/tg) and wild-type PCs was investigated in detail. Previously (Luthman et al, 2011) described a contribution of STD to the translation of input irregularity into output spike rate. I replicated these results of the effect of STD, which was demonstrated using individual conductance traces of one of the 450 GABA_A synapses. In principle, this would also have been possible with a simpler model such as a leaky integrate and fire or an AdEx model with 450 separate synapses. However, the detailed model was chosen to investigate the contribution of other intrinsic neuronal mechanisms, such as specific ion channels or calcium dynamics. The intrinsic properties of the FTN neuron are not significant for the current study, but they can be examined in the future. The population response was also reconstructed from individual synaptic conductance to understand why irregular spike trains injected less inhibitory conductance into the CN neuron than regular trains and why this decrease depended on STD. Tottering spike trains had a larger proportion of short ISIs, which led to a stronger STD of the inhibitory synaptic conductance. In this way, STD selectively cut off higher frequency components of the input spike trains, effectively acting as a low-pass filter. Wild-type spike trains had a smaller proportion of short ISIs and therefore were less affected by the low-pass filtering effect of STD, which resulted in less reduced PC-FTN synaptic conductance and smaller depression. The reduced GABA_A conductance in response to irregular spike trains in the presence of STD led to a higher CN firing rate than the regular trains with and without STD. As a consequence, the accelerated CN neuron firing rate in response to the increased irregularity of the tottering spike trains can be explained by the STD-dependent decrease of GABA_A conductance at high PC-FTN convergence ratios. However, the accelerated CN neuron firing rate in response to tottering PC input did not depend on STD for convergence ratio of 1. The irregularity-based acceleration of firing rate for one-

to-one PC-FTN connections might be explained by the involvement of other mechanisms such as the existence of longer periods without PC inhibition (Luthman et al., 2011).

STD is a form of synaptic plasticity caused by the depletion of neurotransmitters in the presynaptic neurons. The changes caused by STD decay to baseline in order of milliseconds. Due to STD neurons can adjust the strength of their responses depending on the input frequencies (Abbott et al., 1997), giving the postsynaptic neuron an increased sensitivity to lower-frequency input strengthening the synaptic weight. Higher-frequency input rapidly deactivates the synapse. Dynamical synapses such as PC-FTN synapses display low-pass filtering properties. In the FTN neuron model STD is assumed to be caused by the decreased probability of presynaptic transmitter release (Shin et al, 2007), which makes the conductance evoked by a synaptic input dependent on the prior input firing rate.

It was recently shown, that synapses can adjust their energy expenditure and optimize the energy-information rate balance. This can be achieved by changing the dynamics of STD. Stronger depression and slower recovery will preserve metabolic energy and decrease the release probability. In this way the parameters of STD define the information-energy flow in neurons. Thus, increasing the STD level will decrease both the information rate and the energy consumption of the synapse at the release site. It was shown by Salmasi et al (2019) that when the release of neurotransmitters is asynchronous and associated with the noise in release, the effect of STD would be greater than from the synchronous release associated with the signal component of release. The signal to noise ratio of the release site can be enhanced by STD. Moreover, Salmasi and collaborators demonstrated that in the cases when synchronous spike-evoked release is depressed less or recovers faster than the asynchronous release, STD can enhance the information transmission. In the cases where the dynamics of synchronous and asynchronous releases are the same, STD decreases the information rate of the release site and preserves the energy. STD is one of the mechanisms that contributes to temporal selectivity.

Thus, STD is shown to be an important mechanism in the effect of 4-AP on treating DBN. The regularisation of Purkinje cell input with 4-AP is expected to have a beneficial effect on nystagmus occurrence by stabilizing gaze holding. To study this hypothesis at a systems level it might be possible to use the eye-movement model by (Glasauer et al, 2008) to construct a population response by utilising the output from the cellular model as an input to the system-level model. This will help to predict the respective eye movements during DBN and after 4-AP treatment, as described in (Glasauer et al, 2008). Also, since it was shown that STD is the link between irregularity and firing rate, which leads to nystagmus, it would be logical to

suggest that blocking STD might prevent nystagmus. This needs to be confirmed by further experiments.

As for the model limitations, the mutation that is characteristic for tg/tg leads to plenty of physiological and morphological alterations compared to wild-type, which is not accounted for in this model. The same CN model was used for both tg/tg and wild-type cases, without changing synaptic characteristics for tg/tg. There are other factors which can also affect CN firing rate, such as the use of anaesthesia, which also was not accounted for.

To understand the mechanism of the termination of absence seizures by CN stimulation, a network model based on single-compartment spiking neurons - Adaptive Exponential Integrate-and-fire models - was chosen after a long set of trials and errors described in Chapter 3. I simulate a thalamocortical network model with adaptive exponential integrate-and-fire neurons, because with appropriate parameter values it can reproduce up to 96% of spike-times of a regular - spiking Hodgkin-Huxley-type model (Brette and Gerstner, 2005). Also, this model can reproduce most of the known electrophysiological features, while focusing on the interactions between large network populations, which is the perfect compromise between the computational cost and level of details. The model displays complex intrinsic properties such as low-threshold spiking, regular spiking, fast spiking and adaptation. The conductance change in the post-synaptic neurons is modelled by alpha synapses. This model cannot reproduce the effect of pharmacological manipulations such as specific ion channel blocking, but this was anyway out of the project scope. Of course, the use of an isolated network brings bias to the results, as the effect of other elements of the real network are not accounted for. For example, the TC neurons were stimulated externally by the CN input, and this input is excitatory only. In a real life scenario there are many types of stimulation possibilities. I have tried to address some of them by investigating the effect of jitter and other input types, such as inhibitory and biphasic, but there are much more possibilities. The CN input can be also formed from a mixed excitatory-inhibitory stimuli of various proportions. Another model limitation is caused by the brain background activity. The ongoing activity in the model is sustained by 1 Hz constant input, which is obviously not the case for real brain background activity. Also, the exact proportion of TC neurons receiving CN input might be dynamic depending on the circumstances.

I have found that depending on the time constants of the inhibitory synaptic conductance, the model can show different dynamics and be in various states, such as asynchronous-irregular for 5 ms and oscillatory for 15 ms. An increase in the inhibitory decay time constant reflects a

change from GABA_A dominated inhibition to more GABA_B, which can result in GSWDs, given that the “wave” components of GSWDs are related to slow GABA_B - mediated K⁺ currents. Also, depending on tau_w, the model can show bistability, displaying either bursting or asynchronous irregular state or spontaneous GSWDs termination.

I provide CN input to all thalamocortical neurons to analyse the mechanism of reverting from abnormal oscillatory activity to the normal AI state. The obtained results clearly show that the input from the CN can indeed control oscillatory activity in thalamocortical networks. Moreover, it has been shown that it is more effective to provide the CN input at the peak of the GSWD, and it is least effective in resetting oscillatory activity while provided in the middle of the bursts, displaying phase-dependence. This finding potentially may increase the efficacy of therapeutic applications of CN stimulation and optimise it in closed-loop systems for terminating the seizures.

If the model findings could be extrapolated to other types of epilepsy, where more serious treatment options would be considered, then possible clinical application of this model could be deep brain stimulation. The most common region for its application is the anterior thalamic nucleus stimulation. Intracranial deep brain stimulation is a very promising relatively new method of alleviation of the various neurologic diseases symptoms. Among them, the most established is Parkinson’s disease treatment. For epileptic patients, Cooper et al pioneered in the cerebellar (cortex) stimulation in 1974 (Cooper et al., 1974).

As shown in this thesis, CN stimulation has a powerful deoscillating effect on the ictal thalamocortical network, so it is likely that CN stimulation will also have an alleviating effect in more severe kinds of intractable epilepsy. There are studies where DBS is applied to deep CN (Vedam-Mai et al., 2016), which might be a preferred region of stimulation to treat epilepsy. Vedam-Mai et al (2016) applied deep CN stimulation to ataxic mice (ataxia, along with the cortical spike-and-wave discharges, is the symptom exhibited by tg/tg mutants, who are the model for absence seizures) and observed marginal improvement in their stride. Further investigations are required to establish to what extent these findings for ataxia and absence epilepsy can be utilised to treat other types of seizures because absence epilepsy will unlikely be considered for such an intervention as deep brain stimulation due to its benign nature (Kros et al, 2015). Also, further investigations are required to confirm these initial observations and establish the frequency and duration of the stimulus application.

10

Conclusions

10.1 Summary of the results: findings and limitations

I was investigating the mechanisms underlying cerebellar contribution to two pathologies: nystagmus and absence epilepsy.

As a result of detailed single neuron modelling, I have proposed the mechanism of STD contribution to the synaptic conductance on the PC – FTN firing rate, which explains previous modelling results inconsistency (Glasauet et al 2011, Glasauer and Rossert, 2008) with experimental data (Alvina and Khodakhah, 2010). In particular, I have shown that irregular pathological PC input trains seen during DBN lead to increased depression of the synaptic conductance, a decreased total inhibitory conductance injected into FTN neuron, higher FTN firing rate (6 versus 4 spikes with and without STD respectively), disregarding the synchronicity level. Accelerated FTN firing rate results in nystagmus symptoms. When the PC input was regularised with 4-AP, FTN firing was decelerated and no nystagmus symptoms should be observed. These explanation is in line with the experimental findings (Alvina and Khodakhah, 2010).

As a result of a AdEx network ensembles modelling, I can conclude that the network can switch its dynamics depending on the inhibitory synaptic conductance. Thus, when the inhibitory time constant of 5 ms, the network exhibits AI behaviour. When it is set to 15 ms, the network shows GSWDs dynamics, which is characteristics of absence epilepsy. Such a dramatic change in the network dynamics can be explained on the basis of GABA-mediated inhibition. Thereby, elevation of the inhibitory time constant corresponds to the shift from GABA_A-dominated inhibition to slow GABA_B-mediated K⁺ currents (wave of GSWDs, Destexhe, 1998). My simulation results substantiate that CN can control oscillatory activity in thalamocortical networks. Moreover, the potency of CN input displays phase-dependence. According to my simulations, the absence seizure termination is the most effective when CN input arrived at the peak of GSWDs, while the effectiveness is low between the GSWD bursts. These findings could be applied in therapy of absence epilepsy, using deep brain stimulation, in particular, in CN stimulation to terminate seizures.

10.2 Open questions and future directions

The role of the cerebellum in motor diseases is well established. It is well known that cerebellar lesions cause motor deficits and discoordination of movements. Recently the scientific community became interested in non-motor diseases caused by cerebellar dysfunction (Reeber et al., 2013). As some of the cerebellar functions are cognition and emotions, which implied by its architecture and connectivity, impairment in cerebellum would lead to disruption of these functions. It would be interesting to widen the range of pathologies caused by cerebellar dysfunction from the motor to non-motor. One of the most interesting non-motor pathologies is an autism spectrum disorder (Fatemi et al., 2012), which might even be associated with epilepsy (Levisohn, 2007).

Two models that detailed in this Thesis describe cerebellum: biologically detailed single neuron model of downbeat nystagmus (FTN model of downbeat nystagmus) and thalamus interconnected with the cortex (AdEx thalamocortical model of absence epilepsy). The possible extension of this work would be the incorporation of the cerebellar nucleus into the existing thalamocortical AdEx network model to study cerebellar-thalamocortical loops, which might be involved in different pathological conditions, such as essential tremor (Tröster et al., 2002), primary generalized dystonia (DeLong and Wichmann, 2012), progressive supranuclear palsy (Brusa et al., 2014) and others.

There are two possible ways to address the limitations of the current version of the thalamocortical network model. The easier one would be to research in greater details the biphasic response type of the thalamocortical part of the network to CN stimuli. Biphasic (excitatory and inhibitory) response type might serve as a model of mixed input from CN neurons and other structures, such as zona incerta for instance (Figure 10.1). Another way follows.

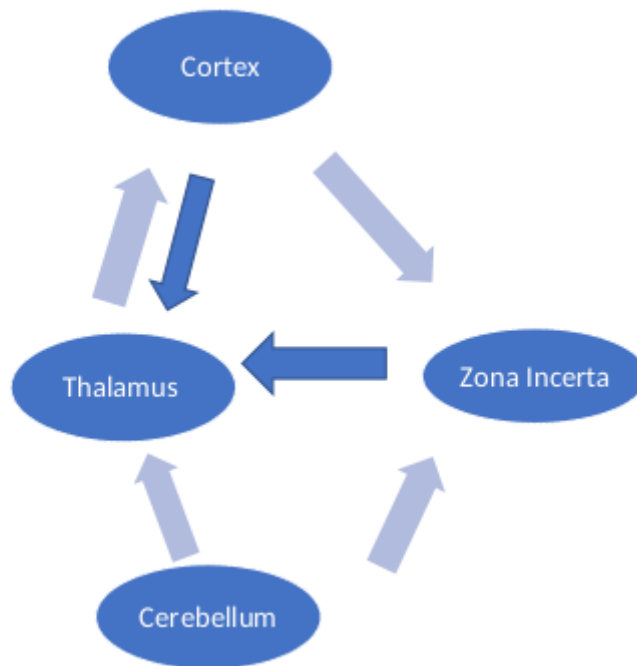


Figure 10.1. Schematic representation of thalamocortical network and subthalamus (zona incerta).

In experimental *in vivo* research (Kros et al., 2015), it was shown that thalamic neurons respond to CN stimulation in various ways. The majority of them (61%) responded with increased firing, which was successfully reproduced with the help of thalamocortical model modified from (Destexhe, 2009). 9.5 % of neurons responded with the increased firing rate, and 11.5 % of neurons displayed a delayed response, which were successfully reproduced in this Thesis. However, 10.3% of responses was not possible to model with the set of parameters described above in the thesis. A possible explanation to this might be that thalamic neurons respond in biphasic way not to the CN stimulus but to the stimulation from basal forebrain (Beierlein, 2014), which is not modelled in the Thesis. Thalamic circuit activities that formed of thalamocortical and reticular thalamic neurons are shown to be regulated by a number of afferent systems. One of them are cholinergic efferent projections from basal forebrain, which target the RE nucleus, which inhibits TC neurons. TC neurons are showed to be expressing muscarinic acetylcholine (ACh) receptors which block Potassium currents upon their activation (Bista et al., 2012) and a resting membrane potential depolarization due to activation of nicotinic ACh receptors. This depolarization happens due to the T-type Ca^{2+} -channel inactivation (McCormick & Bal, 199) and promotes a switch from bursting to tonic firing

(Beierlein, 2014). RE neurons also have both nicotinic and muscarinic ACh receptors, however, the effect of their activation on the membrane potential appears to be opposite. In particular, after the fast nicotinic AChR-mediated depolarization, the long-lasting muscarinic AChR-mediated hyperpolarization follows (Hu et al. 1989b), which is a biphasic response. Therefore, the input from basal forebrain leads to the RE neuronal inhibition, which on its turn, leads to the disinhibition of TC neurons and to switch into tonic firing mode from bursting. Therefore, the current AdEx model could be able to reproduce the biphasic input if the external stimulation would slowly inhibit the RE nucleus, simulating the input from the basal forebrain. The parameters of the external input should be adjusted in such a way that the input is simulated both muscarinic and nicotinic ACh afferents from basal forebrain.

10.3 List of publications

- Julia Goncharenko, Lieke Kros, Reinoud Maex, Neil Davey, Christoph Metzner, Chris I. De Zeeuw, Freek E. Hoebeek, and Volker Steuber. Phase dependence of the termination of absence seizures by cerebellar input to thalamocortical networks. *BMC Neuroscience*, 20:157, 2019.
URL: <https://bmcneurosci.biomedcentral.com/articles/supplements/volume-20-supplement-1>, doi:10.1186/s12868-019-0538-0.
- J. Goncharenko, L Kros, N Davey, C Metzner, C De Zeeuw, and V Steuber. Modulation of epileptic activity in thalamo-cortical networks by input from the cerebellar nuclei. In *BMC Neuroscience*, 18(Suppl.1). 2017.
URL: <https://bmcneurosci.biomedcentral.com/articles/10.1186/s12868-017-0370-3>.
- Julia Goncharenko, Neil Davey, Volker Steuber, and Maria Schilstra. The role of cerebellar short-term synaptic plasticity in the pathology and medication of downbeat nystagmus. *BMC Neuroscience*, 17(1):P51, 2016.
URL: <http://dx.doi.org/10.1186/s12868-016-0283-6>, doi:10.1186/s12868-016-0283-6.

Bibliography

Abadi R. V., 2002. Mechanisms underlying nystagmus. *Journal of the Royal Society of Medicine*, 95(5), pp.231–234. doi:10.1258/jrsm.95.5.231

Abbott, L.F., Varela, J.A., Sen, K. and Nelson, S.B., 1997. Synaptic depression and cortical gain control. *Science*, 275(5297), pp.221-224.

Alviña, K. and Khodakhah, K., 2010. The therapeutic mode of action of 4-aminopyridine in cerebellar ataxia. *Journal of Neuroscience*, 30(21), pp.7258-7268.

Anchisi, D., Scelfo, B. and Tempia, F., 2001. Postsynaptic currents in deep cerebellar nuclei. *Journal of Neurophysiology*, 85(1), pp.323-331.

Andersen, B.B., Korbo, L. and Pakkenberg, B., 1992. A quantitative study of the human cerebellum with unbiased stereological techniques. *Journal of Comparative Neurology*, 326(4), pp.549-560.

Azevedo, F.A., Carvalho, L.R., Grinberg, L.T., Farfel, J.M., Ferretti, R.E., Leite, R.E., Jacob Filho, W., Lent, R., and Herculano-Houzel, S., 2009. Equal numbers of neuronal and nonneuronal cells make the human brain an isometrically scaled-up primate brain. *J. Comp. Neurol.* 513, pp.532–541.

Bal, T., Debay, D. and Destexhe, A., 2000. Cortical feedback controls the frequency and synchrony of oscillations in the visual thalamus. *Journal of Neuroscience*, 20(19), pp.7478-7488.

Barthó, P., Slézia, A., Varga, V., Bokor, H., Pinault, D., Buzsáki, G. and Acsády, L., 2007. Cortical control of zona incerta. *Journal of Neuroscience*, 27(7), pp.1670-1681.

Bastian, A.J., 2011. Moving, sensing and learning with cerebellar damage. *Current opinion in neurobiology*, 21(4), pp.596-601.

Beierlein M., 2014. Synaptic mechanisms underlying cholinergic control of thalamic reticular nucleus neurons. *The Journal of Physiology* 592(19), pp.4137-4145.

Berg, A.T., Shinnar, S., Levy, S.R. and Testa, F.M., 1999. Newly diagnosed epilepsy in children: presentation at diagnosis. *Epilepsia*, 40(4), pp.445-452.

Best & Taylor, "The living body", fourth edition, 1965, chapter 12: The central nervous system, *The Brain or Encefalon*, pp 529 - 533

Birdno, M.J., Kuncel, A.M., Dorval, A.D., Turner, D.A., Gross, R.E. and Grill, W.M., 2011. Stimulus features underlying reduced tremor suppression with temporally patterned deep brain stimulation. *Journal of neurophysiology*, 107(1), pp.364-383.

Bista P., Meuth S.G., Kanyshkova T., Cerina M., Pawlowski M., Ehling P., Landgraf P., Borsotto M., Heurteaux C., Pape H.C., Baukrowitz T. & Budde T., 2012. Identification of the muscarinic pathway underlying cessation of sleep-related burst activity in rat thalamocortical relay neurons. *Pflugers Arch* 463, pp.89–102.

Blumenfeld, H. and McCormick, D.A., 2000. Corticothalamic inputs control the pattern of activity generated in thalamocortical networks. *Journal of Neuroscience*, 20(13), pp.5153-5162.

Brette, R. and Gerstner, W., 2005. Adaptive exponential integrate-and-fire model as an effective description of neuronal activity. *Journal of neurophysiology*, 94(5), pp.3637-3642.

Brusa, L., Ponzo, V., Mastropasqua, C., Picazio, S., Bonni, S., Di Lorenzo, F., Iani, C., Stefani, A., Stanzione, P., Caltagirone, C. and Bozzali, M., 2014. Theta burst stimulation modulates cerebellar-cortical connectivity in patients with progressive supranuclear palsy. *Brain stimulation*, 7(1), pp.29-35.

Campbell, D.B. and Hess, E.J., 1999. L-type calcium channels contribute to the tottering mouse dystonic episodes. *Molecular pharmacology*, 55(1), pp.23-31.

Catterall, W.A., Striessnig, J., Snutch, T.P. and Perez-Reyes, E., 2003. International Union of Pharmacology. XL. Compendium of voltage-gated ion channels: calcium channels. *Pharmacological reviews*, 55(4), pp.579-581.

Clark, D.A, Mitra P.P. and Wang S.S.-H., 2001. Scalable architecture in mammalian brains. *Nature*, 411, 189-193.

Cooper I.S., Amin I., Gilman S., Waltz J.M., 1974. The Effect of Chronic Stimulation of Cerebellar Cortex on Epilepsy in Man. In: Cooper I.S., Riklan M., Snider R.S. (eds) *The Cerebellum, Epilepsy, and Behavior*. Springer, Boston, MA.

Courchesne, E., Townsend, J., Akshoomoff, N.A., Saitoh, O., Yeung-Courchesne, R., Lincoln, A.J., James, H.E., Haas, R.H., Schreibman, L. and Lau, L., 1994. Impairment in shifting attention in autistic and cerebellar patients. *Behavioral neuroscience*, 108(5), p.848.

Crunelli, V. and Leresche, N., 2002. Childhood absence epilepsy: genes, channels, neurons and networks. *Nature Reviews Neuroscience*, 3(5), pp.371-382.

D'Angelo, E. & Casali, S., 2012. Seeking a unified framework for cerebellar function and dysfunction: From circuit operations to cognition. *Frontiers in neural circuits*, 6. p.116.

Davison, A.P., Brü derle D, Eppler J, Kremkow J, Muller E, Pecevski D, Perrinet L, Yger P. 2008. PyNN: a common interface for neuronal network simulators. *Frontiers in Neuroinformatics*, 2(11).

Davison, A.P., Hines, M. and Muller, E., 2009. Trends in programming languages for neuroscience simulations. *Frontiers in neuroscience*, 3, p.36.

Davison A, Porting a model from NEURON to PyNN: a case study, 2017; <http://andrewdavison.info/notes/porting-NEURON-PyNN/>, accessed 1 January 2020

DeLong, M. and Wichmann, T., 2012. Deep brain stimulation for movement and other neurologic disorders. *Annals of the New York Academy of Sciences*, 1265, p.1.

Destexhe, A., Bal, T., McCormick, D.A. and Sejnowski, T.J., 1996. Ionic mechanisms underlying synchronized oscillations and propagating waves in a model of ferret thalamic slices. *Journal of neurophysiology*, 76(3), pp.2049-2070.

Destexhe, A., 2008. Corticothalamic feedback: a key to explain absence seizures. In *Computational neuroscience in epilepsy*, pp.184-214.

Destexhe, A., 2009. Self-sustained asynchronous irregular states and up-down states in thalamic, cortical and thalamocortical networks of nonlinear integrate-and-fire neurons. *Journal of computational neuroscience*, 27(3), p.493.

Destexhe, A., 1999. Can GABAA conductances explain the fast oscillation frequency of absence seizures in rodents?. *European Journal of Neuroscience*, 11(6), pp.2175-2181.

Destexhe, A., Contreras, D. and Steriade, M., 1998. Mechanisms underlying the synchronizing action of corticothalamic feedback through inhibition of thalamic relay cells. *Journal of neurophysiology*, 79(2), pp.999-1016.

Destexhe, A. and Sejnowski, T.J., 1995. G protein activation kinetics and spillover of gamma-aminobutyric acid may account for differences between inhibitory responses in the hippocampus and thalamus. *Proceedings of the National Academy of Sciences*, 92(21), pp.9515-9519.

Destexhe, A., Contreras, D., Steriade, M., Sejnowski, T.J. and Huguenard, J.R., 1996. In vivo, in vitro, and computational analysis of dendritic calcium currents in thalamic reticular neurons. *Journal of Neuroscience*, 16(1), pp.169-185.

De Zeeuw, C.I., Wylie, D.R., DiGiorgi, P.L. and Simpson, J.I., 1994. Projections of individual Purkinje cells of identified zones in the flocculus to the vestibular and cerebellar nuclei in the rabbit. *Journal of Comparative Neurology*, 349(3), pp.428-447.

De Zeeuw, C.I. and Berrebi, A.S., 1995. Postsynaptic targets of Purkinje cell terminals in the cerebellar and vestibular nuclei of the rat. *European Journal of Neuroscience*, 7(11), pp.2322-2333.

Eppler, J.M., Helias, M., Muller, E., Diesmann, M. and Gewaltig, M.O., 2009. PyNEST: a convenient interface to the NEST simulator. *Frontiers in neuroinformatics*, 2, p.12.

Fatemi, S.H., Aldinger, K.A., Ashwood, P., Bauman, M.L., Blaha, C.D., Blatt, G.J., Chauhan, A., Chauhan, V., Dager, S.R., Dickson, P.E. and Estes, A.M., 2012. Consensus paper: pathological role of the cerebellum in autism. *The Cerebellum*, 11(3), pp.777-807.

Felix, R., 2002. Insights from mouse models of absence epilepsy into Ca²⁺ channel physiology and disease etiology. *Cellular and molecular neurobiology*, 22(2), pp.103-120.

Fisher, R., Salanova, V., Witt, T., Worth, R., Henry, T., Gross, R., Oommen, K., Osorio, I., Nazzaro, J., Labar, D. and Kaplitt, M., 2010. Electrical stimulation of the anterior nucleus of thalamus for treatment of refractory epilepsy. *Epilepsia*, 51(5), pp.899-908.

Fletcher, C.F., Lutz, C.M., O'Sullivan, T.N., Shaughnessy Jr, J.D., Hawkes, R., Frankel, W.N., Copeland, N.G. and Jenkins, N.A., 1996. Absence epilepsy in tottering mutant mice is associated with calcium channel defects. *Cell*, 87(4), pp.607-617.

Fourcaud-Trocmé, N., Hansel, D., Van Vreeswijk, C. and Brunel, N., 2003. How spike generation mechanisms determine the neuronal response to fluctuating inputs. *Journal of Neuroscience*, 23(37), pp.11628-11640.

Gauck, V. and Jaeger, D., 2003. The contribution of NMDA and AMPA conductances to the control of spiking in neurons of the deep cerebellar nuclei. *Journal of Neuroscience*, 23(22), pp.8109-8118.

Garcia, S., Guarino, D., Jaillet, F., Jennings, T.R., Präpper, R., Rautenberg, P.L., Rodgers, C., Sobolev, A., Wachtler, T., Yger, P. and Davison, A.P., 2014. Neo: an object model for handling electrophysiology data in multiple formats. *Frontiers in neuroinformatics*, 8, p.10.

Glasauer, S. and Rössert, C., 2008. Modelling drug modulation of nystagmus. In *Progress in brain research*, Vol. 171, pp.527-534. Elsevier.

Glasauer, S., Rössert, C. and Strupp, M., 2011. The role of regularity and synchrony of cerebellar Purkinje cells for pathological nystagmus. *Annals of the New York Academy of Sciences*, 1233(1), pp.162-167.

Glenn, L.L. and Steriade, M., 1982. Discharge rate and excitability of cortically projecting intralaminar thalamic neurons during waking and sleep states. *Journal of Neuroscience*, 2(10), pp.1387-1404.

Glickstein, M., 2007. What does the cerebellum really do?. *Current Biology*, 17(19), pp.R824-R827.

Gloor, P. and Fariello, R.G., 1988. Generalized epilepsy: some of its cellular mechanisms differ from those of focal epilepsy. *Trends in neurosciences*, 11(2), pp.63-68.

Gornati, S.V., Schäfer, C.B., Rooda, O.H.E., Nigg, A.L., De Zeeuw, C.I. and Hoebeek, F.E., 2018. Differentiating cerebellar impact on thalamic nuclei. *Cell reports*, 23(9), pp.2690-2704.

Gray, C.M. and McCormick, D.A., 1996. Chattering cells: superficial pyramidal neurons contributing to the generation of synchronous oscillations in the visual cortex. *Science*, 274(5284), pp.109-113.

Grillner, G.S.S., 2010. *Handbook of Brain Microcircuits*. Oxford University Press.

Gschwind, M.A. and Seeck, M., 2016. Modern management of seizures and epilepsy. *Swiss medical weekly*, 146, p.w14310.

Harvard Brain Tissue Resource Center, McLean Hospital, Belmont, MA. 1-800-BRAIN BANK

Heron, S.E., Phillips, H.A., Mulley, J.C., Mazarib, A., Neufeld, M.Y., Berkovic, S.F. and Scheffer, I.E., 2004. Genetic variation of CACNA1H in idiopathic generalized epilepsy. *Annals of neurology*, 55(4), pp.595-596.

Hansel, D. and Mato, G., 2001. Existence and stability of persistent states in large neuronal networks. *Physical Review Letters*, 86(18), p.4175.

Heuzeroth, H., Wawra M., Fidzinski, P., Dag, R, Holtkamp, 2019. The 4-Aminopyridine Model of Acute Seizures in vitro Elucidates Efficacy of New Antiepileptic Drugs. *Frontiers in Neuroscience*, 13, p.677.

Hines, M.L. and Carnevale, N.T., 1997. The NEURON simulation environment. *Neural computation*, 9(6), pp.1179-1209.

Hines, M.L. and Carnevale, N.T., 2001. NEURON: a tool for neuroscientists. *The Neuroscientist*, 7(2), pp.123-135.

Hines, M.L. and Carnevale, N.T., 2000. Expanding NEURON's repertoire of mechanisms with NMODL. *Neural computation*, 12(5), pp.995-1007.

Hoebeek, F.E., Stahl, J.S., Van Alphen, A.M., Schonewille, M., Luo, C., Rutteman, M., van den Maagdenberg, A.M.J.M., Molenaar, P.C., Goossens, H.H.L.M., Frens, M.A. and De Zeeuw, C.I., 2005. Increased noise level of purkinje cell activities minimizes impact of their modulation during sensorimotor control. *Neuron*, 45(6), pp.953-965.

Hu B., Steriade M. & Deschenes M., 1989b. The effects of brainstem peribrachial stimulation on perigeniculate neurons: the blockage of spindle waves. *Neuroscience*, 31, pp.1–12.

Hüfner, K., Stephan, T., Kalla, R., Deutschländer, A., Wagner, J., Holtmannspötter, M., Schulte-Altdorneburg, G., Strupp, M., Brandt, T. and Glasauer, S., 2007. Structural and functional MRIs disclose cerebellar pathologies in idiopathic downbeat nystagmus. *Neurology*, 69(11), pp.1128-1135.

Huguenard, J.R. and Prince, D.A., 1994. Intrathalamic rhythmicity studied in vitro: nominal T-current modulation causes robust antioscillatory effects. *Journal of Neuroscience*, 14(9), pp.5485-5502.

<http://www.opensourcebrain.org/projects/31>, accessed 25 May 2020

<http://andrewdavison.info/notes/porting-NEURON-PyNN/>, accessed 14 March 2019

<https://github.com/NeuralEnsemble/PyNN/issues/559>, accessed 14 March 2019

<http://neuralensemble.org/PyNN>, accessed 14 March 2019

http://neuralensemble.org/docs/PyNN/data_handling.html, accessed 14 March 2019

<http://www.nest-initiative.org>, accessed 14 March 2019

<https://senselab.med.yale.edu/ModelDB/ShowModel.cshtml?model=150024>, accessed 14 March 2019

<https://senselab.med.yale.edu/modeldb/searchFulltext.cshtml?g=birdno+et+al+2011>, accessed 14 March 2019

Pi, H.J., Hangya, B., Kvitsiani, D., Sanders, J.I., Huang, Z.J. and Kepecs, A., 2013. Cortical interneurons that specialize in disinhibitory control. *Nature*, 503(7477), p.521.

Izhikevich, E.M., 2003. Simple model of spiking neurons. *IEEE Transactions on neural networks*, 14(6), pp.1569-1572.

Izhikevich, E.M., 2004. Which model to use for cortical spiking neurons?. *IEEE transactions on neural networks*, 15(5), pp.1063-1070.

Izhikevich, E.M. and Edelman, G.M., 2008. Large-scale model of mammalian thalamocortical systems. *Proceedings of the national academy of sciences*, 105(9), pp.3593-3598.

Jeanmonod, D., Magnin, M. and Morel, A., 1996. Low-threshold calcium spike bursts in the human thalamus: Common physiopathology for sensory, motor and limbic positive symptoms. *Brain*, 119(2), pp.363-375.

Kalla, R., Glasauer, S., Schautzer, F., Lehnen, N., Büttner, U., Strupp, M. and Brandt, T., 2004. 4-aminopyridine improves downbeat nystagmus, smooth pursuit, and VOR gain. *Neurology*, 62(7), pp.1228-1229.

Kalla, R., Glasauer, S., Büttner, U., Brandt, T. and Strupp, M., 2007. 4-aminopyridine restores vertical and horizontal neural integrator function in downbeat nystagmus. *Brain*, 130(9), pp.2441-2451.

Kandel, E.R., Schwartz, J.H. and Jessell, T.M. eds., 2000. *Principles of neural science*, Vol. 4, pp.1227-1246. Ch. 42. The cerebellum. New York: McGraw-hill.

Kernighan, B.W. and Pike, R., 1984. *The Unix programming environment* (Vol. 270). Englewood Cliffs, NJ: Prentice-Hall.

Kim, D., Song, I., Keum, S., Lee, T., Jeong, M.J., Kim, S.S., McEnery, M.W. and Shin, H.S., 2001. Lack of the burst firing of thalamocortical relay neurons and resistance to absence seizures in mice lacking $\alpha 1G$ T-type Ca^{2+} channels. *Neuron*, 31(1), pp.35-45.

Knierim J, 1997. *Neuroscience Online, the Open Access Neuroscience Electronic; Section 4, Chapter 5: Cerebellum*

Kros, L., Eelkman Rooda, O.H., Spanke, J.K., Alva, P., van Dongen, M.N., Karapatis, A., Tolner, E.A., Strydis, C., Davey, N., Winkelman, B.H. and Negrello, M., 2015. Cerebellar output controls generalized spike-and-wave discharge occurrence. *Annals of neurology*, 77(6), pp.1027-1049.

Ladenbauer, J., Augustin, M., Shiau, L. and Obermayer, K., 2012. Impact of adaptation currents on synchronization of coupled exponential integrate-and-fire neurons. *PLoS computational biology*, 8(4), p.e1002478.

Leenders, A.M., Van Den Maagdenberg, A.M., Da Silva, F.H.L., Sheng, Z.H., Molenaar, P.C. and Ghijsen, W.E., 2002. Neurotransmitter release from tottering mice nerve terminals with reduced expression of mutated P-and Q-type Ca^{2+} -channels. *European Journal of Neuroscience*, 15(1), pp.13-18.

Leiner, H.C., Leiner, A.L. and Dow, R.S., 1989. Reappraising the cerebellum: What does the hindbrain contribute to the forebrain? *Behavioral neuroscience*, 103(5), p.998.

Leiner, H.C., Leiner, A.L. and Dow, R.S., 1993. Cognitive and language functions of the human cerebellum. *Trends in neurosciences*, 16(11), pp.444-447.

Leigh, R.J., 2003. Potassium channels, the cerebellum, and treatment for downbeat nystagmus.

Leigh, R.J. and Zee, D.S., 2006. Diagnosis of nystagmus and saccadic intrusion. *The neurology of eye movements*, pp.475-558.

Llinás, R.R. and Steriade, M., 2006. Bursting of thalamic neurons and states of vigilance. *Journal of neurophysiology*, 95(6), pp.3297-3308.

Loiseau, P., Duche, B. and Cohadon, S., 1992. The prognosis of benign localized epilepsy in early childhood. *Epilepsy Research. Supplement*, 6, pp.75-81.

Luthman, J., Hoebeek, F.E., Maex, R., Davey, N., Adams, R., De Zeeuw, C.I. and Steuber, V., 2011. STD-dependent and independent encoding of input irregularity as spike rate in a computational model of a cerebellar nucleus neuron. *The Cerebellum*, 10(4), pp.667-682.

Marti, S.R., Straumann, D. and Glasauer, S.E., 2005. The origin of downbeat nystagmus: an asymmetry in the distribution of on-directions of vertical gaze-velocity Purkinje cells. *Annals of the New York Academy of Sciences*, 1039(1), pp.548-553.

Matsushita, K., Wakamori, M., Arii, T., Oda, S.I., Mori, Y. and Imoto, K., 2002. Bidirectional Alterations in Cerebellar Synaptic Transmission of tetrodotoxin and rolling Ca^{2+} Channel Mutant Mice. *Journal of Neuroscience*, 22(11), pp.4388-4398.

Miyasho, T., Takagi, H., Suzuki, H., Watanabe, S., Inoue, M., Kudo, Y. and Miyakawa, H., 2001. Low-threshold potassium channels and a low-threshold calcium channel regulate Ca^{2+} spike firing in the dendrites of cerebellar Purkinje neurons: a modeling study. *Brain research*, 891(1-2), pp.106-115

McCormick, D.A. and Bal, T., 1997. Sleep and arousal: thalamocortical mechanisms. Annual review of neuroscience, 20(1), pp.185-215.

Noebels, J.L., 2005. Calcium channel “gating” and absence epilepsy. Epilepsy currents, 5(3), pp.95-97.

Ovsepian, S.V., Steuber, V., Le Berre, M., O’Hara, L., O’Leary, V.B. and Dolly, J.O., 2013. A defined heteromeric KV1 channel stabilizes the intrinsic pacemaking and regulates the output of deep cerebellar nuclear neurons to thalamic targets. The Journal of physiology, 591(7), pp.1771-1791.

Palkovits, M., Mezey, É., Hamori, J. and Szentagothai, J., 1977. Quantitative histological analysis of the cerebellar nuclei in the cat. I. Numerical data on cells and on synapses. Experimental Brain Research, 28(1-2), pp.189-209.

Pedroarena, C.M. and Schwarz, C., 2003. Efficacy and short-term plasticity at GABAergic synapses between Purkinje and cerebellar nuclei neurons. Journal of Neurophysiology, 89(2), pp.704-715.

Person, A.L. and Raman, I.M., 2012. Purkinje neuron synchrony elicits time-locked spiking in the cerebellar nuclei. Nature, 481(7382), p.502.

Peyser, A., Deepu, R., Mitchell, J., Appukuttan, S., Schumann, T., Eppler, J.M., Kappel, D., Hahne, J., Zajzon, B., Kitayama, I. and Fardet, T., 2017. NEST 2.14. 0 (No. FZJ-2017-07289). Jülich Supercomputing Center.

Qian, J. and Noebels, J.L., 2000. Presynaptic Ca²⁺ influx at a mouse central synapse with Ca²⁺ channel subunit mutations. Journal of Neuroscience, 20(1), pp.163-170.

R Development Core Team, 2008. R: A language and environment for statistical computing. R Foundation for Statistical Computing, Vienna, Austria. ISBN 3-900051-07-0, URL <http://www.R-project.org>

Rall, W., 1967. Distinguishing theoretical synaptic potentials computed for different somadendritic distributions of synaptic input. *Journal of neurophysiology*, 30(5), pp.1138-1168.

Reeber, S.L., Otis, T.S. and Sillitoe, R.V., 2013. New roles for the cerebellum in health and disease. *Frontiers in systems neuroscience*, 7, p.83.

Salmasi, M., Loebel, A., Glasauer, S. and Stemmler, M., 2019. Short-term synaptic depression can increase the rate of information transfer at a release site. *PLoS computational biology*, 15(1), p.e1006666.

Sekirnjak, C., Vissel, B., Bollinger, J., Faulstich, M. and Du Lac, S., 2003. Purkinje cell synapses target physiologically unique brainstem neurons. *Journal of Neuroscience*, 23(15), pp.6392-6398.

Sherman, S.M. and Guillery, R.W., 2006. Exploring the thalamus and its role in cortical function. MIT press.

Sherman, S.M., 2011. Functioning of circuits connecting thalamus and cortex. *Comprehensive Physiology*, 7(2), pp.713-739.

Sherman SM. Thalamus plays a central role in ongoing cortical activity functioning. *Nat Neurosci*. 2016;19-4:533–41.

Shin, S.L., Rotter, S., Aertsen, A. and De Schutter, E., 2007. Stochastic description of complex and simple spike firing in cerebellar Purkinje cells. *European Journal of Neuroscience*, 25(3), pp.785-794.

Silveri, M.C., Di Betta, A.M., Filippini, V., Leggio, M.G. and Molinari, M., 1998. Verbal short-term store-rehearsal system and the cerebellum. Evidence from a patient with a right cerebellar lesion. *Brain: a journal of neurology*, 121(11), pp.2175-2187.

Snead III, O.C., 1992. Evidence for GABAB-mediated mechanisms in experimental generalized absence seizures. *European journal of pharmacology*, 213(3), pp.343-349.

Stahl, J.S., James, R.A., Oommen, B.S., Hoebeek, F.E. and De Zeeuw, C.I., 2006. Eye movements of the murine P/Q calcium channel mutant tottering, and the impact of aging. *Journal of neurophysiology*, 95(3), pp.1588-1607.

Stahl, J.S., Thumser, Z.C. and Oommen, B.S., 2012. The ataxic mouse as a model for studying downbeat nystagmus. *Journal of Vestibular Research*, 22(5, 6), pp.221-241.

Steriade, M., 1974. Interneuronal epileptic discharges related to spike-and-wave cortical seizures in behaving monkeys. *Electroencephalography and clinical neurophysiology*, 37(3), pp.247-263.;

Steriade, M. and Contreras, D., 1995. Relations between cortical and thalamic cellular events during transition from sleep patterns to paroxysmal activity. *Journal of Neuroscience*, 15(1), pp.623-642.

Sterratt, D., Graham, B., Gillies, A. and Willshaw, D., 2011. *Principles of computational modelling in neuroscience*. Cambridge University Press.

Strupp, M., Zingler, V.C., Arbusow, V., Niklas, D., Maag, K.P., Dieterich, M., Bense, S., Theil, D., Jahn, K. and Brandt, T., 2004. Methylprednisolone, valacyclovir, or the combination for vestibular neuritis. *New England Journal of Medicine*, 351(4), pp.354-361.

Strupp, M., Zwergal, A. and Brandt, T., 2007. Episodic ataxia type 2. *Neurotherapeutics*, 4(2), pp.267-273.

Steuber, V. and Willshaw, D., 2004. A biophysical model of synaptic delay learning and temporal pattern recognition in a cerebellar Purkinje cell. *Journal of computational neuroscience*, 17(2), pp.149-164.

Steuber, V., Schultheiss, N.W., Silver, R.A., De Schutter, E. and Jaeger, D., 2011. Determinants of synaptic integration and heterogeneity in rebound firing explored with data-driven models of deep cerebellar nucleus cells. *Journal of computational neuroscience*, 30(3), pp.633-658.

Telgkamp, P., Padgett, D.E., Ledoux, V.A., Woolley, C.S. and Raman, I.M., 2004. Maintenance of high-frequency transmission at Purkinje to cerebellar nuclear synapses by spillover from boutons with multiple release sites. *Neuron*, 41(1), pp.113-126.

Temkin O. *The Falling Sickness*, 2nd ed. Baltimore: Johns Hopkins, 1971.

Thach, W.T., 1970. Discharge of cerebellar neurons related to two maintained postures and two prompt movements. II. Purkinje cell output and input. *Journal of Neurophysiology*, 33(4), pp.537-547.

Tissot, S.A.D. *Traité de l'épilepsie*. François Grasset et Comp; Lausanne: 1783.

Touboul, J. and Brette, R., 2008. Dynamics and bifurcations of the adaptive exponential integrate-and-fire model. *Biological cybernetics*, 99(4-5), p.319.

Traub, R.D., Contreras, D., Cunningham, M.O., Murray, H., LeBeau, F.E., Roopun, A., Bibbig, A., Wilent, W.B., Higley, M.J. and Whittington, M.A., 2005. Single-column thalamocortical network model exhibiting gamma oscillations, sleep spindles, and epileptogenic bursts. *Journal of neurophysiology*, 93(4), pp.2194-2232.

Tröster, A.I., Woods, S.P., Fields, J.A., Lyons, K.E., Pahwa, R., Higginson, C.I. and Koller, W.C., 2002. Neuropsychological deficits in essential tremor: an expression of cerebello-thalamo-cortical pathophysiology?. *European Journal of Neurology*, 9(2), pp.143-151.

Tyrrell, T. and Willshaw, D., 1992. Cerebellar cortex: its simulation and the relevance of Marr's theory. *Philosophical Transactions of the Royal Society of London. Series B: Biological Sciences*, 336(1277), pp.239-257.

Vedam-Mai, V., McFarland, K., Zhang, Q., Kim, H., Nathu, R., Kurtovic, S., Savery, K., Ashizawa, T. and Okun, M., 2016. Evaluating the effects of deep brain stimulation (DBS) in mice with spinocerebellar ataxia (SCA1): 1074. *Movement Disorders*, 31.

Voogd, J., Schraa-Tam, C.K., van der Geest, J.N. and De Zeeuw, C.I., 2012. Visuomotor cerebellum in human and nonhuman primates. *The Cerebellum*, 11(2), pp.392-410.

Wakamori, M., Yamazaki, K., Matsunodaira, H., Teramoto, T., Tanaka, I., Niidome, T., Sawada, K., Nishizawa, Y., Sekiguchi, N., Mori, E. and Mori, Y., 1998. Single tottering mutations responsible for the neuropathic phenotype of the P-type calcium channel. *Journal of Biological Chemistry*, 273(52), pp.34857-34867.

Walker, M.F., Tian, J., Shan, X., Tamargo, R.J., Ying, H. and Zee, D.S., 2008. Lesions of the cerebellar nodulus and uvula impair downward pursuit. *Journal of neurophysiology*, 100(4), pp.1813-1823.

Weisz, J.R., Sandler, I.N., Durlak, J.A. and Anton, B.S., 2005. Promoting and protecting youth mental health through evidence-based prevention and treatment. *American psychologist*, 60(6), p.628.

Wikimedia Commons/Life Science Databases

Zhou, L. and Shine, H.D., 2003. Neurotrophic factors expressed in both cortex and spinal cord induce axonal plasticity after spinal cord injury. *Journal of neuroscience research*, 74(2), pp.221-226.

Appendix

i. Conference papers

P293 Phase dependence of the termination of absence seizures by cerebellar input to thalamocortical networks

Julia Goncharenko¹, Lieke Kros², Reinoud Maex¹, Neil Davey¹, Christoph Metzner³, Chris de Zeeuw², Freek Hoebeek², Volker Steuber¹

¹University of Hertfordshire, Biocomputation Research Group, Hatfield, United Kingdom; ²Erasmus MC, Department of Neuroscience, Rotterdam, Netherlands; ³Technische Universität Berlin, Department of Software Engineering and Theoretical Computer Science, Berlin, Germany

Correspondence: Julia Goncharenko (i.goncharenko@herts.ac.uk)

BMC Neuroscience 2019, 20(Suppl 1): P293

Absence seizures are the most common form of epilepsy in children. They start and finish abruptly, last for 10–20 seconds and can be detected by generalised spike-and-wave discharges (GSWDs) in the electroencephalogram. These GSWDs are based on neuronal oscillations in thalamocortical networks, which can be caused by excessive inhibition in the thalamus or excessive cortical activity. Absence seizures can be triggered by switching of the normal asynchronous neuronal activity in thalamocortical networks to synchronised oscillations, and terminated by the reverse process, switching from synchronised oscillations to asynchronous activity.

Experimental studies have shown that thalamic stimulation can disrupt oscillatory activity in thalamocortical networks. More recently, it was also found that optogenetic activation of neurons in the cerebellar nuclei (CN) can stop epileptic absence seizures and reset the oscillatory activity, for example in a closed loop system [1]. However, the underlying mechanism of the termination of absence seizures by CN stimulation is not yet clear.

To investigate the mechanism of the termination of absence seizures by thalamic input from the CN we used computer simulations. We simulate a thalamocortical network model with adaptive exponential integrate-and-fire neurons, displaying complex intrinsic properties such as low-threshold spiking, regular spiking, fast spiking and adaptation [2]. The network activity can exhibit oscillatory or asynchronous irregular (AI) dynamics, depending on the time

constants of the inhibitory synaptic conductance, which are 5 ms (AI) and 15 ms (oscillatory), respectively. An increase in the inhibitory decay time constant reflects a change from GABAA dominated inhibition to more GABAB, which can result in GSWDs, given that the “wave” components of GSWDs are related to slow GABAB -mediated K⁺ currents [3].

We provide CN input to all thalamocortical neurons to analyse the mechanism of reverting from abnormal oscillatory activity to the normal AI state. Our results confirm that input from the CN can control oscillatory activity in thalamocortical networks. Furthermore, they show that the effectiveness of this input exhibits phase-dependence. In our simulations, CN input terminates epileptic absence seizures most effectively when it arrives at the peak of GSWDs, while seizure termination is least efficient for input between the GSWD bursts. This finding is potentially relevant for therapeutic applications of CN stimulation to terminate seizures. However, the simulations *in silico* did not take several biological factors such as indirect pathways from the CN to the thalamus into account that may explain differences with animal models of epilepsy [1].

References

1. Kros L, Eelkman Roda OHJ, Spanke JK, et al. Cerebellar Output Controls Generalised Spike-and-Wave Discharge Occurrence. *Annals of neurology* 2015, 77(6):1027–1049.
2. Destexhe A. Self-sustained asynchronous irregular states and up-down states in thalamic, cortical and thalamocortical networks of nonlinear integrate-and-fire neurons. *Journal of Computational Neuroscience* 2009, 27:493–506.
3. Destexhe A. Spike-and-Wave Oscillations Based on the Properties of GABAB Receptors. *Journal of Neuroscience* 1998, 18(21):9099–9110.

P255 Modulation of epileptic activity in thalamo-cortical networks by input from the cerebellar nuclei

Julia Goncharenko¹, Lieke Kros², Neil Davey¹, Christoph Metzner¹, Chris de Zeeuw², Freek Hoebeek², Volker Steuber¹

¹Centre for Computer Science and Informatics Research, University of Hertfordshire, Hatfield, AL10 9AB, UK; ²Department of Neuroscience, Erasmus MC, Wytemaweg 80, 3015 CN, Rotterdam, the Netherlands

Correspondence: Julia Goncharenko (i.goncharenko@herts.ac.uk)

BMC Neuroscience 2017, 18 (Suppl 1):P255

Epilepsy is one of the most prevalent neurological diseases in humans, affecting people of all ages. One of the most common forms of epilepsy in children is absence epilepsy [1]. Characteristic symptoms of absence epilepsy are sudden seizures that are accompanied by periods of behavioral arrest and impaired consciousness [1]. As in other forms of epilepsy, these seizures are electrophysiologically described by neuronal oscillations in thalamo-cortical networks and appear as generalized spike-and wave discharges (GSWDs) in the electroencephalogram (EEG) [2]. Oscillatory activity in cerebral cortex and thalamus can be caused by excessive inhibition in thalamus or by excessive cortical activity [2]. It has been suggested that the initiation of absence seizures can be triggered by events that switch neuronal activity in thalamo-cortical networks from normal asynchronous activity to synchronised oscillations [2].

Previous experimental studies have shown that oscillatory activity in thalamo-cortical networks and the accompanying GSWDs can be disrupted by stimulation of the thalamus [3]. Recently, it has been found that optogenetic activation of neurons in the cerebellar nuclei (CN) is a powerful tool to stop epileptic absence seizures using a closed-loop system in two unrelated mouse models [4]. Due to their anatomical bottleneck location, CN neurons can control the balance of excitation and inhibition in thalamus, resetting the oscillatory activity in thalamo-cortical loops. However, the mechanism underlying the disruption of thalamo-cortical oscillations and absence seizures by stimulation of the CN remains unknown.

Here we use computer simulations to investigate the mechanisms underlying the termination of absence seizures by optogenetic stimulation of CN neurons. We simulate a thalamo-cortical network model of adaptive exponential integrate-and-fire neurons, displaying complex

intrinsic properties such as low-threshold spiking, regular spiking, fast spiking and adaptation [5]. The network activity can exhibit oscillatory or asynchronous irregular (AI) dynamics, depending on the level of adaptation in cortical cells [5]. We use electrophysiologically recorded spike trains that result from optogenetic activation of CN neurons in mouse models of absence epilepsy as input to the network model to analyse the mechanism of reverting abnormal oscillatory activity to the normal AI state. Our results illustrate how input from the CN can control oscillatory activity in thalamo-cortical networks and therefore provide a mechanism to terminate epileptic absence seizures.

References

1. Berg AT, Berkovic SF, Brodie MJ, et al.: Revised terminology and concepts for organization of seizures and epilepsies: report of the ILAE Commission on Classification and Terminology, 2005–2009. *Epilepsia* 2010, 51:676–685.
2. Snead OC III: Basic mechanisms of generalized absence seizures. *Ann Neurol* 1995, 37(2):146–157.
3. Paz JT, Davidson TJ, Frechette ES, et al.: Closed-loop optogenetic control of thalamus as a tool for interrupting seizures after cortical injury. *Nat Neurosci* 2013, 16:64–70.
4. Kros L, Eelkman Roda OHJ, Spanke JK, et al.: Cerebellar Output Controls Generalised Spike-and-Wave Discharge Occurrence. *Ann Neurol* 2015, 77(6):1027–1049.
5. Destexhe A.: Self-sustained asynchronous irregular states and up-down states in thalamic, cortical and thalamocortical networks of nonlinear integrate-and-fire neurons. *J Comput Neurosci* 2009, 27:493–506.

P51 The role of cerebellar short-term synaptic plasticity in the pathology and medication of downbeat nystagmus

Julia Goncharenko¹, Neil Davey¹, Maria Schilstra¹, Volker Steuber¹

¹Centre for Computer Science and Informatics Research, University of Hertfordshire, Hatfield, AL10 9EJ, UK

Correspondence: Julia Goncharenko - i.goncharenko@herts.ac.uk

BMC Neuroscience 2016, 17(Suppl 1):P51

Downbeat nystagmus (DBN) is a common eye fixation disorder that is linked to cerebellar pathology. DBN patients are treated with 4-aminopyridine (4-AP), a K channel blocker, but the underlying mechanism is unclear. DBN is associated with an increased activity of floccular target neurons (FTNs) in the vestibular nuclei. It was previously believed that the reason for the increased activity of FTNs in DBN is a pathological decrease in the spike rate of their inhibitory Purkinje cell inputs, and that the effect of 4-AP in treating DBN could be mediated by an increased Purkinje cell activity, which would restore the inhibition of FTNs and bring their activity back to normal [1]. This assumption, however, has been questioned by *in vitro* recordings of Purkinje cells from tottering (*tg/tg*) mice, a mouse model of DBN. It was shown that therapeutic concentrations of 4-AP did not increase the spike rate of the Purkinje cells, but that they restored the regularity of their spiking, which is impaired in *tg/tg* mice [2].

Prompted by these experiments, Glasauer and colleagues performed computer simulations to investigate the effect of the regularity of Purkinje cell spiking on the activity of FTNs [3]. Using a conductance based FTN model, they found that changes in the regularity of the Purkinje cell input only affected the FTN spike rate when the input was synchronized. In this case, increasing the regularity of the Purkinje cell spiking resulted in larger gaps in the inhibitory input to the FTN and an increased FTN spike rate. These results predict that the increased irregularity in the Purkinje cell activity in DBN should lead to a decreased activity of the FTNs, rather than the increased activity that is found in experiments, and they are therefore unable to explain the therapeutic effect of 4-AP.

However, the model by Glasauer and colleagues does not take short-term depression (STD) at the Purkinje cell—FTN synapses into account. We hypothesized that this absence of STD could explain the apparent contradiction between the experimental [2] and computational [3] results. To study the role of STD in the pathology and 4-AP treatment of DBN, we used a

morphologically realistic conductance based model of a cerebellar nucleus (CN) neuron [4, 5] as an FTN model to simulate the effect of irregular versus regular Purkinje cell input. The coefficients of variation of the irregular and regular Purkinje cell spike trains during DBN and after 4-AP treatment, respectively, were taken from recordings from wild-type and tg/tg mice [6], which served as a model system for DBN. We presented the FTN model with synchronized and unsynchronized input and found that, for both conditions, irregular (DBN) input trains resulted in higher FTN spike rates than regular (4-AP) ones. In the presence of unsynchronized Purkinje cell input, the acceleration of the FTN spike output during simulated DBN and the deceleration during simulated 4-AP treatment depended on STD at the Purkinje cell synapses. Our results provide a potential explanation for the pathology and 4-AP treatment of pathological nystagmus.

References

1. Glasauer S, Kalla R, Buttner U, Strupp M, Brandt T. 4-aminopyridine restores visual ocular motor function in upbeat nystagmus. *J Neurol Neurosurg Psychiatry*. 2005;76:451–3.
2. Alvina K, Khodakhah K. The therapeutic mode of action of 4-aminopyridine in cerebellar ataxia. *J Neurosci*. 2010;30:7258–68.
3. Glasauer S, Rössert C, Strupp M. The role of regularity and synchrony of cerebellar Purkinje cells for pathological nystagmus. *Ann NY Acad Sci*. 2011;1233:162–7.
4. Steuber V, Schultheiss NV, Silver RA, de Schutter E, Jaeger D. Determinants of synaptic integration and heterogeneity in rebound firing explored with data-driven models of deep cerebellar nucleus cells. *J Comp Neurosci*. 2011;30:633–58.
5. Luthman J, Hoebeek FE, Maex R, Davey N, Adams R, de Zeeuw CI, Steuber V. STD-dependent and independent encoding of input irregularity as spike rate in a computational model of a cerebellar nucleus neuron. *Cerebellum*. 2011;10:667–82.
6. Hoebeek FE, Stahl JS, van Alphen AM, Schonewille M, Luo C, Rutteman M, van den Maagdenberg AM, Molenaar PC, Goossens HH, Frens MA, et al. Increased noise level of Purkinje cell activities minimizes impact of their modulation during sensorimotor control. *Neuron* 2005, 45(6):953–965.

ii. Experimental data analysis: $1/ISI(t)$ plotted for all 39 data files.

